Università Ca' Foscari Venezia

Graduate School Global Change Science and Policy

PhD Programme
in Science and Management of Climate Change
Ciclo XXV
Anno di discussione 2013

A long-term climatology of medicanes

Tesi di Dottorato di Leone Cavicchia, matricola 955709
Settore scientifico disciplinare di afferenza: FIS/06

Coordinatore del Dottorato:
Prof. Carlo Barbante

Tutore del dottorando:
Dr. Silvio Gualdi

Co-tutore del dottorando:
Prof. Hans von Storch

Now as to sudden blasts, which arise as has been said from exhalations of the earth, and fall back again to the earth drawing over it an envelope of cloud; these occur in a variety of forms. The fact is that their onrush is quite irregular, like that of mountain torrents (as we have pointed out is the view of certain persons), and they give forth thunder and lightning. If travelling with a heavier momentum they burst a great gap in a dry cloud, they produce a storm called by the Greeks a cloudburst; but if they break out from a downvard curve of cloud with a more limited rotation, they cause a whirl unaccompanied by fire - I mean by lightning - that is called a typhoon, which denotes a whirling cloudburst. This brings down with it a portion of heat torn from a cloud, which it turns and whirls round, increasing its own downward velocity by its weight, and shifting from place to place with a rapid whirl; it is specially disastrous to navigators, as it twists round and shatters not only the yards, but the vessels themselves, leaving only the slender remedy of pouring out vinegar in advance of its approach, vinegar being a very cold substance. The same whirlwind when beaten back by its very impact snatches things up and carries them back with it to the sky, sucking them high aloft.

But if it bursts out of a larger cavern of downward pressing cloud but not so wide a one as in the case of a storm, and is accompanied by a crashing noise, this is what they call a whirlwind, which overthrows everything in its neighbourhood. When the same rages hotter and with a fiery flow, it is called a prester*, as while sweeping away the things it comes in contact with it also scorches them up. But a typhoon does not occur with a northerly wind, nor a cloudburst with snow or when snow is lying. If it flared up as soon as it burst the cloud, and had fire in it, did not catch fire afterwards, it is a thunderbolt. It differs from a fiery pillar in the way in which a flame differs from a fire: a fiery pillar spreads out its blast widely, whereas a thunderbolt masses together its onrush. On the other hand a tornado differs from a whirlwind by returning, and as a whizz differs from a crash; a storm is different from either in its extent it is caused by the scattering rather than the bursting of a cloud. There also occurs a darkness caused by a cloud shaped like a wild monster this is direful to sailors. There is also what is called a column, when densified and stiffened moisture raises itself aloft; in the same class also is a waterspout, when a cloud draws up water like a pipe.*

Pliny the Elder, *Naturalis historia*, Book 2, Chapters 49-50

Contents

Introduction

Over the last decades, the occasional occurence over the Mediterranean Sea of sub-synoptic scale storms presenting several similarities with tropical cyclones has been reported. Given their resemblance to tropical storms, and in particular considering the strong winds associated with them, these systems have been referred to in the recent literature as "medicanes" (from *Medi*terrranean hurri*canes*).

Medicanes are considered rare phenomena, since only a few have been directly observed - the number of cases well documented in the literature is around ten. It has to be noted however that, due to their marine character and their sub-synoptic scale, most of the medicanes that have been observed and documented are the cases associated with impacts and damage on coastal areas. It is thus likely that a substantial number of medicanes that occurred in the past have not been detected at all.

Indeed, the availability of observations of such storms by in-situ weather reports is generally poor, and limited to ships cruising nearby. Since the 1980s, more cases have been detected by searching for structures similar to those of observed medicanes in satellite imagery. However, due to the difficulty encountered in defining unequivocally a set of conditions to assess on firm grounds detection of medicanes, even after inspection of a large amount of satellite images the number of known medicanes is still limited to a few tens.

Contemporary meteorological analyses capture most cases of medicanes because of high grid resolution and powerful initialisation techniques, which include the use of satellite data. However, when running frozen analysis systems, which are the basis of re-analysis such as NCEP/NCAR, a homogeneous description of the statistics of the sub-synoptic scale formation and life cycles of medicanes cannot be expected because of changing density and quality of observations on synoptic and sub-synoptic scales. Instead, changing statistics from such an inhomogeneous data set will represent more the effect of changing observational efficiency than changes in the physical phenomenon. Moreover, the reanalysis products currently available do not have

a high enough spatial resolution to describe accurately small-scale cyclones such as medicanes.

Thus, it is not possible to construct homogeneous statistics of the formation and life cycle of medicanes for the past decades by analysing re-analyses. The same problem holds for the case of polar lows and for tropical cyclones. In both cases, a dynamical downscaling strategy has been been employed, in which large-scale state descriptions provided by re-analysis are dynamically downscaled, using the concept of spectral nudging, running an atmospheric limited area model in climate mode. In the present study, we apply the same methodology to the study of medicanes, exploiting the added value of downscaling to obtain atmospheric fields at high resolution.

At first, in order to assess the robustness of this method, we simulate four medicanes studied in the literature. As in the previous studies on polar lows and typhoons, we examine how well known cases of the formation and life cycle of medicanes can be reproduced.

We then run the system for the six decades of NCEP/NCAR reanalysis, to identify and track all medicanes, estimate their trends and variability and investigate the factors responsible for the genesis of medicanes.

Finally, we repeat the downscaling simulation the projections of the IPCC A2 future climate scenario and estimate the impact of climate change on the statistics of medicanes.

This Thesis is organized as follows. In Chapter 1 a general overview of medicanes features is given, reviewing the findings of observational and modeling studies in the literature. In Chapter 2 the main technical aspects of the current work are described. The regional model configuration used for the downscaling and the objective procedure for the detection of medicanes in the model output are discussed in detail. In Chapter 3 the results on the simulation of four historical medicanes are presented, focussing on their robustness. The results on the statistical properties of the medicanes in the six decades of NCEP reanalysis and on their linkage to large-scale factors are discussed in Chapter 4. Finally, the findings on the changing statistics of medicanes in a warming climate are presented in Chapter 5.

Chapter 1

Medicanes: hurricanes in the Mediterranean Sea

1.1 An overview of Mediterranean cyclogenesis

Due to its peculiar geographical features, such as the steep orography surrounding the basin and the complex land-sea distribution, the Mediterranean region is characterized by a large number of low pressure systems. Given the spatial scales involved, it has been possible to accomplish a systematic characterization and classification of the statistical properties and genesis mechanisms of Mediterranean cyclones only in recent years, when high resolution data have become available.

The total number of cyclones detected depends on the resolution of the atmospheric fields used for the analysis and on the details of the detection procedure adopted, but there is a good agreement on the geographical distribution of cyclones formation. Fig. 1.1 shows the distribution of the cyclones detected in a high-resolution dataset over the Mediterranean. A number of areas emerges where a large number of cyclones are detected (see the map in Fig. 1.3 for the geographical names used in the text): the gulf of Genoa, the area around the island of Cyprus, the region corresponding to the Atlas mountains in northern Africa, and the part of the Iberian peninsula south of the Pyrenees mountains. According to Trigo et al. (1999b) the cyclonic activity over the aforementioned regions accounts for around half of the total number of cyclones detected in the whole Mediterranean region.

Other quantities, such as the mean radius, lifetime and intensity are somehow more sensitive on the choice of the data used for the analysis, but even in that case there is a reasonable agreement between different analyses on

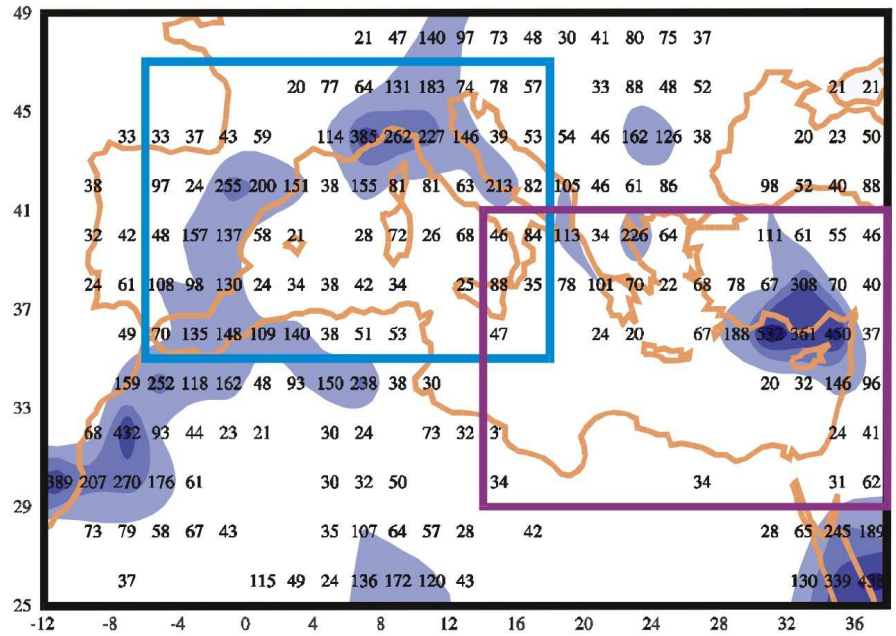

Figure 1.1: Number of cyclones detected in a three-years (Jun 1998 to May 2001) sample of operational analyses from the ECMWF at T319 resolution. 2,248 cyclones are detected in the Eastern Mediterranean (purple frame) and 2,910 in the Western Basin (blue frame).
(From Gil et al. 2003).

the main features. As an example, in Fig. 1.2 are reported the distributions of mean radius, lifetime, track length and geostrophic circulation from a recent analysis obtained from the ERA-40 dataset (Campins et al., 2011). In Fig. 1.3 are reported the seasonal cycles of cyclogenesis events over the western and eastern parts of the basin, and in the regions where most of the activity is concentrated. The overall distribution in both parts of the basin show a flattish shape with a maximum in Summer and a minimum in Winter, whereas the seasonality in the most active areas shows sharper peaks.

The vertical structure of cyclones in the western part of the basin has been investigated in detail in Campins et al. (2006). It was found that the greatest percentage of western Mediterranean cyclones are shallow ones, extending only about up to 850 hPa. The deep cyclones (extending up to the 300 hPa level) account for approximately 25% of the total number (Fig. 1.4). Moreover, deep cyclones are found mainly during Winter. The mean vertical profiles show that Mediterranean cyclones tend to have a warm core in the lower layers, and a cold core in the upper layers (Fig. 1.5). The

relative humidity profiles show a clear seasonal difference, with higher values in Winter (Fig. 1.6).

According to Trigo et al. (1999a), cyclogenesis in the Mediterranean can be divided into three different idealized seasons, each exhibiting specific features. Winter (Fig. 1.7 a) is dominated by baroclinic processes along the northern coast of the basin. The main genesis center is the gulf of Genoa, where the formation mechanism is orographical cyclogenesis in the lee of the Alps (Buzzi and Tibaldi, 1978). Another formation region is found in the Aegean Sea, due to both the influence of the orography in the Balkans and of upper-level troughs. The interaction of upper-level troughs with low-level weak stability is also responsible for cyclogenesis in the third region, the Black Sea.

During Spring (Fig. 1.7 b) and Summer (Fig. 1.7 c) cyclogenesis events tend to be more scattered throughout the basin, compared to Winter. A number of distinctive patterns for those seasons can be however singled out. The Saharan lows in Spring are due to the interplay between the temperature gradients over northern Africa and the effect of the lee of the Atlas mountains. The lows in the Middle-East are associated with the expansion of the Asian trough over the eastern Mediterranean, forced by the Asian monsoon (Rodwell and Hoskins, 1996). During Summer, Saharan, Iberian and Middle-East lows all show a strong diurnal cycle, an indication of the role of thermal forcing.

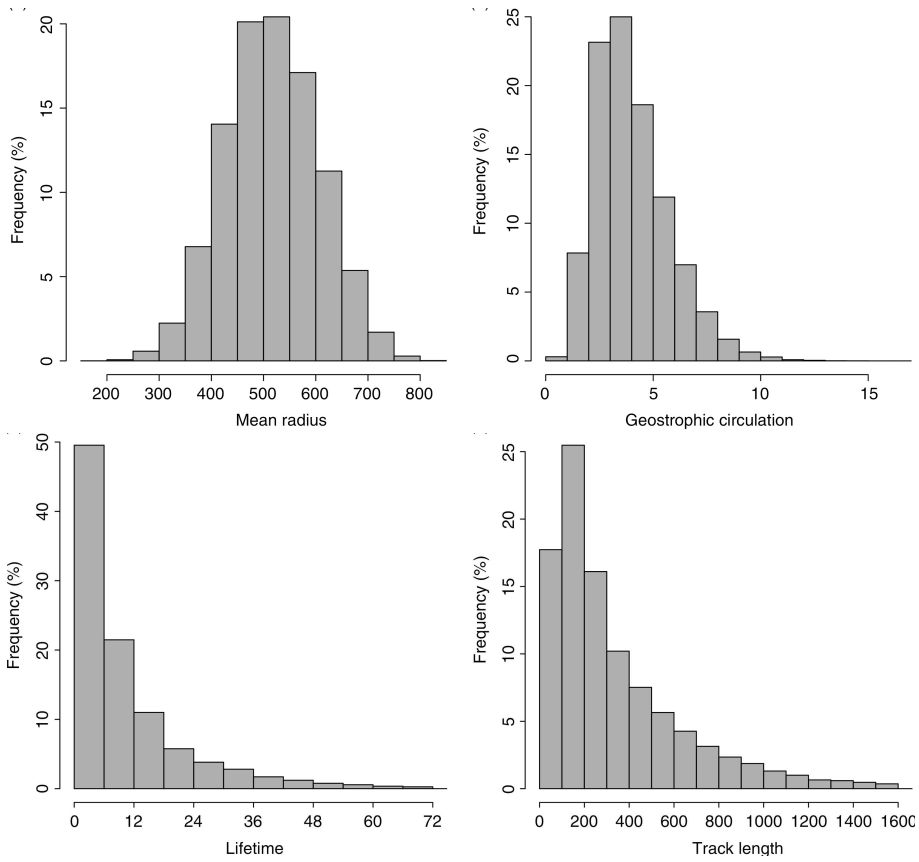

Figure 1.2: Histograms of (top left) mean radius (R, in km), of (top right) geostrophic circulation (in GCU, 1 GCU=$10^7 m^2 s^{-1}$) of (bottom left) lifetime (t, in hours) of all the cyclone centres and of (bottom right) track length (d, in km) of all the cyclones with a lifetime o fat least 12h, detected in the ERA-40 reanalyses.
(From Campins et al. 2011).

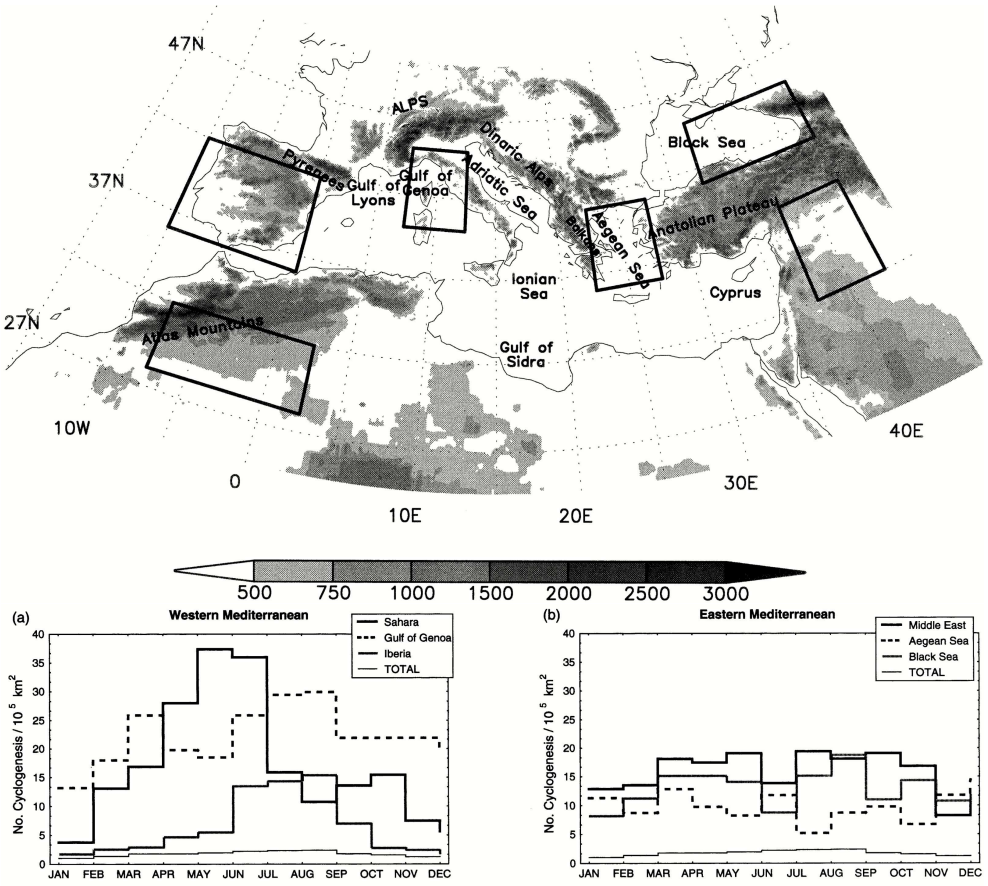

Figure 1.3: Total number of cyclogenesis events detected per 10^5 km^2 within the most active regions (indicated by boxes in the map) in the (a) western and (b) eastern Mediterranean, during the 1987-96 period in ECMWF re-analyses. The total number of cyclogenesis events detected in the whole basin per unit area is represented by the bottom line.
(From Trigo et al. 1999a).

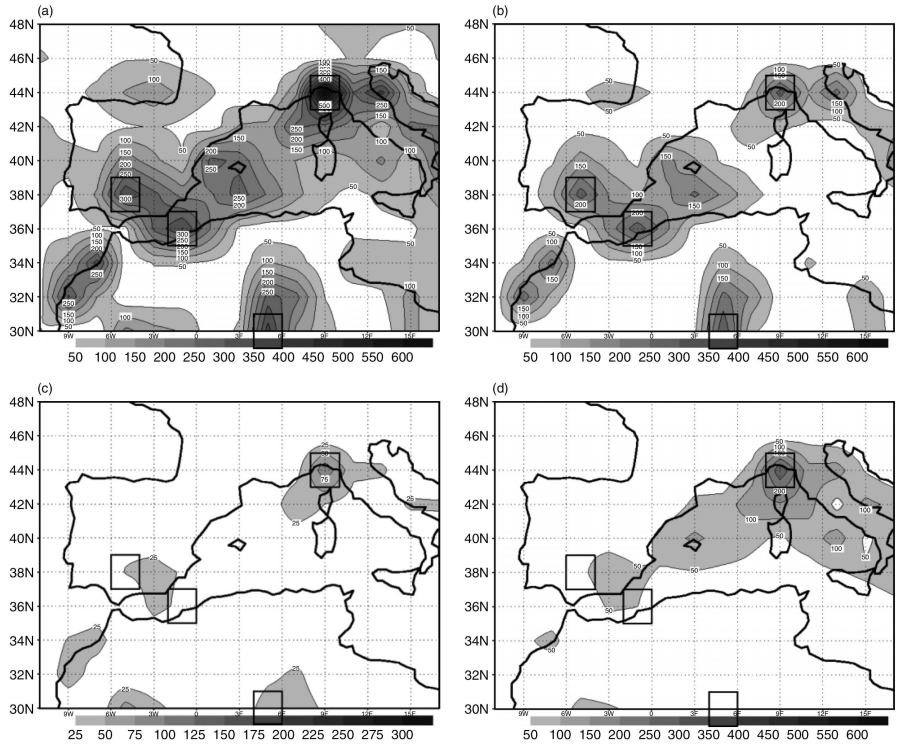

Figure 1.4: Total number of cyclone centres detected in 0.5° resolution HIRLAM operational analyses (1995-2003) for (a) all the database, (b) shallow (extending to the 850 hPa level), (c) middle-depth (extending up to the 300 hPa level) and (d) deep (extending up to the 300 hPa level) ones. Contour interval 50 cyclone centres (25 for middle-depth centres).
(From Campins et al. 2006).

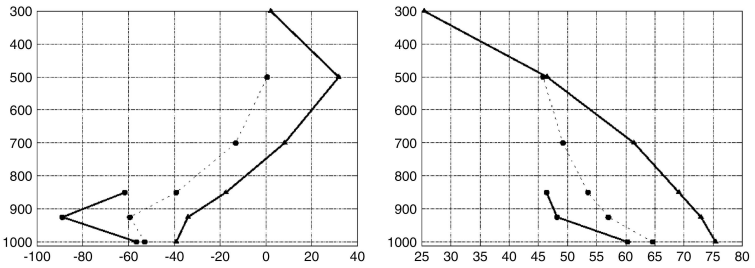

Figure 1.5: Mean vertical proles of laplacian of temperature (left) and relative humidity (right) for cyclones grouped by thickness (a negative value of ∇T indicates a warm core, a positive ∇T a cold core). Shallow cyclones are represented by solid lines with dots, middle-depth cyclones by dashed lines with dots and deep cyclones by solid lines with triangles.
(From Campins et al. 2006).

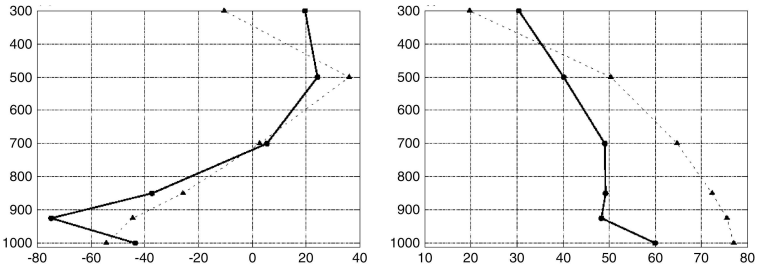

Figure 1.6: Same as Figure 1.5 for cyclones detected in Summer (solid lines with dots) and Winter (dashed lines with triangles).

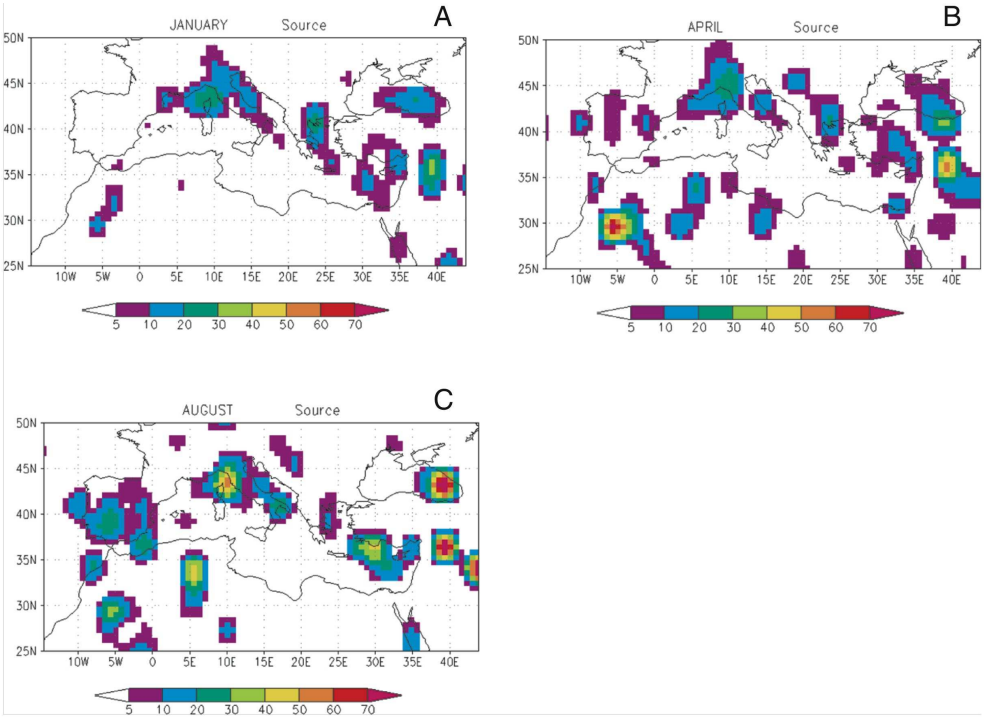

Figure 1.7: Number of cyclogenesis events detected per 2.25° x 2.25° in January (A), April (B), and August (C) from 1979 to 1996 in ECMWF re-analyses.
(From Trigo et al. 1999a).

1.2 Observational evidence of medicanes

Among the large quantity of cyclones developing over the Mediterranean Sea, reports of a number of small but exceptionally severe storms, feared by sailors for the harm produced to ships and causing damages on coastal areas, date back to ancient times. In the last centuries, after European sailors started to navigate the Atlantic Ocean, those storms have been compared to hurricanes, due to the strength of the associated winds. However it is only in the last decades of 20th century, after the advent of satellite imagery in the 80's, that the evidence of this peculiar kind of storms started to emerge in a modern meteorological sense. Due to their resemblance with hurricanes, those mesoscale Mediterranean storms in recent years have been referred to as "medicanes" (from *Medi*terranean hurri*canes*).

The first account in the scientific literature of a Mediterranean storm exhibiting some resemblance with hurricanes has been reported in Ernst and Matson (1983). The storm was detected in satellite images from January 1982 south of the Ionian Sea (Fig. 1.9). Limited observations from ships cruising nearby and temperature profiles inferred from satellita data (Fig. 1.10) provided further evidence of the eye structure and warm core of the storm. It was suggested that the dynamical evolution of the cyclone was similar to that of tropical storms, characterized by intense convection and a warm core, but it was not possible to collect conclusive evidence in support of this hypothesis at the time.

Another well documented case of a subsynoptic vortex in the Mediterranean with hurricane-like features is described in Rasmussen and Zick (1987). The vortex developed between September 27th and October 2nd 1983 in the Western Mediterranean (Fig. 1.11). The analysis of the synoptic charts reveals the presence of a cold cut-off low in the area where the vortex is formed, between Sicily and Tunisia (Fig. 1.12). The available atmospheric soundings (Fig. 1.13) are compatible with the presence of a warm core and vertical symmetry, inferred by the thickness analysis of synoptic charts (not shown): the horizontal wind is unidirectional up to 250 hPa and the wind speed is constant up to 400 hPa, as expected in a warm-core system. It is suggested in Rasmussen and Zick (1987) that the formation and sustainment of the vortex relies on convection and air-sea interaction rather than on baroclinic instability.

The event of January 1995 (Lagouvardos et al., 1999; Pytharoulis et al., 2000) is, among the historical cases studied in the literature, the one where the hurricane-like features of medicanes emerge in the clearest way. Fig. 1.14 shows the cloud structure associated with the storm, where a well defined spiral-shape structure with an eye in the middle is visible. Measurements

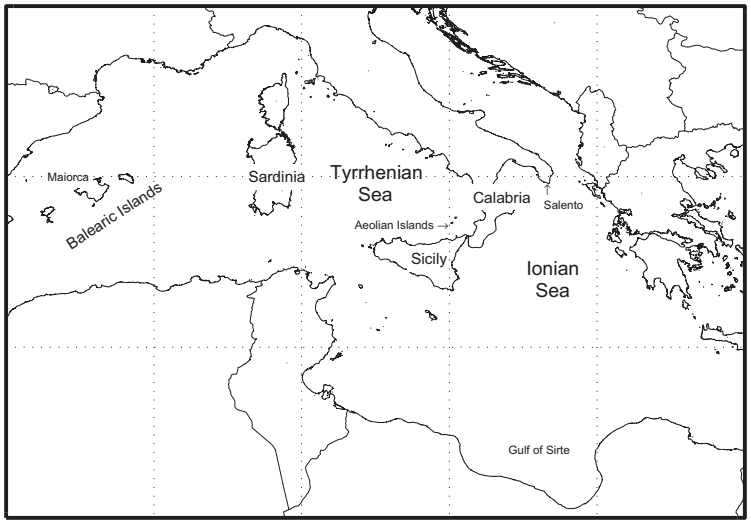

Figure 1.8: Map of central Mediterranean including geographical locations mentioned in the text.

from a German meteorologcal vessel that crossed the storm reveal the presence of a warm core (Fig. 1.15).

Another case of mesoscale hurricane-like storm documented in great detail occurred in October 1996 (Reale and Atlas, 2001). Besides the observation of the typical cloud structure and surface atmospheric fields associated with medicanes, both the vertical structure and surface fluxes have been analyzed in detail for this case. The analysis of the vertical section of the wind and temperature fields in proximity of the storm (Fig. 1.16) reveals several signatures of a tropical-like vortex, such as an almost perfect vertical symmetry, a windless air column above the center of the storm, and a positive temperature anomaly. Moreover, an extremely low vertical wind shear is observed in the region where the cyclone develops, ~ 5 m s^{-1}, whereas the typical value for baroclinic cyclones in the Mediterranean is around 25 m s^{-1} (Fig. 1.17). The authors conclude from the aforementioned evidence that, although the system is surrounded by a baroclinic environment, baroclinicity has almost no role in the development of the storm.

Finally, the medicane of September 2006 (Moscatello et al., 2008a,b; Davolio et al., 2009) over southern Italy is a very interesting case under different perspectives. With respect to all the events described above this storm is characterized by the strongest intensity, an extremely small radius, and short lifetime. Moreover, it is the only case where the medicane properties have been measured by ground weather radars, thanks to the transit

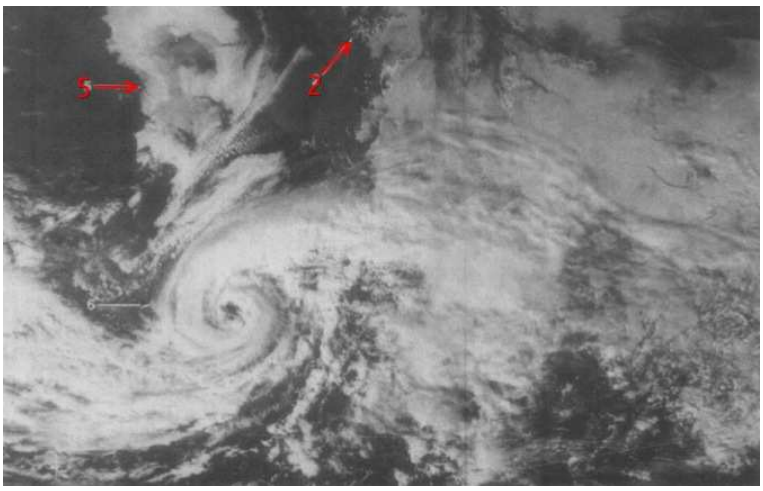

Figure 1.9: NOAA-7 visible band image of January 1982 storm (taken on 26 January 1982 at 12:36 GMT). Arrow number 5 indicates southern Apulia, arrow number 2 corresponds to the coast of Albania.
(Adapted from Ernst and Matson 1983).

of the storm over the Salento peninsula. The wind profile as measured from a weather station along the trajectory of the storm is shown in Fig. 1.18, while the sea level pressure field as reconstructed from a network of weather radars is reported in Fig. 1.19.

The main features of medicanes and the typical values of their parameters, derived from the few observed events described above, can be summarized as follows:

- A *radius* between 70 km and 200 km.
- A *lifetime* between ∼12 hours and ∼5 days.
- The *travelled distance* is between ∼700 km and ∼ 3000 km.
- A clearly defined *eye* develops in most cases, and is visible for as long as three days. In some cases the eye does not appear, while in some others it develops twice (disappearing when the storm crosses land areas).
- *Wind speed* up to ∼40 m/s.
- The most frequent *genesis regions* are the Balearic islands and the Ionian sea.

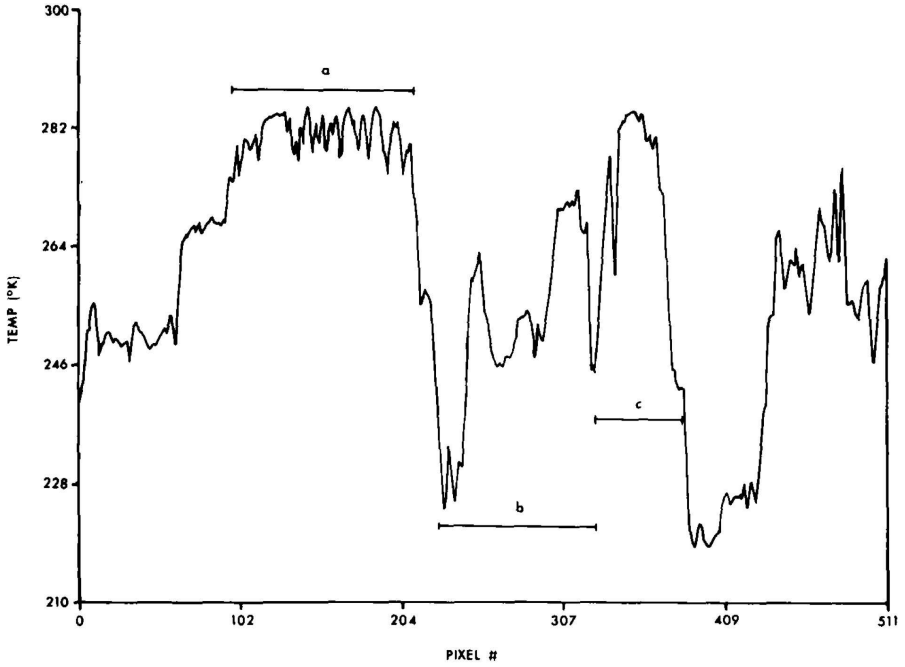

Figure 1.10: Radiometric transect of temperature (derived from thermal infrared data) on a line crossing the center of the storm. The section indicated with *c* corresponds to the eye of the storm.
(From Ernst and Matson 1983).

- Most of the medicanes occur during *Autumn*, but some have been detected also in Winter and Spring.

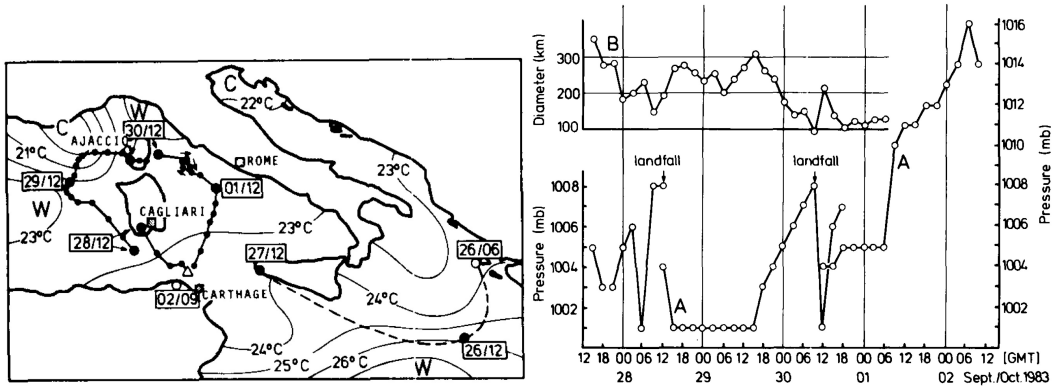

Figure 1.11: Left: track of low pressure center (solid line) and sea surface temperature reconstructed from satellite data and ship measurements (contours). Right: time evolution of the minimum pressure and diameter of the vortex.
(From Rasmussen and Zick 1987).

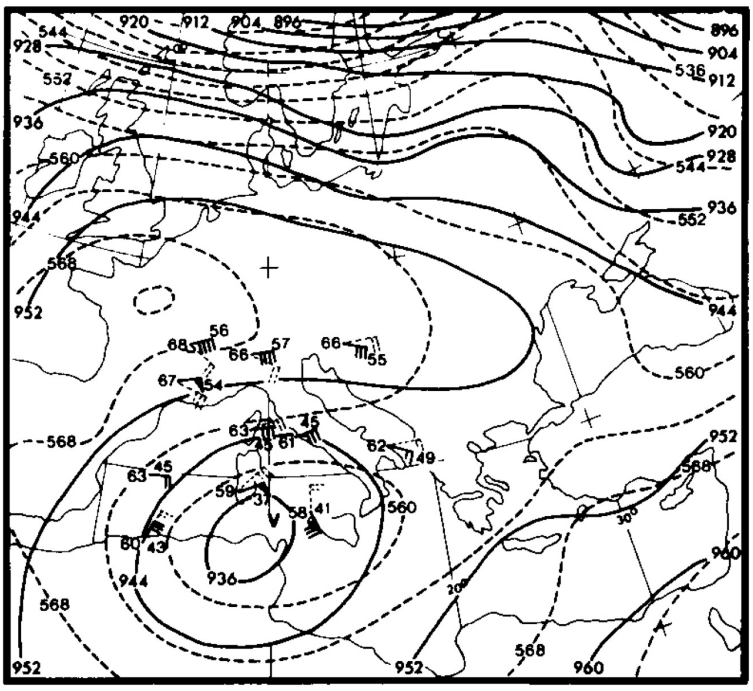

Figure 1.12: 300 mb (solid lines) and 1000/500mb thickness (dashed lines), at 00.00 GMT 28 September 1983, showing a cold cut-off low over the western Mediterranean.
(From Rasmussen and Zick 1987).

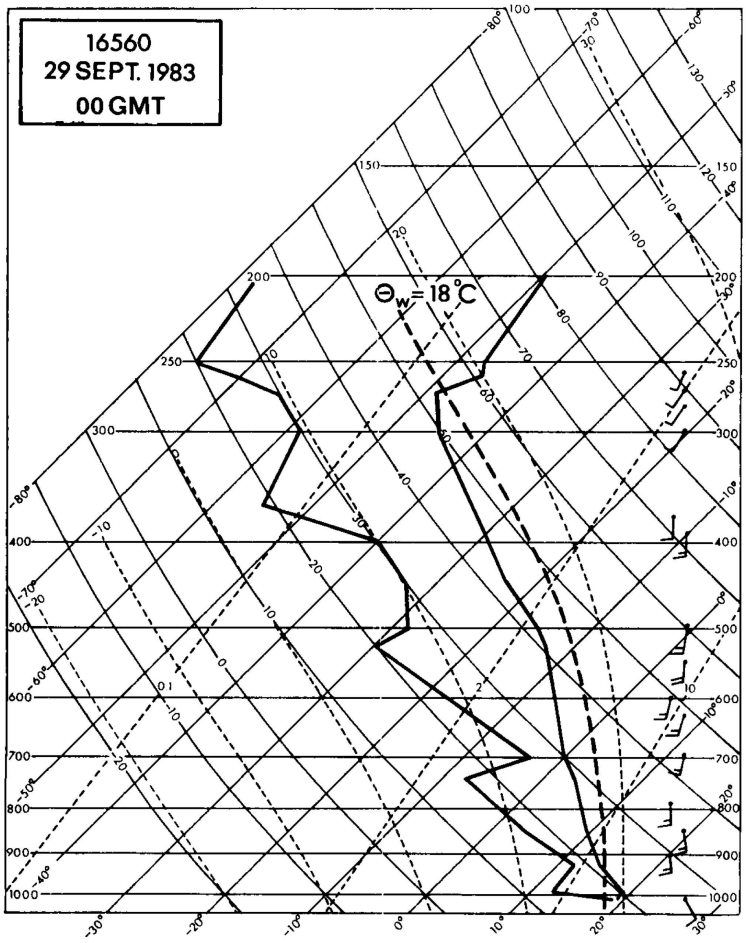

Figure 1.13: Radio sounding in Cagliari, Sardinia at 00 on Septermber 29 1983. The moist adiabatic at $\theta = 18$ C is represented by the dashed line. (From Rasmussen and Zick 1987).

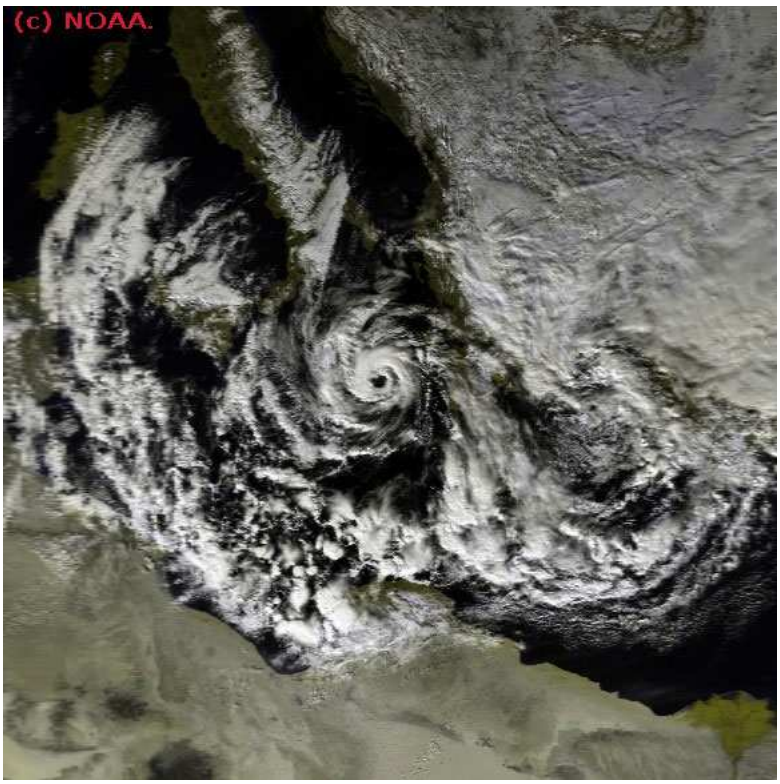

Figure 1.14: Satellite picture of January 1995 medicane.

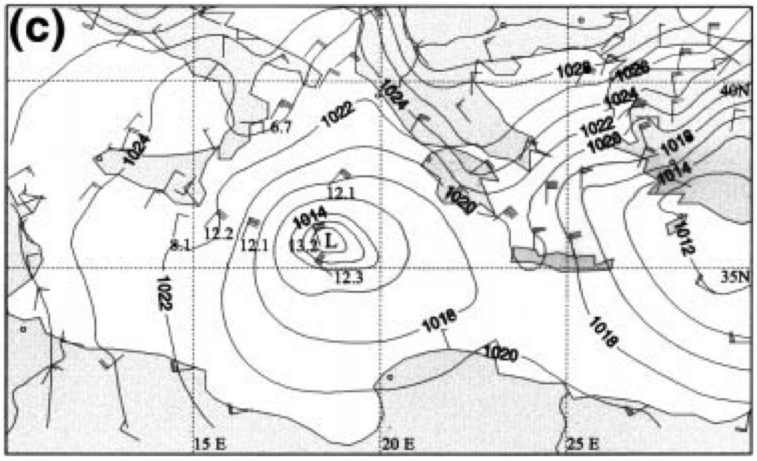

Figure 1.15: Sea level pressure (solid lines), wind (pennants) and surface air temperature values measured by ships (0600 UTC on 16 January 1995). (From Lagouvardos et al. 1999).

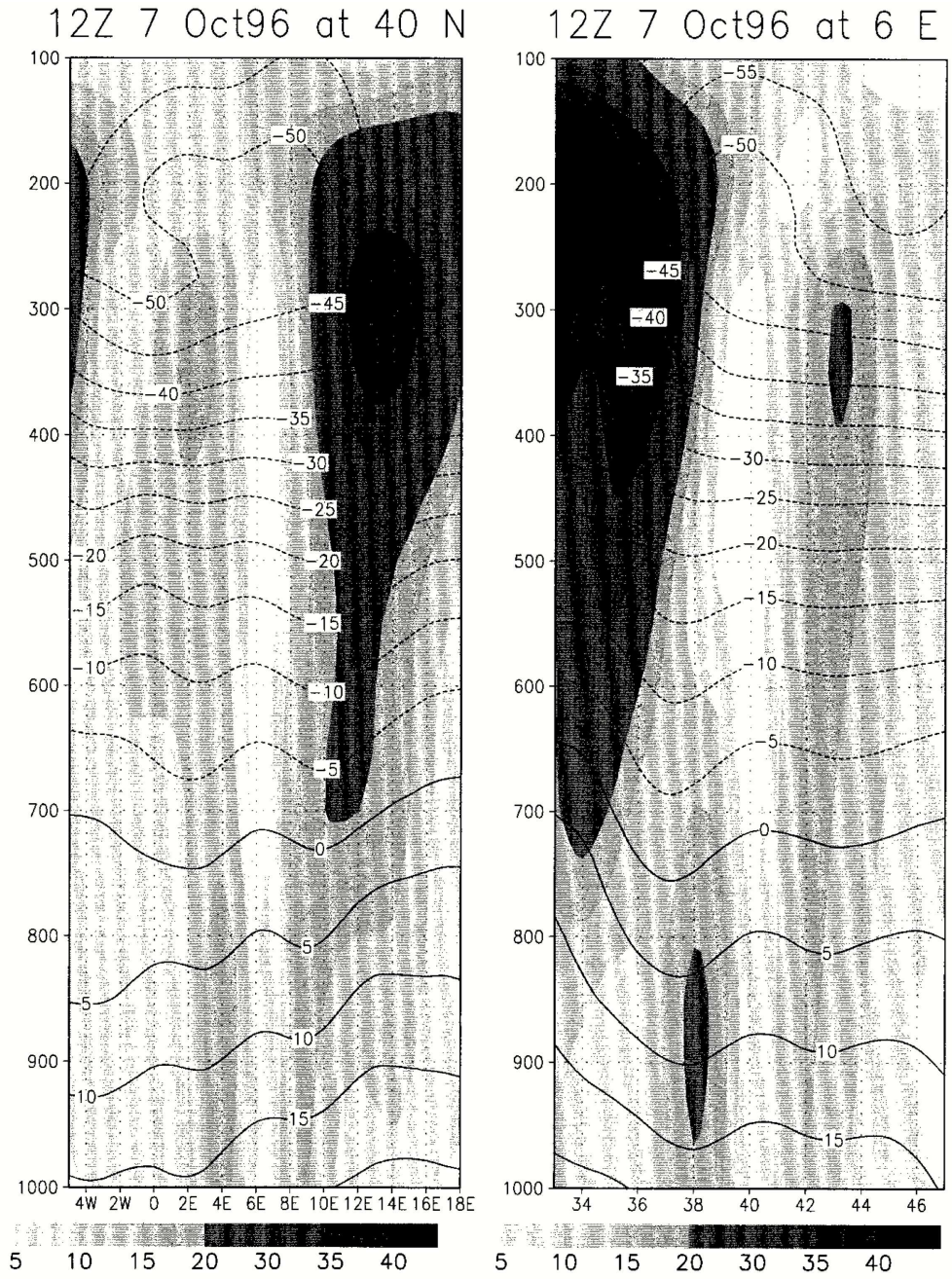

Figure 1.16: Vertical section of wind (m/s, shaded) and temperature (°C, contours) across the storm center at (left) 40N and at (right) 6E at 1200 UTC 7 Oct 1996.
(From Reale and Atlas 2001).

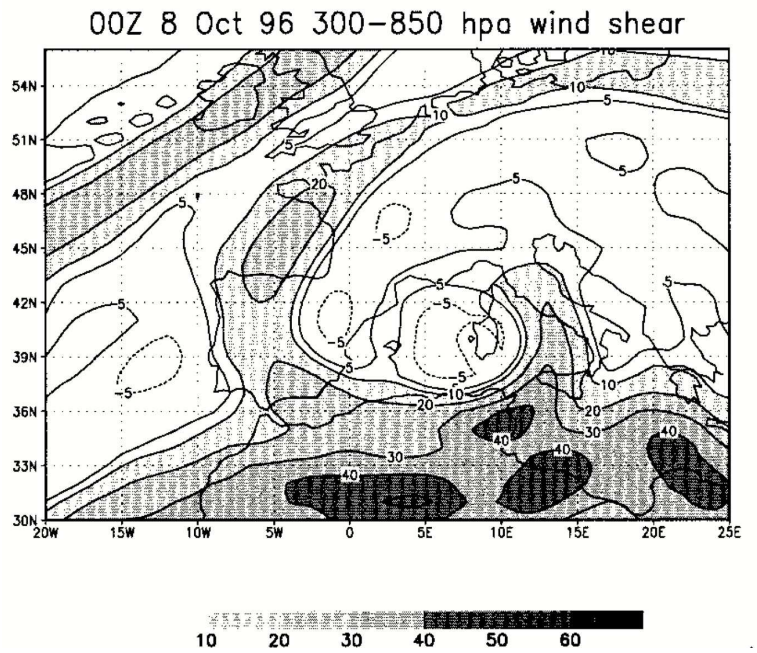

Figure 1.17: October 1996 medicane: baroclinic shear at 0000 UTC 8 Oct 1996, represented as the difference in wind speed (m/s) between the 300- and the 850-hPa levels.
(From Reale and Atlas 2001).

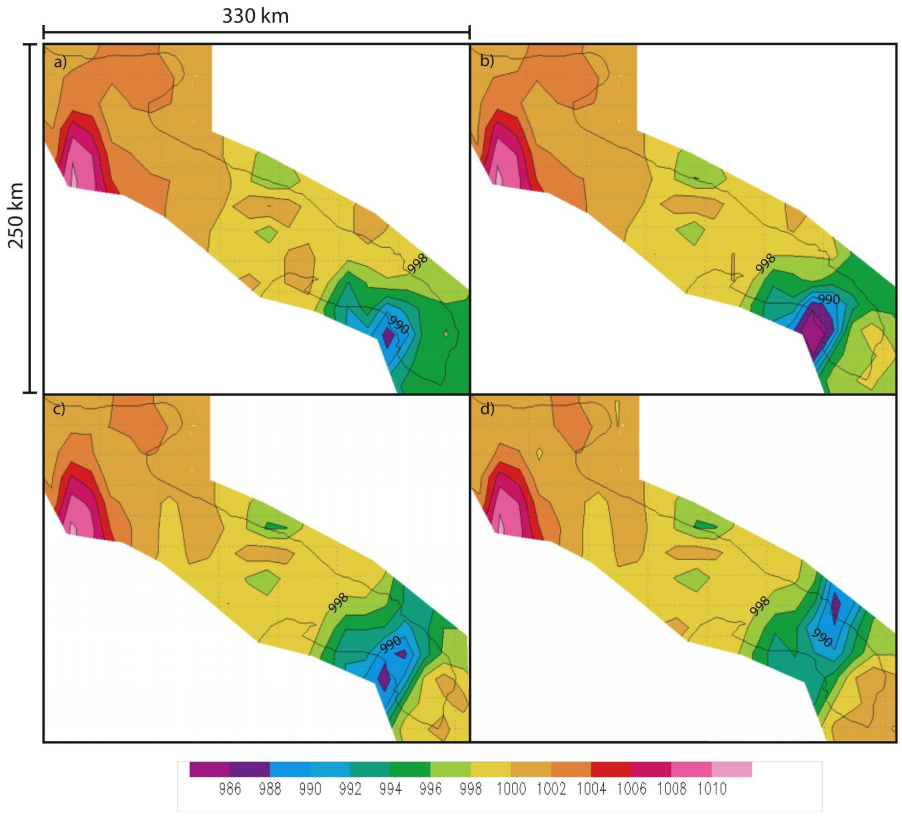

Figure 1.18: September 2006 medicane: mean sea-level pressure in hPa (colours) at (a) 0900 UTC, (b) 0915 UTC, (c) 0930 UTC, and (d) 0945 UTC, on 26 September 2006. The isobars are interpolated from the measurements of 33 surface stations distributed along the south-eastern part of Italy. The depicted region corresponds to the Salento peninsula (see Fig. 1.8).
(From Moscatello et al. 2008a).

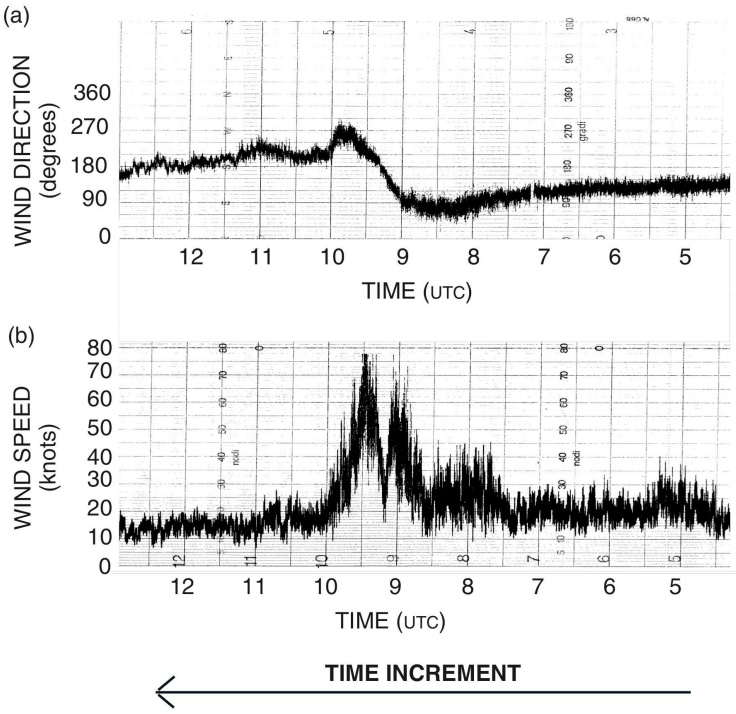

Figure 1.19: September 2006 medicane: wind speed and direction measurement from a weather station located at Galatina airport, in the lower part of Salento (see Fig. 1.8). The peak in wind speed corresponds to the eye wall. (From Moscatello et al. 2008a).

1.3 Theoretical analysis of medicanes formation and comparison with tropical cyclones

As it was discussed in Sec. 1.2, the analysis of the observational evidence reveals several similarities between medicanes and tropical cyclones, such as the shape of the cloud cover exhibiting an eye, the structure of the wind field, the vertical symmetry and the presence of a warm core.

Moreover, the study of the dynamical properties of observed medicane cases suggests that, even if they occur in baroclinic environments, the development and sustainment of medicanes relies on air-sea interaction and convection rather than on baroclinic instability.

In order to understand to what extent the analogy can be held valid, it is useful to review a number of facts about hurricanes at tropical latitudes.

1.3.1 Intensity and genesis probability of tropical cyclones

It has been shown (Emanuel, 1986, 1999; Bister and Emanuel, 2002) that the intensity of tropical cyclones is controlled by the thermodynamics of the surrounding environment, through the following relationship defining the *maximum potential wind speed*, V_p:

$$V_p^2 = \frac{C_K}{C_D}\frac{T_S - T_O}{T_O}(h_s^* - h^*)\,, \tag{1.1}$$

where C_K and C_D are the surface exchange coefficients for enthalpy and momentum, T_S and T_O are the sea surface and entropy-weighted outflow temperatures, h^* the specific enthalpy of the air near the surface, and h_s^* the enthalpy of air in contact with the ocean. As its name suggests, V_p represents a theoretical estimate of the wind speed that *can* be achieved by a tropical cyclone given specific values of the environmental factors. This upper limit is seldom reached in real-world cyclones (see Fig. 1.20). The potential wind speed represents a good estimate of the maximum intensity of hurricanes, however. Moreover, the space and time patterns of V_p give an approximate indication of the regions where favorable conditions for the formation of tropical cyclones can be encountered (Fig. 1.21).

It has been empirically determined by the analysis of a large sample of hurricanes, that tropical cyclones develop only when the sea surface temperature in the area is higher than 26 degrees C. Such a temperature can be explained as the value needed in order for the atmospheric instability to be

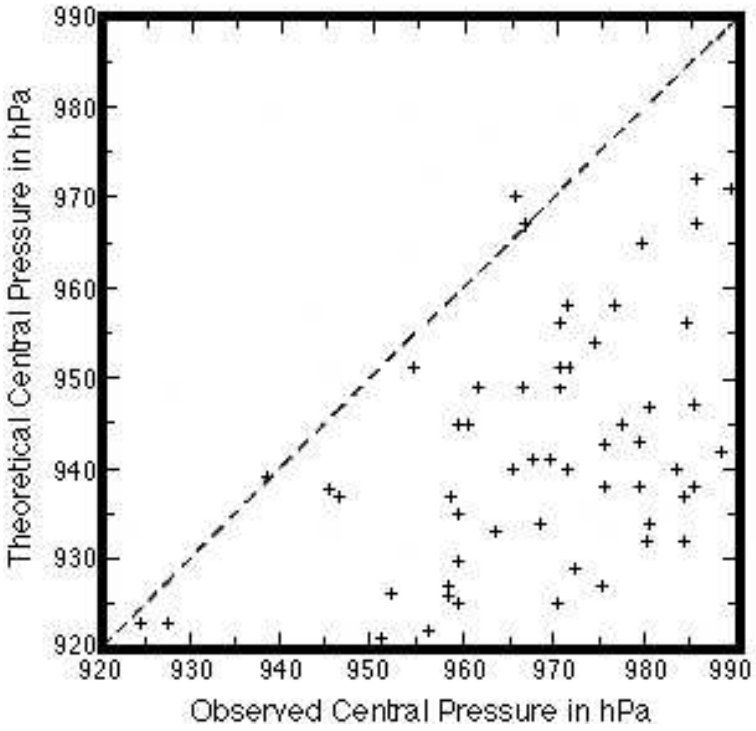

Figure 1.20: Observed minimum central pressures (abscissa) versus potential minimum pressure (ordinate) calculated using climatological SSTs and atmospheric profiles at the locations of observed Atlantic hurricanes.
(From Schade 1994).

large enough for the onset of hurricanes, taking into account the temperatures in the high troposphere (Palmen, 1948).

While a quantitative theory has been formulated for the intensity of tropical cyclones, such a formulation is lacking for the genesis process. There is however a wide agreement on the factors influencing hurricanes formation. A number of empirical indices parametrizing tropical cyclogenesis have been defined in the literature; the main advantage of those indices lies in the fact that, being based on large-scale factors, they can be used to estimate the probability of hurricanes formation when the spatial scale of the data is not high enough to properly resolve the cyclogenesis processes. The Genesis Potential Index (GPI) as introduced in Camargo et al. (2007b) and Emanuel and Nolan (2004) is defined as:

$$GPI = |10^5 \eta|^{\frac{3}{2}} \left(\frac{H}{50}\right) \left(\frac{V_p}{70}\right)^3 (1 + 0.1V_s)^{-2}\,, \tag{1.2}$$

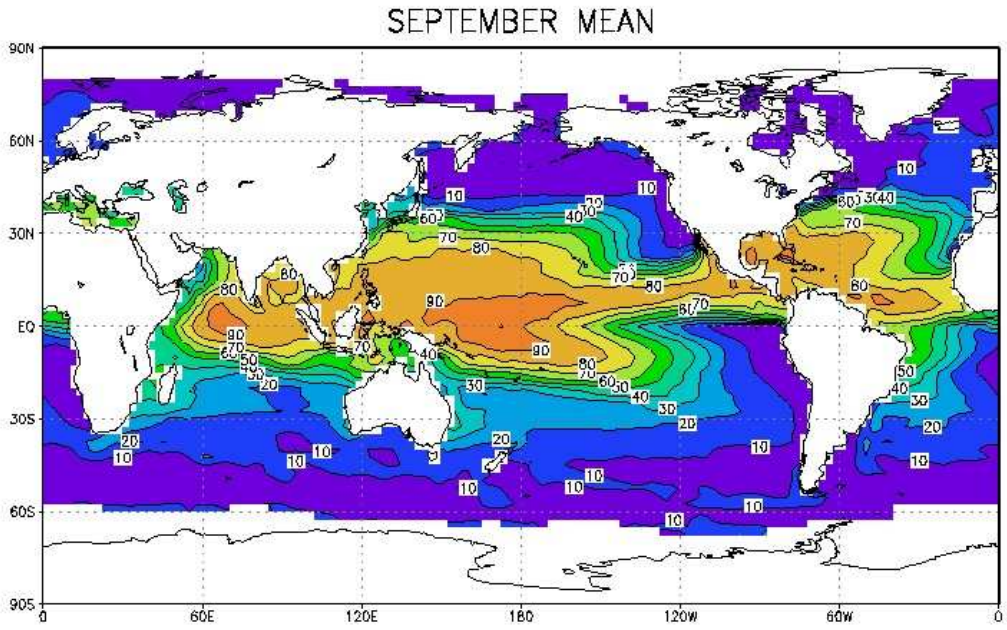

Figure 1.21: Climatological maximum potential wind speed from NCEP 1 reanalyses (Kalnay et al., 1996) for the month of September.
(From http://wind.mit.edu/ emanuel/pcmin/climo.html).

where η is the absolute vorticity in the lower troposphere (850 hPa), H is the relative humidity in the middle troposphere (600 hPa), V_p is given in Eq. (1.1), and V_s is the module of the difference of winds at 850 and 250 hPa.

As a representative illustration of the applications of genesis indices, Fig. 1.22 shows the climatological value of the GPI index for the peak months of tropical cyclones activity, compared with the locations of the observed cyclones over the 1970-2005 period.

An alternative index, based on a different combination of environmental factors, is the Yearly Genesis Parameter introduced in Gray et al. (1975) and Gray (1979), defined as:

$$YGP = |f| \left(\zeta_r \frac{f}{|f|}\right) (V_s + 3)^{-1} \times E \left(\frac{\partial \theta_e}{\partial p} + 5\right) \left(\frac{RH - 40}{30}\right) , \qquad (1.3)$$

where f is the Coriolis parameter, ζ_r the relative vorticity at 925 hPa, V_s the

vertical wind shear between 925 and 200 hPa, E the thermal energy of water above 26° C in the top 60 meters of the ocean, $\frac{\partial \theta_e}{\partial p}$ the vertical gradient of the equivalent potential temperature between 925 and 500 hPa and RH the average relative humidity between 500 and 700 hPa.

A comparison of the ability of the different indices defined above to reproduce the main statistical properties of observed hurricanes in different regions of the world has been performed in Menkes et al. (2012)[1]. In Figs. 1.23 and 1.24, are reported respectively the mean number of hurricanes per year, the seasonal cycle and the inter-annual variability, as predicted by the different indices.

The global performance of the different indices is comparable, but there are significative differences at the regional scale. Even if they reproduce qualitatively the main features of cyclogenesis, a number of flaws (such as the overestimation of simulated cyclogenesis in unfavourable seasons, or the poor correlation on interannual timescales) prevents all the indices to be used as a robust quantitative tool to estimate cyclogenesis, specially at the regional scale. The reason for the aforementioned discrepancies is due to the role of stochastic processes that control cyclogenesis, that are not represented in the indices.

1.3.2 The case of medicanes

Several medicanes have been observed during Winter, when the temperature of Mediterranean Sea water is well below the 26° C threshold for tropical cyclogenesis, with measured SST values of around 15° C. Usually V_p is too small in such conditions to support tropical cyclones. However, as it was mentioned in Sec. 1.2 above, the formation of medicanes is often associated to the presence of a synoptic cold low in the middle troposphere. It was suggested in Emanuel (2005) that the presence of a cold cut-off low can play a key role in increasing the atmosphere instability, thus allowing vortices with dynamical features similar to those of hurricanes to develop even over waters with temperatures such as those found in Winter in the Mediterranean Sea.

This mechanism can be formulated theoretically as follows. Approximating the atmospheric lapse rate as moist adiabatic, and assuming that the advection of the cold low in the upper layers triggers convection so that the lapse rate is unchanged, the maximum potential wind speed in presence of a

[1]The two further indices analyzed are variations of the GPI and YGP indices described above. The TCS index is obtained by substituting in the GPI the factor V_p with a factor depending on the SST, whereas the CYGP index is obtained by the YGP replacing the thermal factor with a parametrization of convective precipitation.

cold cut-off low, V_{cl}, is given by:

$$V_{cl}^2 = V_p^2 - \frac{C_K}{C_D}(\phi'_{cl} - \phi'_s)\,, \tag{1.4}$$

where ϕ'_{cl} and ϕ'_s represent the departures of the geopotential from the background state respectively in the cold low and at the surface, and V_p is has been defined in Eq. (1.1). As an example, in the case of January 1995 medicane, plugging the values inferred from the reanalyses (see Fig. 1.25) in Eq. (1.4), the additional contribution to the potential intensity due from the presence of the cold low amounts to about 40 m/s.

Given the small number of observed medicane events, it is hard to give a robust assessment of the factors influencing the genesis of medicanes. In Tous and Romero (2013) a number of factors associated to the genesis probability of tropical cyclones, as discussed above, have been analyzed for twelve medicane cases. It was found that during the twelve medicane events considered in the study, the Genesis Potential Index for tropical cyclones takes values significantly higher than those found during the intense "ordinary" Mediterranean cyclones.

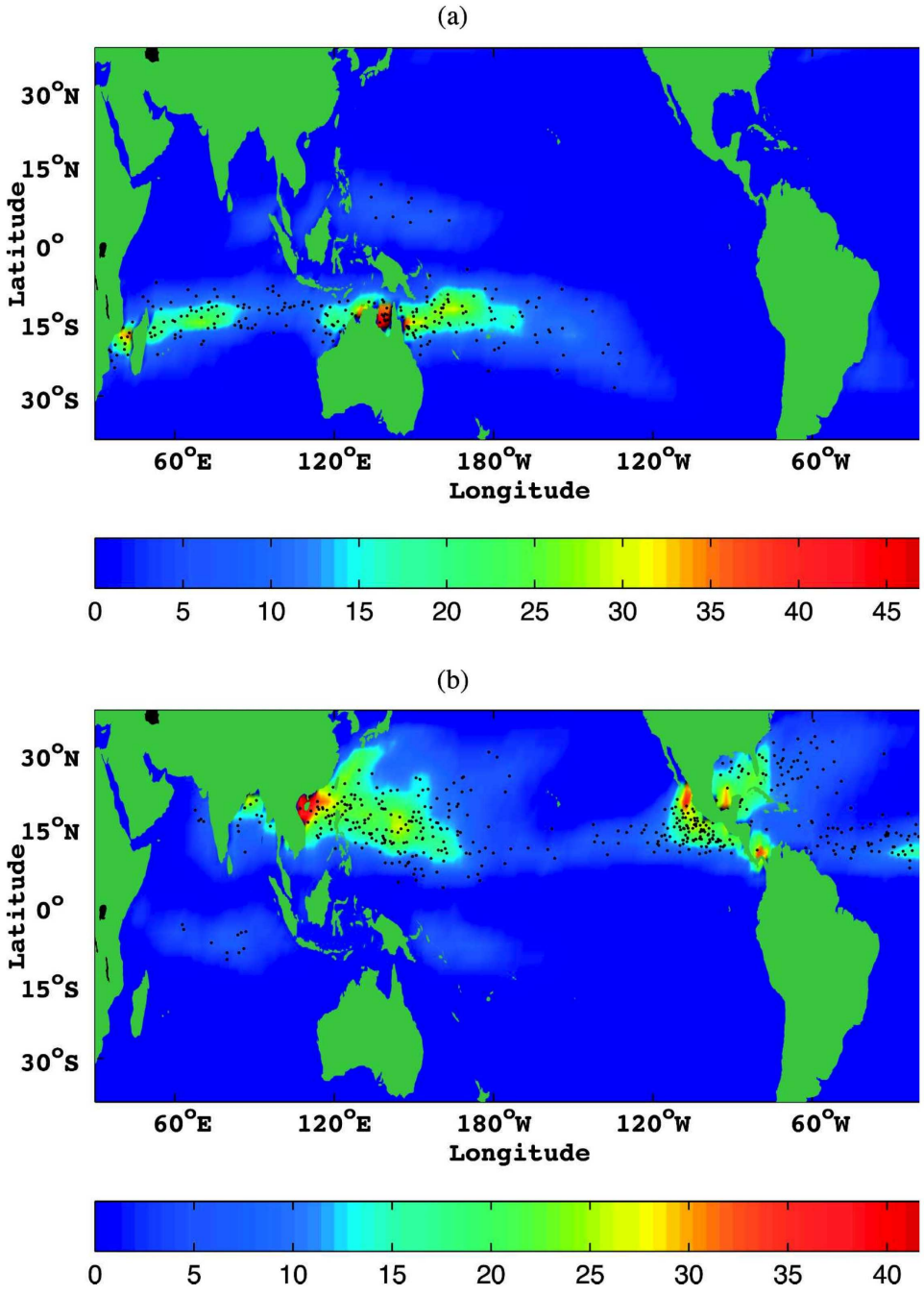

Figure 1.22: Genesis potential index climatology in (a) February and (b) September. The black dots show individual genesis events over the period from (a) 1970 to 2004 and (b) 1970 to 2005.
(From Camargo et al. 2007a).

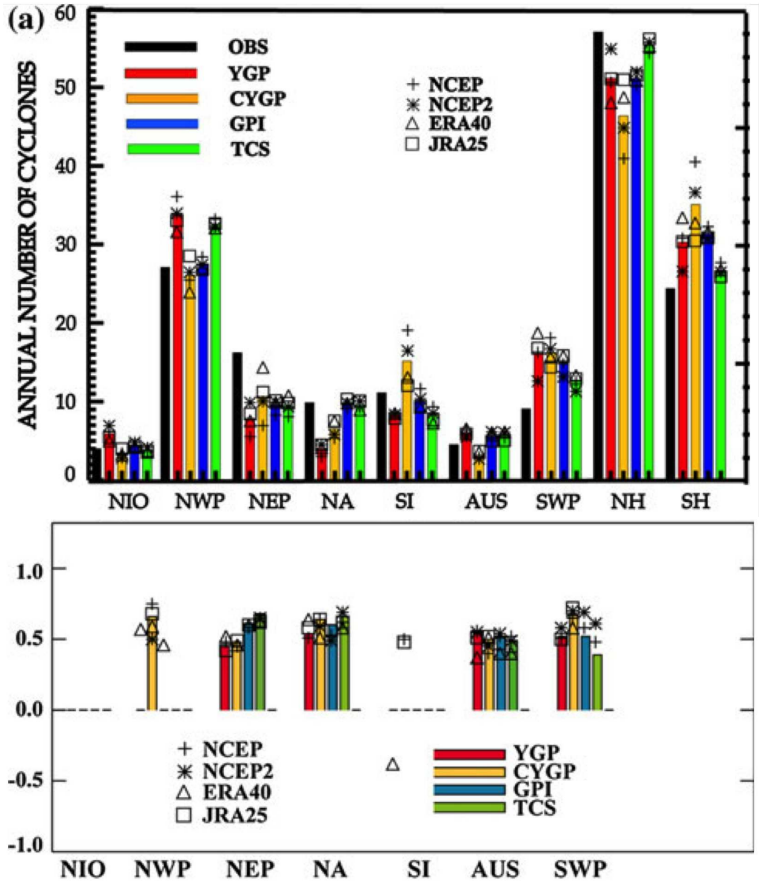

Figure 1.23: Histograms of annual mean number of cyclones (top) and correlation of box-averaged interannual observed cyclogenesis and indices (bottom), in different regions. In addition, total numbers for the northern hemisphere (NH) and southern hemisphere (SH) are shown for all indexes. The colourbars represent the numbers predicted for the different indices in reanalyses data, and each reanalysis result is added on each colourbar as indicated.
(From Menkes et al. 2012).

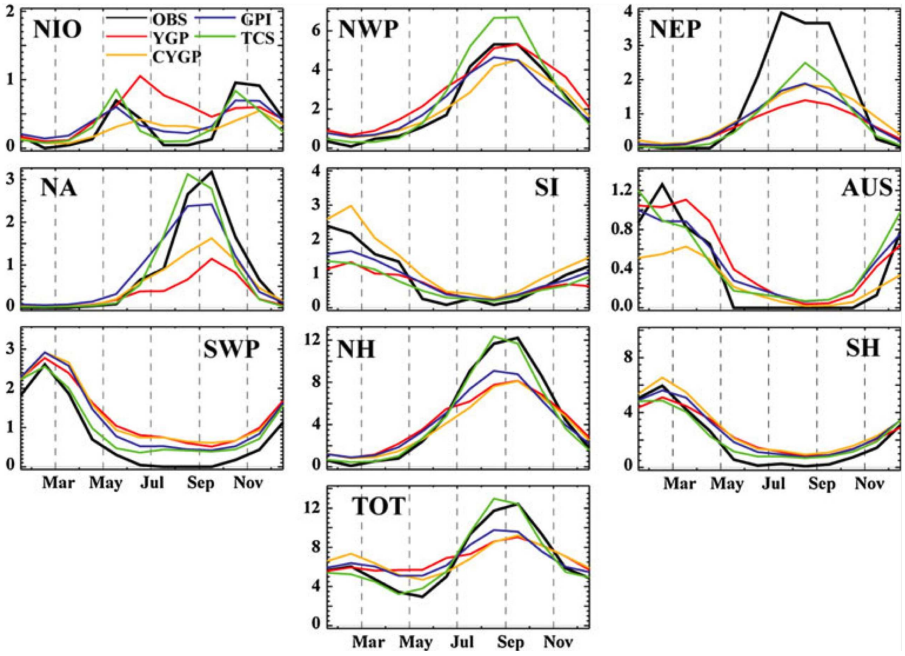

Figure 1.24: Seasonal variation of observed cyclogenesis compared with that predicted by genesis indices calculated in reanalyses, in different regions. (From Menkes et al. 2012).

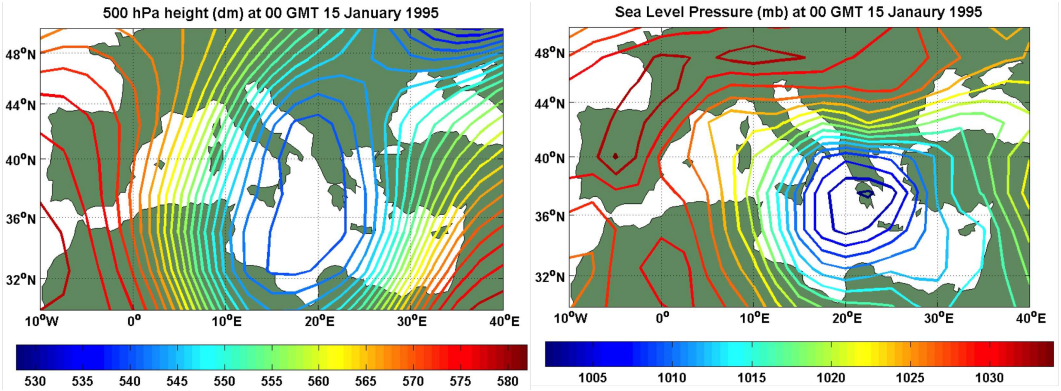

Figure 1.25: 500 hPa geopotential height (dm, left) and sea level pressure (hPa, right), at 00:00GMT on 15 January 1995. Analyses from NCAR/NCEP 1 reanalysis data (Kalnay et al., 1996).
(From Emanuel 2005).

1.4 Modelling and climatological studies on medicanes

Several event-based modelling studies have addressed different aspects of the dynamics and formation of medicanes.

In Fita et al. (2007) seven historical medicanes were simulated in a non-hydrostatic axisymmetric model, confirming the warm-core and vertically symmetric structure of the storms and highlighting the important role played in the development of medicanes by the moisture content of the environment and by the vertical profile of the atmosphere, including the presence of a cold low in the upper levels. In Miglietta et al. (2011b) sensitivity tests have been performed for the September 2006 medicane, varying the sea surface temperature. It was found that a decrease of 3 degrees in the sea surface temperature would have inhibited the formation of the medicane. The role of surface heat fluxes on the trajectory and intensification of medicanes has been investigated in Tous et al. (2012).

The attempts to give a systematic assessment of the frequency and statistical properties of medicanes, on the other hand, have faced so far a number of difficulties. Medicanes are considered rare phenomena, due to the small number of observations. Apart from the medicanes studied in the literature, mentioned in Sec 1.2 above, only a few more cases are known. A list of possible medicanes events, detected in satellite images from various sources is maintained on the website `http://www.uib.es/depart/dfs/meteorologia/METEOROLOGIA/MEDICANES`, and amounts to a few tens of events over a 25 years period (1982-2007).

Objective detection in reanalyses datasets, a procedure routinely used for synoptic scale cyclones, is not applicable in the case of medicanes. The spatial scale of medicanes, that can be as low as less than one hundred kilometers, is a challenge even for the most modern reanalysis products. As an example, in Fig. 1.26 is reported the comparison of the pressure field in the 50 km resolution MERRA reanalyses (Rienecker et al., 2011) and 25 km ECMWF operational analysis for two of the historical medicanes described in Sec. 1.2. For the medicane with the smaller radius, the isolines corresponding to the mesoscale cyclonic system are not visible in the MERRA sea level pressure field. On the other hand, products with a resolution high enough to resolve the characteristc spatial scale of medicanes, such as operational analyses or high resolution reanalyses, typically are not available in a homogeneous way for time periods long enough to allow a robust assessment of the statistical properties of rare phenomena such as medicanes.

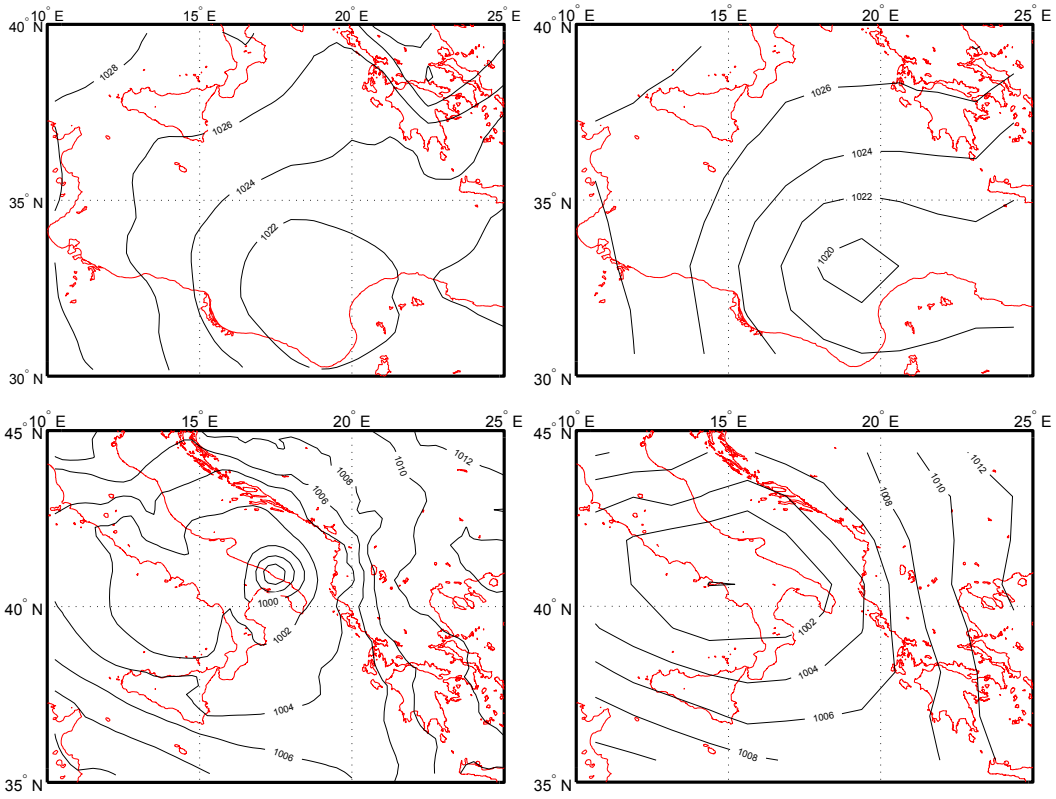

Figure 1.26: Sea level pressure field for January 1995 (top, Jan 16 at 18 UTC) and September 2006 (bottom, Sept 26 at 12 UTC) medicanes in ECMWF operational analysis (left) and NASA-MERRA reanalyses (right).

Satellite-based searches of medicanes also met some difficulties. An exhaustive analysis of satellite imagery in the period 1982-2005 has been performed in Tous and Romero (2013). Around four hundred cyclonic events over 20 years have been classified as possible medicane cases. After the application of strict selection conditions related to the symmetry of the cloud shape and the presence of an eye-like structure, however, only 6 events are classified as medicanes. Some of the cases classified as medicanes in the literature from direct observations do not meet strictly the selection criteria.

This issue reflects, on one hand, the fact that the Mediterranean region is one of the most active cyclogenetic regions in the world, with a climatological average of a few thousands cyclones per year (see Sec. 1.1). Moreover, it is not easy to draw a clear-cut demarcation line between medicanes and "ordinary" Mediterranean cyclones, since medicanes are often baroclinic disturbances in the first phases of their life, that undergo a transition to

tropical-like dynamics whenever a number of favorable environmental factors are present.

Summarizing, the systematic assessment of the statistical properties of medicanes has been hindered so far by several factors:

- the scarcity of direct observations;
- the time range or the spatial resolution of reanalyses-based products is not large enough;
- satellite images alone do not allow to define a sufficient number of criteria to discriminate medicanes from baroclinic cyclones.

Chapter 2

Methods and experimental setup

In this Chapter the main technical aspects behind the results discussed in the Thesis are described. In Sec. 2.1 an overview of the setup of the regional model used for the downscaling is presented. In Sec 2.2 we discuss the details of the detection procedure adopted.

2.1 The dynamical downscaling approach

The dynamical downscaling with a limited area model of atmospheric fields produced by global reanalyses or global circulation models has been proven to be a successful strategy in the study of several regional scale atmospheric processes (Feser et al., 2011), including storminess and cyclones statistics in different regions of the world. The details of the specific model configuration used in the current work are described in the rest of this Section.

The downscaling is performed in the CCLM atmospheric limited area model (Rockel et al., 2008), the climate version of the COSMO weather model. The model features non-hydrostatic equations and has 32 σ vertical levels. The σ levels are pressure-based, terrain-following coordinates[1], as depicted in Fig. 2.1.

We employ two different horizontal resolutions. The "low" resolution simulations use a 0.22° (∼25 km) grid on a domain of 176 x 106 grid points, (see Fig. 2.2). They are driven by initial and boundary conditions derived respectively from NCEP/NCAR 1 reanalyses (Kalnay et al., 1996) for the study

[1]The mathematical definition linking the pressure levels p_0 and the σ levels is given by $\sigma = (p_0 - p_T)/(p_0^s - p_T)$, where p_T is the pressure at the top of the model and p_0^s is the pressure at the surface.

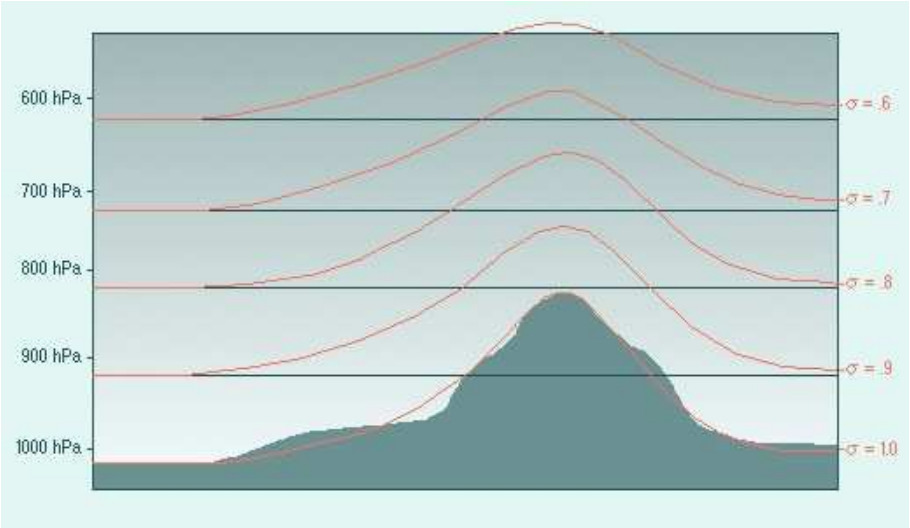

Figure 2.1: An example of σ vertical coordinates.

of past medicanes, and from the ECHAM5 global atmospheric model for the study of medicanes in future climate scenarios. We use the NCEP/NCAR reanalyses, because of their longer period of coverage. Although higher resolution reanalysis products are available, these cover shorter time periods.

The domain covers the whole Mediterranean Sea and the main mountain ranges around it. The grid spacing of 0.22° is the finest that can be used for a single nested downscaling of global grid fields, since the model performance decreases for downscaling factors higher than 10.

The "high" resolution simulations are run at 0.09° (∼10 km) using the fields from the low resolution simulations as boundary conditions, on a domain of 386 x 206 grid points (see Fig. 2.2). Other than the grid resolution, the two model versions do not differ.

For the historical medicanes cases we study in detail the results at both resolutions, and with spectral nudging switched on and off. The aim of spectral nudging (von Storch et al., 2000) is to force the large scale components of the atmospheric fields to stay close to the driving data, while the small scale components are left free to evolve in the regional model. Spectral nudging is applied on the wind field components, for scales larger than 4 NCEP/NCAR grid points, corresponding to 1000 km. Moreover, nudging is applied only on vertical levels above 850 hPa, while wind in the lower layers is left free to interact with the local orography[2]. In both the low and high resolution

[2]The same implementation of spectral nudging has been successfully adopted in similar studies (Feser and von Storch, 2008; Zahn and von Storch, 2008). We performed test simu-

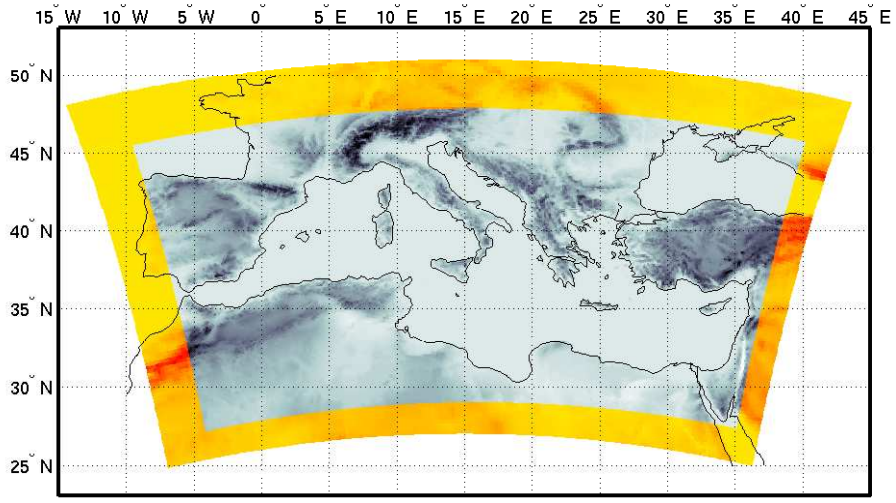

Figure 2.2: Domains of the coarse (yellow) and high (grey) resolution simulations.

simulations the values of the atmospheric fields used as a reference in spectral nudging are the ones provided by the NCEP/NCAR reanalysis.

In the long-term integrations the 25 km resolution was used only as an intermediate technical step for the downscaling, while all the analyses were performed using the spectrally nudged high resolution simulation.

2.2 Objective criteria for the detection of medicanes

2.2.1 An objective detection algorithm

In order to detect automatically occurrence of medicanes in the long-term model output, we developed an *ad-hoc* detection algorithm. The algorithm consists of the following steps:

1. for every hourly model output all the sea level pressure minima with pressure gradient greater than ΔP over 3 grid points are registered.

2. A clustering algorithm assigning to the same track the pressure minima within a radius of 100 km at two consecutive time-steps is applied.

lations with different implementations of spectral nudging, but no significant improvement was observed.

3. Only the tracks respecting the further conditions are saved:

   - The track has to be composed of at least 6 points;
   - At most half of the points can correspond to land-covered model grid points.

4. The following selection criteria on the geometry of the track are applied:

   - the two most distant positions in the track must be separated by at least 200km;
   - a change in the propagation direction at consecutive time-steps greater than $\pi/3$ is allowed for at most half of the point in the track.

5. The following selection criteria related to the storm dynamics are applied

   - fulfillment of symmetry and warm core criteria[3] ($B < 10$ m, -$V_T^{L(U)} > 0$ and -$V_T^{L(D)} > 0$) in a circle of radius R_{wc} for more than 10% of the track or at least 6 hours;
   - the wind speed averaged in a circle of radius 50 km around the pressure minimum has to be higher than a threshold value V_{av} for more than 10% of the track or at least 6 hours;
   - the wind speed at 850 hPa has to be higher than that at 300 hPa (averaged in a circle of radius 50 km around the pressure minimum);
   - the maximum wind speed in a circle of radius 50 km around the pressure minimum has to be higher than a threshold value V_{max} for a time longer than t_{vmax}.

2.2.2 Validation and choice of the thresholds values

No perfect detection algorithm exists; the choice of the detection parameters should thus be aimed at finding the optimal balance between false detections and missed detections of actual storms. This task is extremely challenging for the case of medicanes, given the "grey zone" of storms for which it is hard to assess from satellite observations whether they are medicanes or baroclinic cyclones, as it was discussed in Sec. 1.4.

[3]These criteria are described in detail in App. A.

We proceeded as follows. At first, in order to assess the impact of the different thresholds present in the algorithm on the number of the detected medicanes, a sensitivity test has been performed, varying systematically the values of the relevant parameters and applying the algorithm on the test period 1995-1999[4]. The result is reported in Table 2.1: we find that the dependence on most of the parameters is mild, except for V_{max}, for which an increase of 1 m/s leads to a significant reduction in the number of events.

The algorithm thresholds have been then calibrated in an empirical way, using for validation purposes the limited observational evidence available, including the visual inspection of Meteosat images for the events not reported previously in the literature or in the database mentioned in Sec. 1.4. For the 1995-1999 test period, the optimal choice of parameters, minimizing both false positives and missing detection, would be: ΔP=20 Pa, R_{wc}= 100 km, V_{av}= 18 m/s, V_{max} = 30 m/s, t_{vmax} =4 h. With these values, as it can be read from Table 2.1, eight medicanes are detected. Out of those eight events, three events are historical medicanes discussed in Chapter 3 and three events are present in the database on the website `http://www.uib.es/depart/dfs/meteorologia/METEOROLOGIA/MEDICANES`. For the two remaining events, structures in the cloud cover compatible with those of medicanes are found in satellite images (see Fig. 2.3). However, with those values some of the historical events studied in the literature are not detected; on the other hand setting V_{max} = 29 m/s those historical medicanes are correctly detected. If the V_{max} threshold is lowered to 29 m/s, no conclusive statement on the three additional events detected in the test period is possible from the analysis of corresponding satellite data. The parameters are thus fixed as follows:

- ΔP=20 Pa
- R_{wc}= 100 km
- V_{av}= 18 m/s
- V_{max} = 29 m/s
- t_{vmax} =4 h

In order to assess how robust the long-term statistical properties of medicanes are with respect to the choice of the value of V_{max}, we report for comparison in App. B the results of the analysis over six decades with V_{max}=30 m/s.

[4]The result for the same sensitivity test on a different period is reported for comparison in Tab B.1.

Table 2.1: Number of medicanes detected in a five years period (1995-1999), varying the algorithm parameters as indicated.

R_{wc}= 100 km, t_{vmax}= 6h

V_{av} \ V_{max}	25	26	27	28	29	30
14	21	18	14	10	9	7
15	21	18	14	10	9	7
16	21	18	14	10	9	7
17	21	18	14	10	9	7
18	21	18	14	10	9	7

R_{wc}= 100 km, t_{vmax}= 4h

V_{av} \ V_{max}	25	26	27	28	29	30
14	22	20	16	12	11	8
15	22	20	16	12	11	8
16	22	20	16	12	11	8
17	22	20	16	12	11	8
18	21	20	16	12	11	8

R_{wc}= 150 km, t_{vmax}= 6h

V_{av} \ V_{max}	25	26	27	28	29	30
14	21	18	14	10	9	7
15	21	18	14	10	9	7
16	21	18	14	10	9	7
17	21	18	14	10	9	7
18	21	18	14	10	9	7

R_{wc}= 200 km, t_{vmax}= 6h

V_{av} \ V_{max}	25	26	27	28	29	30
14	21	18	14	10	9	7
15	21	18	14	10	9	7
16	21	18	14	10	9	7
17	21	18	14	10	9	7
18	21	18	14	10	9	7

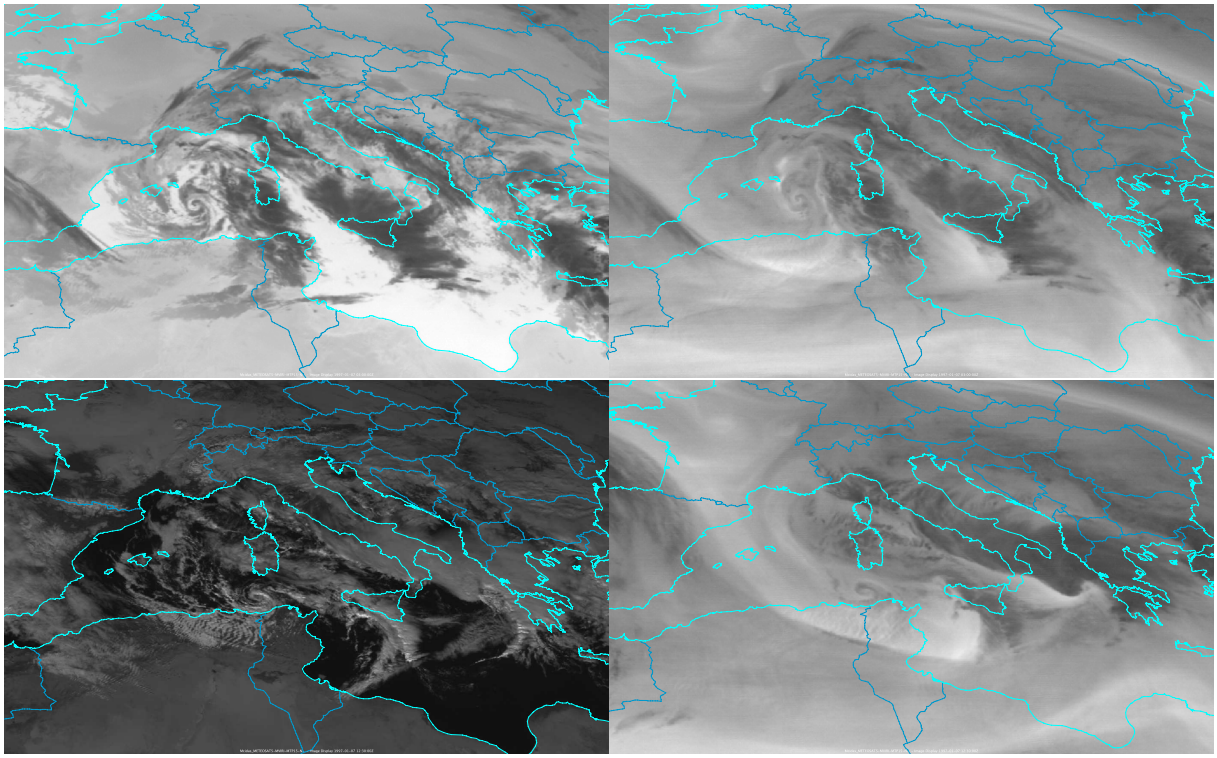

Figure 2.3: METEOSAT7 satellite pictures of a possible medicane in January 1997. Top: infrared channel (left) and water vapor channel (right) on January 07 at 03 UTC. Bottom: visible channel (left) and water vapor channel (right) on January 07 at 12:30 UTC.

Even if the total number of detected medicanes is lower, the main climatological features such as the geographical distribution and seasonal cycle are comparable.

Chapter 3

Analysis of selected historical cases

Papers on which the Chapter is based:
L. Cavicchia and H. von Storch, "The simulation of medicanes in a high-resolution regional climate model", Clim. Dyn., DOI: 10.1007/s00382-011-1220-0

3.1 Selected test cases

We selected four different test cases of historical medicanes documented in the literature to be reproduced in the model simulations. The main characteristics of these cases are reported in Table 3.1.

The choice of these particular events is motivated by the fact that they span a wide range of the typical phenomenological parameters of medicanes,

Table 3.1: Main features of the selected test cases.

Event (YYMM)	Radius	Lifetime	Distance	Eye	Genesis region
9501	150 km	3 days	∼1000 km	yes	Ionian
0609	70 km	1 day	∼500 km	yes	Ionian
9609	150 km	1.5 days	∼2000 km	yes	Balearic
9610	200 km	5 days	∼3000 km	yes (twice)	Balearic

including both typical and extreme values. They are all from recent decades, when observational coverage by satellites was good, and when operational analysis, as done by ECMWF, has good skill also on sub-synoptic scales (Simmons, 2006), so that we have adequate data available for assessing the quality of our simulations. Indeed, we use the following observational data for validation:

1. the NOAA "SeaWinds" product at 6-hour time resolution (Zhang et al., 2006). SeaWinds contains gridded, high resolution ocean surface vector winds and wind stresses on a global 0.25° grid for the period 9 July 1987 - present. The wind speeds are generated by blending observations from instruments mounted on multiple satellites. The accuracy of scatterometer-based wind retrievals is very good for winds up to 20 m/s, while it is highly diminished for higher winds (see e.g. Ebuchi et al. 2002 and Ricciardulli and Wentz 2011)

2. Mean sea level pressure fields from ECMWF operational analysis data, at 0.25° grid resolution.

In order to assess the added value of the dynamical downscaling approach, we also compare the model results with a state-of-the-art reanalysis product, the NASA's MERRA reanalyses (Rienecker et al., 2011), featuring a 0.5 degrees horizontal resolution and 72 vertical levels.

For each of the test cases under study, two ensembles of four simulations each are produced. The ensemble members differ in their start dates, which are separated by intervals of 24 hours. In order to ensure that the simulation results do not depend on initital conditions ("climate mode"), the starting date preceeds the formation of the medicane by about two weeks.

In the first ensemble the evolution of atmospheric variables is forced only through initial and lateral boundary conditions. The members of this ensemble are labelled as "YYMMnn1lo/hi"-"YYMMnn4lo/hi". In the second ensemble there is an additional forcing in the interior of the domain, derived from spectrally nudging wind above 850 hPa. The simulations of this ensemble will be referred to as "YYMMsn1lo/hi"-"YYMMsn4lo/hi".

3.2 Results: surface patterns

In this Section we discuss the model's ability in reproducing the sea level wind and pressure patterns associated with the medicane test cases under study. We begin by discussing only the 2nd realization of the spectrally nudged simulations, i.e, YYMMsn2lo and YYMMsn2hi, in low and high resolution.

The rationale for doing so will become clear in Subsection 3.2.5, when we demonstrate that the spectrally nudged simulations are very close to each other, while the non-nudged cases show some divergence.

3.2.1 15 January 1995 medicane

The January 1995 case (Lagouvardos et al., 1999; Pytharoulis et al., 2000) is probably the most well known medicane, due to the striking similarities between its cloud pattern visible in satellite imagery and that of tropical cyclones.

Synoptic analysis shows a larger scale low moving from the central Mediterranean, northwards of Libya, towards the Ionian coast of Greece in the two days preceding the medicane formation. Ships crossing the Ionian sea measured winds up to 30 m/s associated with the precursor low. By the night of January 15, as the disturbance had reached the coast of Greece, satellite pictures reveal a structure presenting typical hurricane features, that originated in the center of the large scale low and remained approximately stationary as the parent low kept moving eastwards towards the Aegean Sea and Turkey. During the following afternoon the medicane started to move southwestwards and kept travelling towards the coast of Libya during the following 48 hours; during that time observations by ships cruising the Mediterranean reported strong winds, heavy precipitation and positive temperature anomalies in the vicinity of the center of the storm. After making landfall in the Gulf of Sirte the storm dissipated in the next few hours.

Fig. 3.1 shows a comparison of mean sea level pressure on Jan 16 at 00 UTC in ECMWF analysis and in 25 km resolution and 10 km resolution simulations, together with the medicane track as reconstructed respectively in the low resolution and high resolution simulations. In both cases, with the pressure thresholds used, the storm disappears before reaching the Libyan coast. In the low resolution simulation, the part of the track where the storm was moving northwards (marked with red squares) corresponds to the precursor low in the core of which the medicane developed; the second part (blue dots) corresponds to the life cycle of the medicane itself, after it had split from the parent low. In the high resolution simulation the first part of the track, corresponding to the synoptic low, does not appear due to the higher threshold on the pressure gradient. There is a good agreement on the position of the pressure minimum in the three charts. The pressure value at the minimum is 1014 hPa in the ECMWF diagram, 1010 hPa in the MERRA reanalysis, 1016 in the coarse resolution, and 1000 hPa in the high resolution run.

Fig. 3.2 shows the same fields of Fig. 3.1 eighteen hours later, on Jan 16

at 18 UTC. The difference in the positions of the central pressure minima in the two simulations has increased to a few hundred kilometers. The minimum pressure value is 1022 hPa in the ECMWF analysis, 1022 hPa in the MERRA reanalysis, 1022 hPa in the coarse resolution simulation, and 1006 hPa in the high resolution simulation.

Fig 3.3 shows a snapshot of the wind speed in NOAA measurement and model simulations on Jan 16 at 06 UTC. In the satellite measurement the observed wind speed reaches a maximum value of approximately 25 m/s. In the low resolution simulation this value is underestimated by about 30%. In the high resolution simulation, on the other hand, the maximum wind speed agrees with the measured value; moreover, the fine structure of the wind pattern is visible, showing a windless air column above the pressure minimum, corresponding to the cyclone's eye.

3.2.2 26 September 2006 medicane

The September 2006 medicane (Davolio et al., 2009; Moscatello et al., 2008a,b; Miglietta et al., 2011a; Conte et al., 2011) has the smallest radius and shortest lifetime among all known cases. On the other hand, it is the case among the four considered in this work with the strongest wind speed and lowest pressure minimum recorded. It is therefore expected to be a representative test for the model's ability to reproduce smaller medicanes.

The synoptic and observational analysis (Moscatello et al., 2008a) shows a cyclonic disturbance moving across the strait of Sicily and travelling northwards over the Ionian Sea along the coast of Calabria on September 25th. The numerical analysis in Moscatello et al. (2008b) shows that the cyclone was formed the previous night in the lee of the Atlas mountains. During the night of September 26 a strong deepening is observed and, as the cyclone reached the western coast of Salento the following morning, it had evolved to a medicane. The storm then crossed the Salento peninsula, where extreme wind speeds were measured by ground stations and considerable damage was produced. It finally traveled northwestwards over the Adriatic Sea and the afternoon of the same day it made landfall on northern Apulia, where it rapidly dissipated.

Mean sea level pressure on Sept 26 at 12 UTC in ECMWF operational analysis and model simulations, along with the medicane track as reconstructed in the low resolution and high resolution simulations, is shown in Fig. 3.4. The difference in the position of the minimum between the two model simulations reflects the different storm velocities. The pressure value at the minimum is 996 hPa in the ECMWF analysis, coarse resolution simulation, and high resolution simulation. The medicane is not visible in the

MERRA reanalysis.

Wind speed in satellite observation and model simulations on Sept 26 at 12 UTC is shown in Fig. 3.5. The maximum wind speed of 22 m/s reported in the satellite measurements is reproduced with good accuracy in the low resolution simulation, while it is underestimated by about 10-15 percent in the high resolution simulation. It has to be noticed however that, due to the different storm propagation speeds in the two simulations, the fixed-time snapshots might not represent the same phase of the evolution of the actual storm. The simulated wind speed for a location along the track corresponding to that of the low resolution simulation shows indeed a comparable wind speed.

3.2.3 12 September 1996 medicane

The case of September 1996 (Homar et al., 2003) is an example of a typical medicane developing in the Balearic region, one of the areas where medicanes formation is more often encountered.

The system developed between the night and early morning of September 12 off the Valencian coast, where heavy rainfall was reported; an eye structure was already fully developed at the end of this first stage. During the morning of September 12 the storm started to move quickly eastwards crossing Majorca and later in the day the southern extremity of Sardinia. During the following night, the medicane made landfall on the coast of southern Italy and it dissipated.

Fig. 3.6 shows mean sea level pressure charts on Sept 12 at 06 UTC from ECMWF analysis and model simulations, and the medicane track as reconstructed in the 25 km and 10 km resolution simulations. While the track in the coarse resolution simulation ends as the storm reaches Sardinia, in the high resolution simulation the storm is tracked until it reaches the Italian coast. The mesoscale low structure corresponding to the medicane is not visible in the ECMWF and MERRA pressure fields. However analysis of satellite pictures confirms the presence of the storm (see Figs. 1a and 2a in Luque et al. 2007). The value of the pressure minimum is 996 hPa in the coarse resolution, and 990 hPa in the high resolution run.

Fig. 3.7 shows the pressure distributions 24 hours later, after the storm has crossed southern Sardinia. At this stage of the storm evolution, closed isobars are not visible either in the ECMWF and MERRA pressure charts or in the coarse resolution simulation. The medicane is still clearly visible in the high resolution simulation, with a pressure minimum of 1000 hPa.

Fig 3.8 shows the wind speed in NOAA observations and model simulations on Sept 12 at 12 UTC. Both the satellite measurement and the coarse

resolution simulation show a maximum wind value of about 20 m/s, while in the high resolution simulation this value reaches 24 m/s. The characteristic pattern associated with the storm eye is clearly visible in the high resolution simulation.

3.2.4 7 October 1996 medicane

The 6 October 1996 case (Reale and Atlas, 2001) has one of the longest lifetime and largest radius among the known medicanes. During October 6th the medicane developed north of Algeria and deepened while it was moving between the Balearic islands and Sardinia. There are no surface observations available for this part of the track, but satellite pictures show a well defined eye-like structure. On the night of October 8, while the storm was crossing southern Sardinia, it weakened and the eye structure was lost. On the following morning however, as the cyclone traveled eastwards over the Thyrrhenian Sea, it deepened and a smaller eye developed again. Several surface reports about 100 km off the center of the storm indicate winds of 25 m/s. On October 9, as the medicane was travelling north of Sicily, severe damage caused by extreme winds was reported in the Aeolian islands. The medicane started to dissipate while moving southeastwards across Calabria.

Fig. 3.9 shows the mean sea level pressure distribution on Oct 07 at 18 UTC in ECMWF analysis and in the coarse and high resolution simulations, and the medicane track as reconstructed in model simulations. With the thresholds used the storm is tracked only until it approaches the western part of Sicily. There is a good agreement on the position of the pressure minimum in the different charts. The minimum pressure value is of 1004 hPa in the operational analysis, 1000 hPa in the MERRA reanalysis, 1006 hPa in the 25 km resolution simulation, and 998 hPa in the 10 km resolution simulation.

Fig. 3.10 shows the pressure distributions 18 hours later, after the storm has crossed Sardinia. The difference in the positions of the central pressure minima has grown to a few hundred kilometers. The minimum pressure value is 1003 hPa in the ECMWF analysis, 1002 hPa in the MERRA reanalysis, 1005 hPa in the low resolution simulation, and 1003 hPa in the high resolution simulation.

Fig 3.11 shows the wind speed in satellite measurement and model simulations on Oct 7 at 18 UTC. There is an evident mismatch between observations and simulations in the wind speed values of the background pattern. This is probably due to the presence of a Mistral outburst, corresponding to the dark orange (24 m/s) contour in the upper part of the plot, that is not fully reproduced in the model. Outside of this area however, the presence of the

medicane is clearly visible, with simulated winds in the range of 20 m/s. In the NOAA wind field the medicane location corresponds to the cusp in the bottom of the 27 m/s contour.

3.2.5 The role of spectral nudging

In order to assess the robustness of the results shown above, and the effectiveness of the downscaling procedure applied in the study of medicanes long-term statistics, some evidence is required to support the assumption that the ability of the model to reproduce the medicanes does not depend on the specific initial conditions.

Table 3.2 shows the spread of minimum central pressure among the different ensemble members, both nudged and non-nudged, for all the four test cases. The largest spread is observed for the 9501 medicane. Figs. 3.12 and 3.13 show the reconstructed track for the full set of ensemble simulations (with spectral nudging switched on and off, at both 25 km and 10 km resolutions) for the 9501 medicane. As the pictures show, in the low-resolution non-nudged simulations (Fig. 3.12) the medicane development diverges substantially among the ensemble members. In the nudged simulations on the other hand, the medicane evolution is similar in all the simulations. Although the evolution of the storm among the high-resolution simulations (Fig. 3.13) is more similar than in the low-resolution results, the ensemble variability in the spectrally nudged simulations is markedly smaller than in the case without employing the large scale constraint.

In the 0609 case, even if the spread in minimum central pressure among ensemble members reported in Table 3.2 is limited, in two of the four high-resolution non-nudged simulations (not shown) the simulated storms are weaker in comparison with the corresponding nudged simulation - exhibiting in particular smaller pressure gradients. As a result, the tracking algorithm fails to capture the medicane formation and evolution in those ensemble members. Among the nudged simulations, the storm life cycle is correctly reproduced and tracked in all the ensemble members.

In the two remaining cases, the medicane formation and life cycle is tracked in all the simulations, at both low and high resolution. The inter-ensemble variability is bigger in the non-nudged ensembles.

In order to stress the importance of nudging in enhancing the model ability to reliably reproduce the formation and life cycle of medicanes irrespective of initialisation, we show in Fig. 3.14 the tracks of the simulated storm in the nudged high resolution ensemble simulations for the 0609, 9609 and 9610 medicanes.

The results discussed above show how spectral nudging is a crucial feature

Table 3.2: Minumum central pressure spread between ensemble members (as described in Sec. 3.1). The labels #1-#4 indicate the ensemble member; the labels on the first line refer to the different simulations, with the following meaning: "lo nn" refers to low-resolution non-nudged simulations, "lo sn" refers to low-resolution nudged simulations, "hi nn" refers to high-resolution non-nudged simulations, and "hi sn" refers to high-resolution nudged simulations.

		lo nn	lo sn	hi nn	hi sn
9501	#1	1010 hPa	1016 hPa	1002 hPa	998 hPa
(Jan. 16 at 00 UTC)	#2	1010 hPa	1016 hPa	998 hPa	998 hPa
	#3	1016 hPa	1018 hPa	996 hPa	1004 hPa
	#4	1018 hPa	1018 hPa	1000 hPa	1006 hPa
0609	#1	996 hPa	996 hPa	996 hPa	996 hPa
(Sept. 26 at 12 UTC)	#2	998 hPa	996 hPa	996 hPa	996 hPa
	#3	996 hPa	996 hPa	998 hPa	994 hPa
	#4	998 hPa	994 hPa	998 hPa	996 hPa
9609	#1	994 hPa	996 hPa	992 hPa	992 hPa
(Sept. 12 at 06 UTC)	#2	994 hPa	996 hPa	990 hPa	990 hPa
	#3	994 hPa	996 hPa	990 hPa	990 hPa
	#4	996 hPa	996 hPa	992 hPa	994 hPa
9610	#1	1006 hPa	1008 hPa	1002 hPa	1002 hPa
(Oct. 07 at 18 UTC)	#2	1006 hPa	1006 hPa	1002 hPa	998 hPa
	#3	1006 hPa	1008 hPa	1004 hPa	1002 hPa
	#4	1006 hPa	1006 hPa	1006 hPa	1000 hPa

to ensure that the effect of the nonlinear chaotic regional dynamics generated by the regional model do not drive the system to a different large scale state with respect to the one described by the external fields - so that the synoptic conditions triggering the medicane development may not be present.

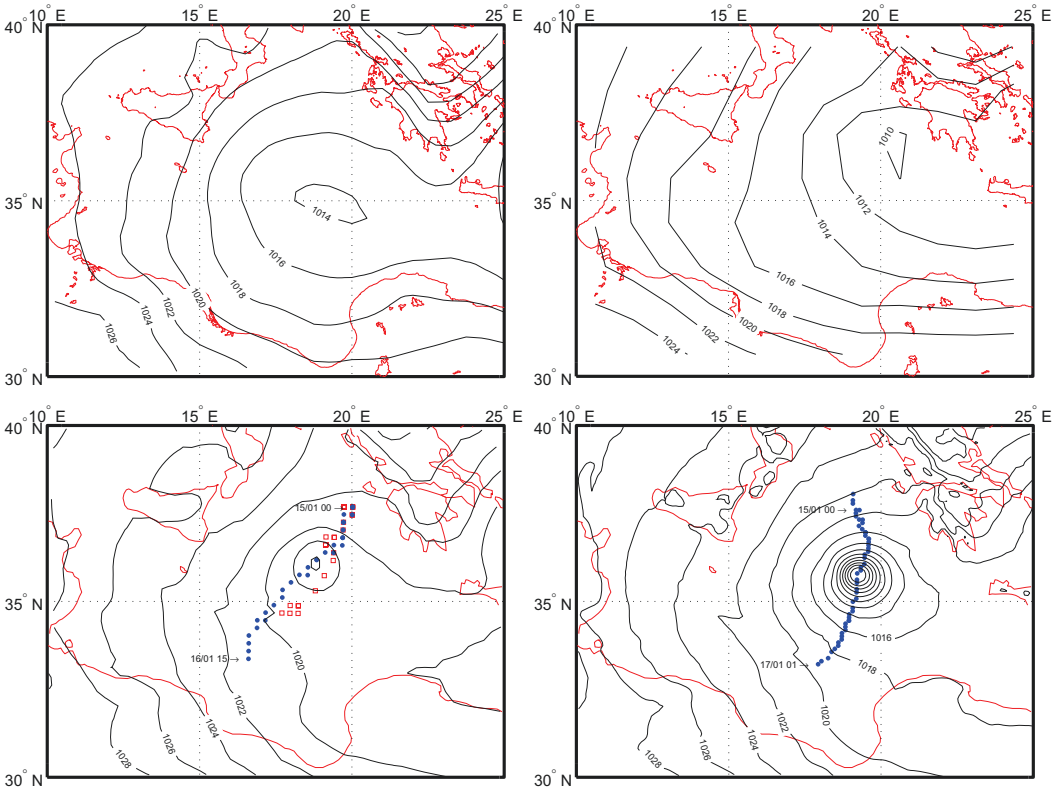

Figure 3.1: Mean sea level pressure fields on Jan 16 at 00 UTC in the ECMWF analysis (top left), MERRA reanalysis (top right), and in the low resolution 9501sn2lo (bottom left) and high resolution 9501sn2hi (bottom right) simulations. Contour lines are plotted at 2 hPa intervals. The label 9501sn2lo/hi refers to the case of January 1995, and the 2nd simulation with a spectrally nudged formulation with low/high grid resolution. "dd/mm hh" labels indicate date and hour associated with the corresponding position. In the second panel two different markers have been used for a better visualization: red empty squares correspond to the part of the track where the storm was moving northwards, blue filled circles to the part where it was moving southwards.

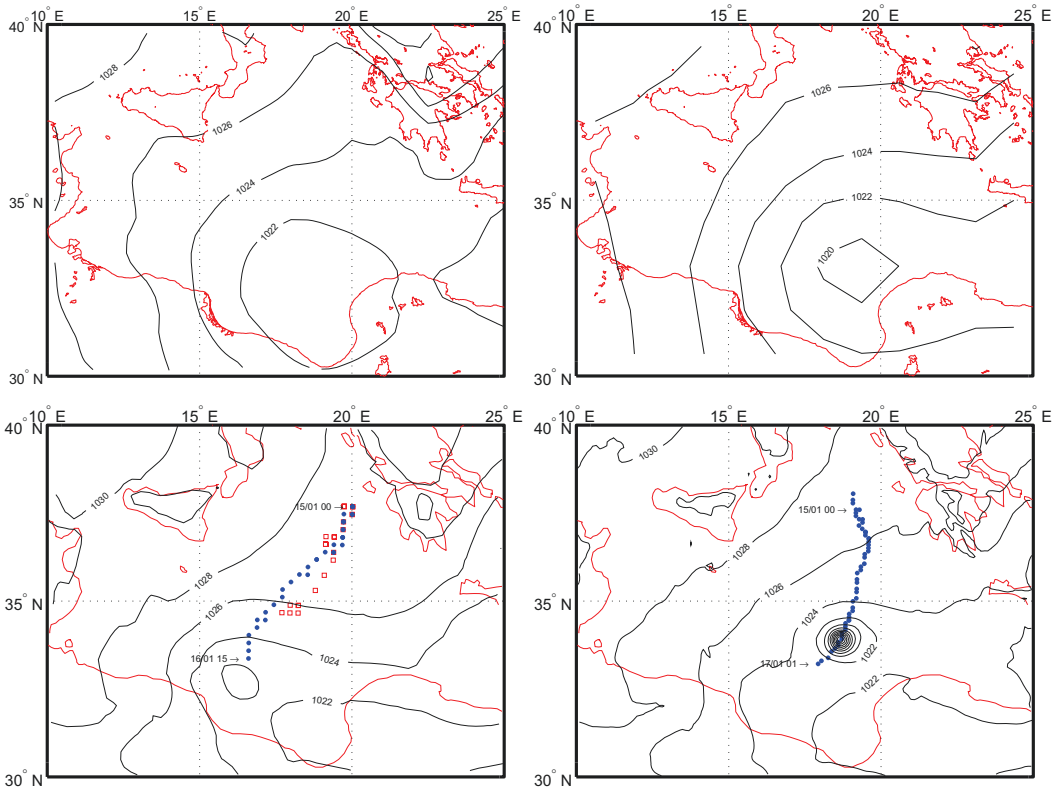

Figure 3.2: The same as Fig. 3.1 on Jan 16 at 18 UTC.

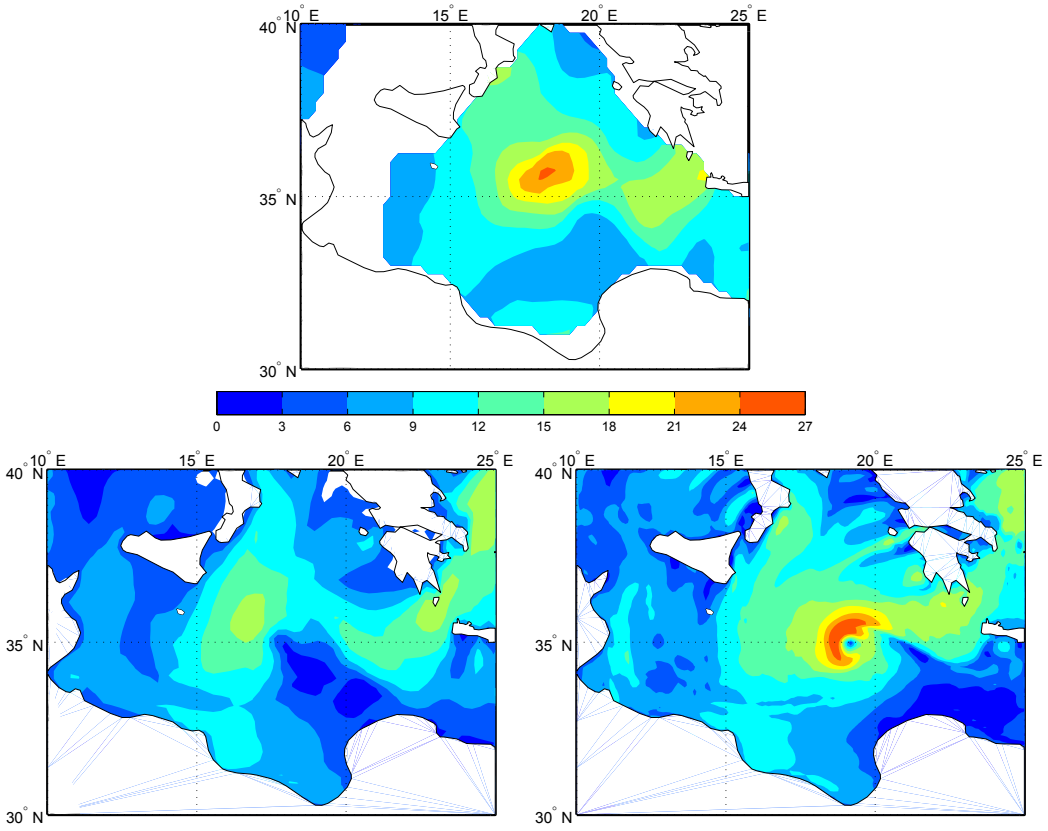

Figure 3.3: Measured wind speed field on Jan 16 at 18 UTC as reconstructed in the NOAA "Blended Sea Winds" (top). 10-meters wind speed in 9501sn2lo (bottom left) and 9501sn2hi (bottom right) simulations. Every contour represents a 3 m/s increment. The label 9501sn2lo/hi refers to the case of January 1995, and the 2nd simulation with a spectrally nudged formulation with low/high grid resolution.

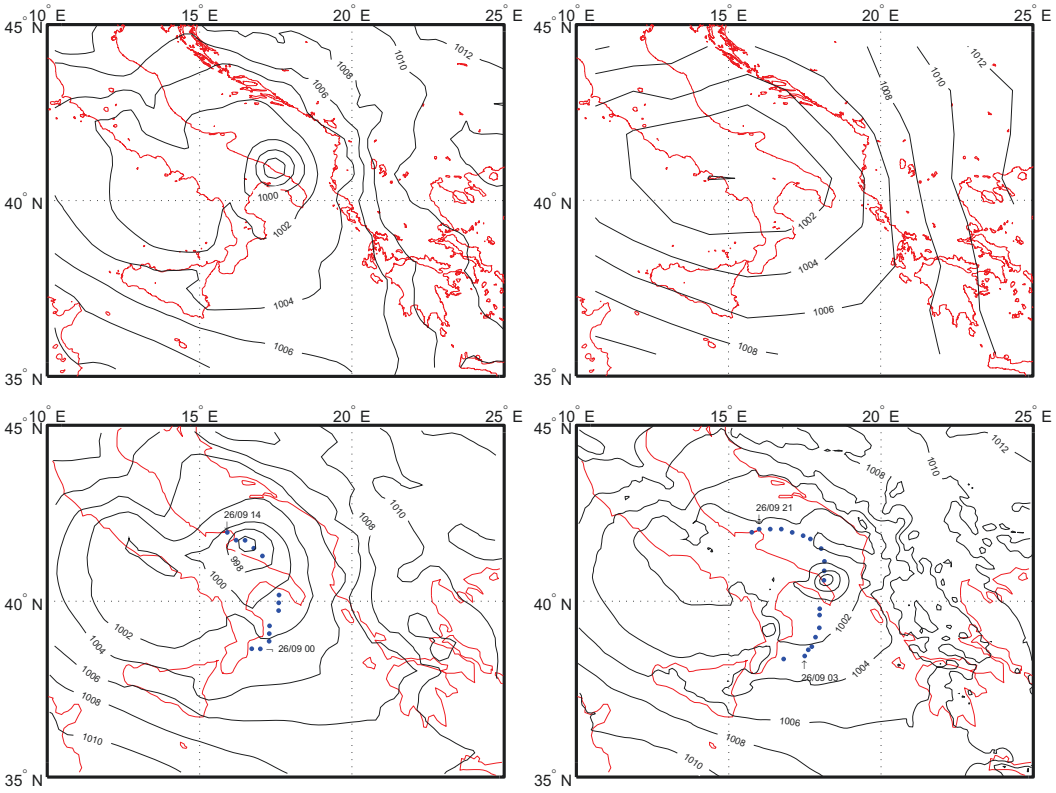

Figure 3.4: Mean sea level pressure fields on Sept 26 at 12 UTC in the ECMWF analysis (top left), MERRA reanalysis (top right), 0609sn2lo (bottom left) and 0609sn2hi (bottom right) simulations. Contour lines are plotted at 2 hPa intervals. The label 0609sn2lo/hi refers to the case of September 2006, and the 2nd simulation with a spectrally nudged formulation with low/high grid resolution. "dd/mm hh" labels indicate date and hour associated with the corresponding position.

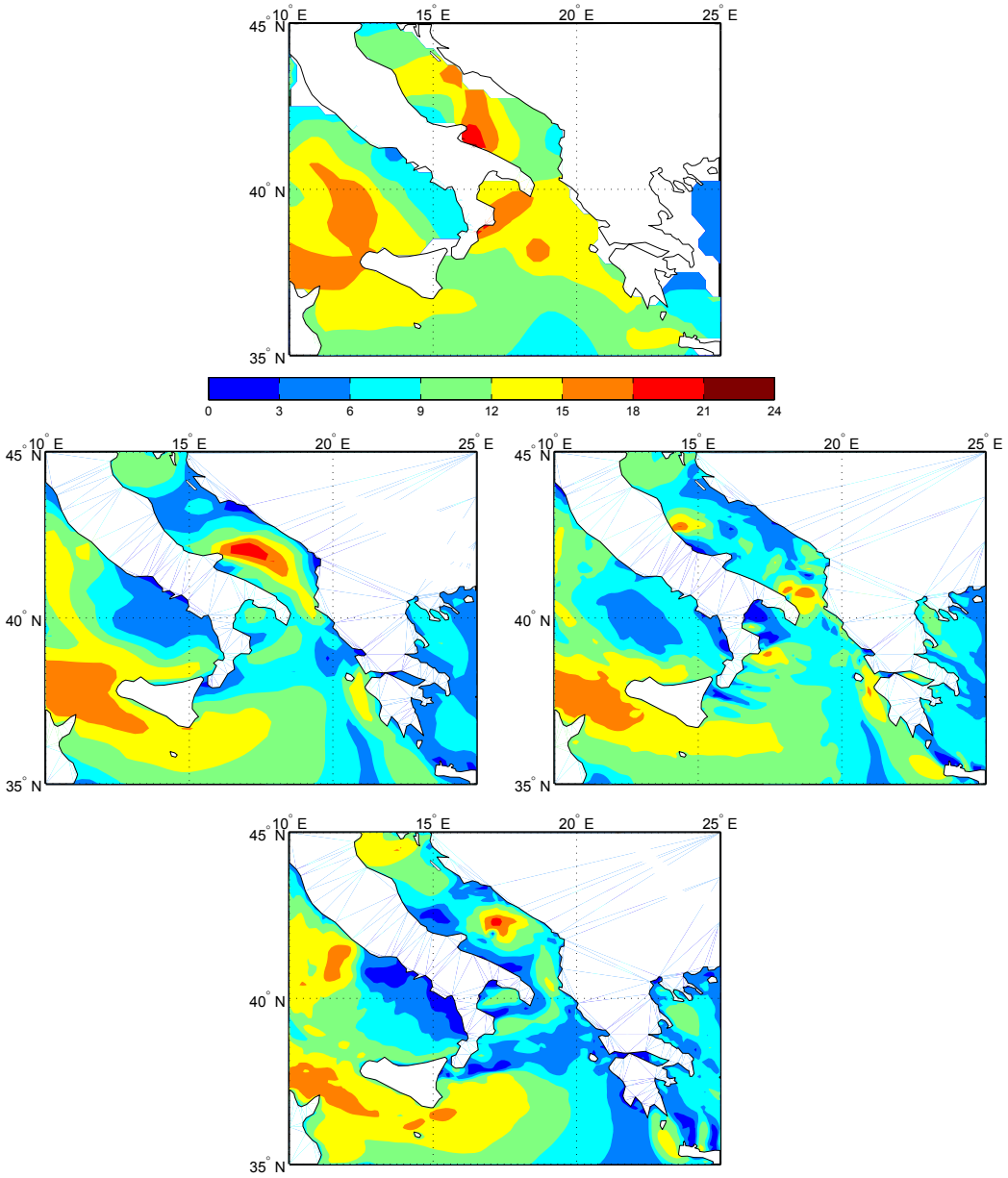

Figure 3.5: Measured wind speed field on Sept 26 at 12 UTC as reconstructed in the NOAA "Blended Sea Winds" (top). 10-meters wind speed in 0609sn2lo (middle left) and 0609sn2hi (middle right) simulations. Bottom: wind speed on Sept 26 at 18 UTC in the 0609sn2hi simulation. Every contour represents a 3 m/s increment. The label 0609sn2lo/hi refers to the case of September 2006, and the 2nd simulation with a spectrally nudged formulation with low/high grid resolution.

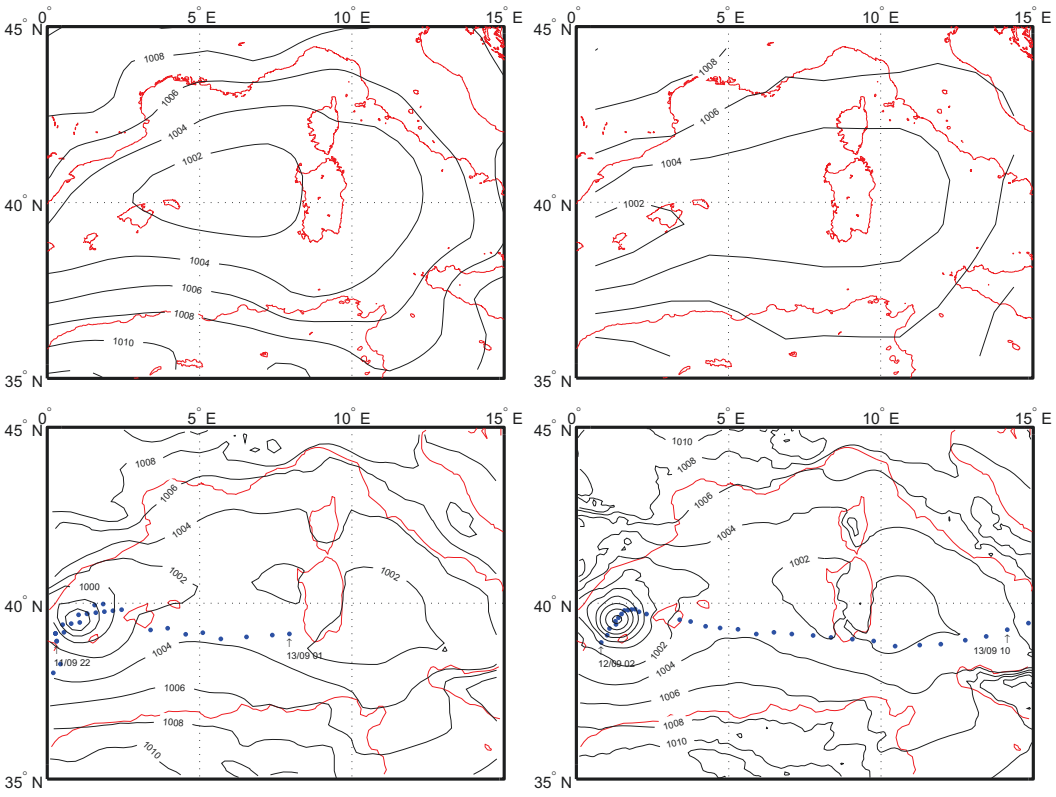

Figure 3.6: Mean sea level pressure fields on Sept 12 at 06 UTC in the ECMWF analysis (top left), MERRA reanalysis (top right), 9609sn2lo (bottom left) and 9609sn2hi (bottom right) simulations. Contour lines are plotted at 2 hPa intervals. The label 9609sn2lo/hi refers to the case of September 1996, and the 2nd simulation with a spectrally nudged formulation with low/high grid resolution. "dd/mm hh" labels indicate date and hour associated with the corresponding position.

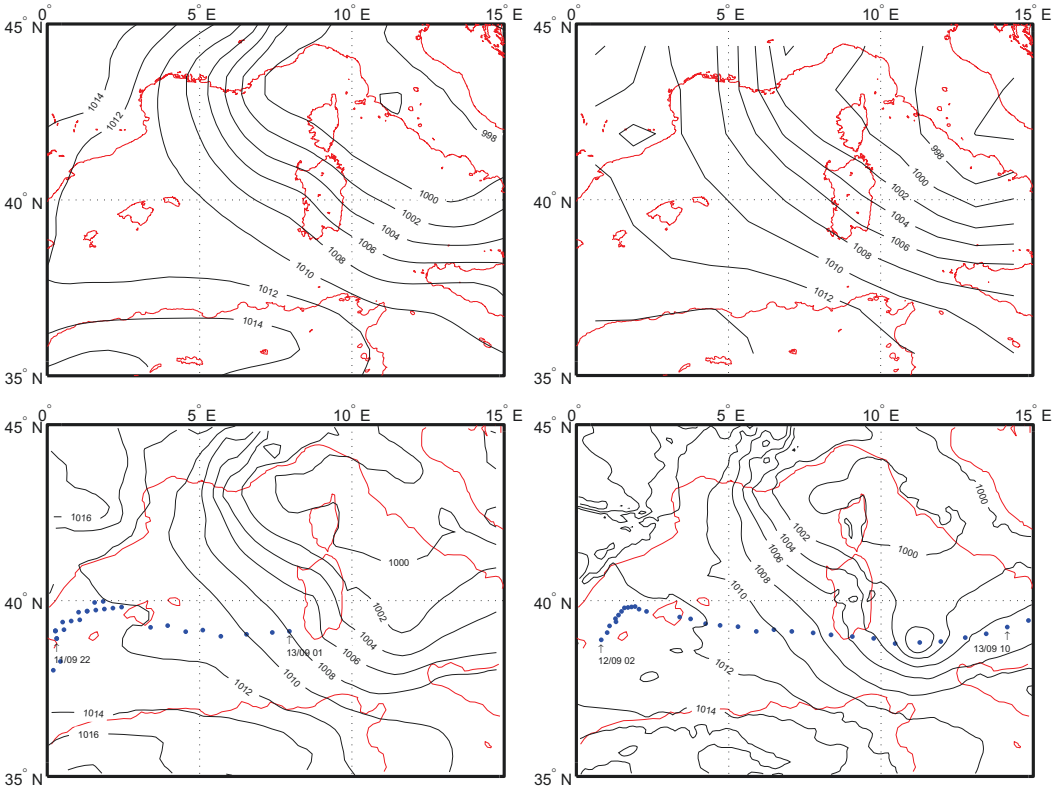

Figure 3.7: The same as Fig. 3.6 on Sept 13 at 06 UTC.

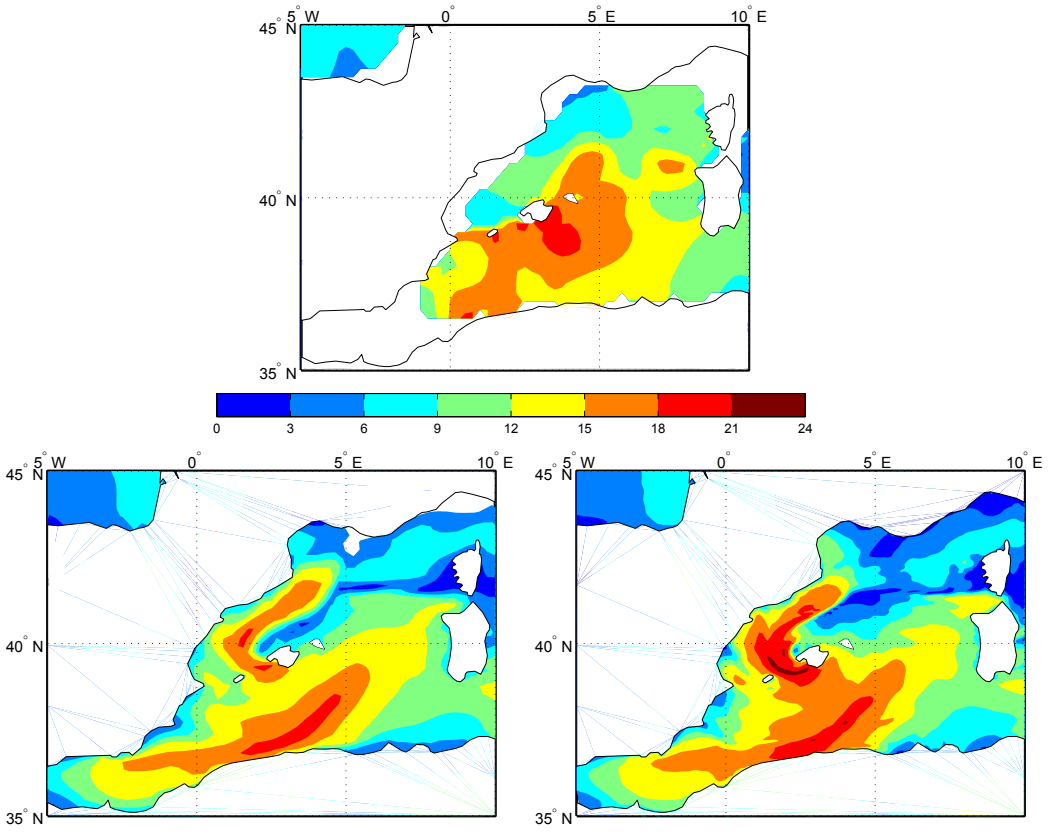

Figure 3.8: Measured wind speed field on Sept 12 at 12 UTC as reconstructed in the NOAA "Blended Sea Winds" (top). 10-meters wind speed in 9609sn2lo (bottom left) and 9609sn2hi (bottom right) simulations. Every contour represents a 3 m/s increment. The label 9609sn2lo/hi refers to the case of September 1996, and the 2nd simulation with a spectrally nudged formulation with low/high grid resolution.

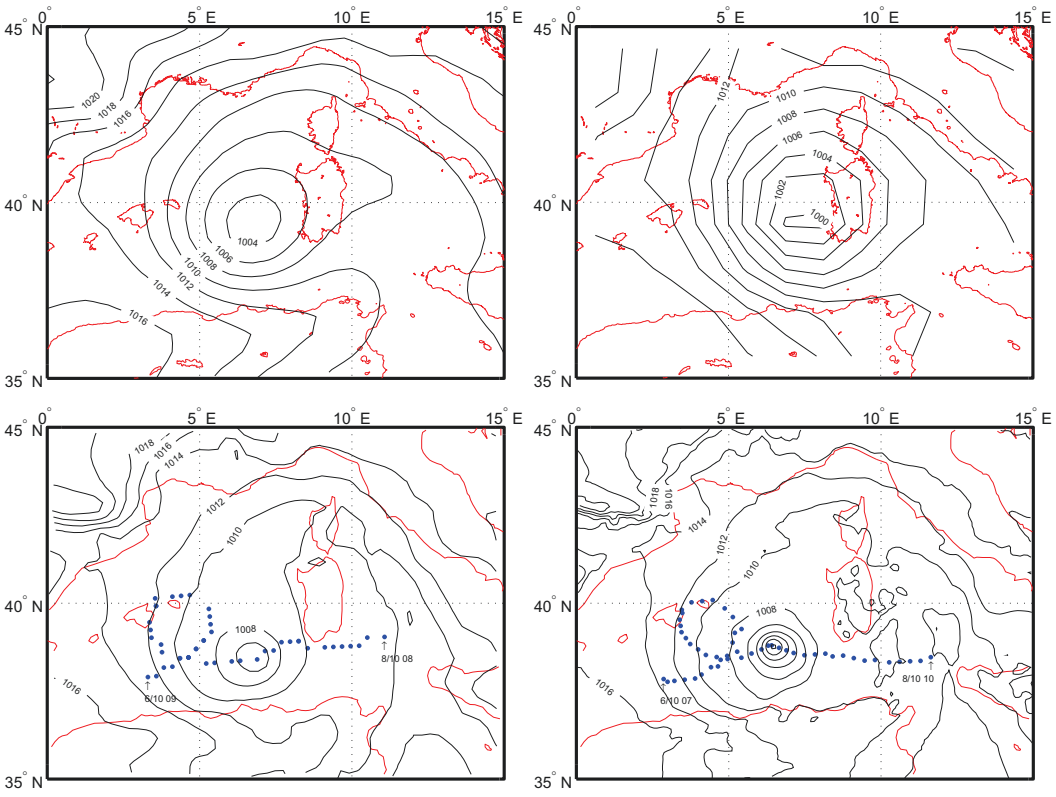

Figure 3.9: Mean sea level pressure fields on Oct 07 at 18 UTC in the ECMWF analysis (top left), MERRA reanalysis (top right), 9610sn2lo (bottom left) and 9610sn2hi (bottom right) simulations. Contour lines are plotted at 2 hPa intervals. The label 9610sn2lo/hi refers to the case of October 1996, and the 2nd simulation with a spectrally nudged formulation with low/high grid resolution. "dd/mm hh" labels indicate date and hour associated with the corresponding position.

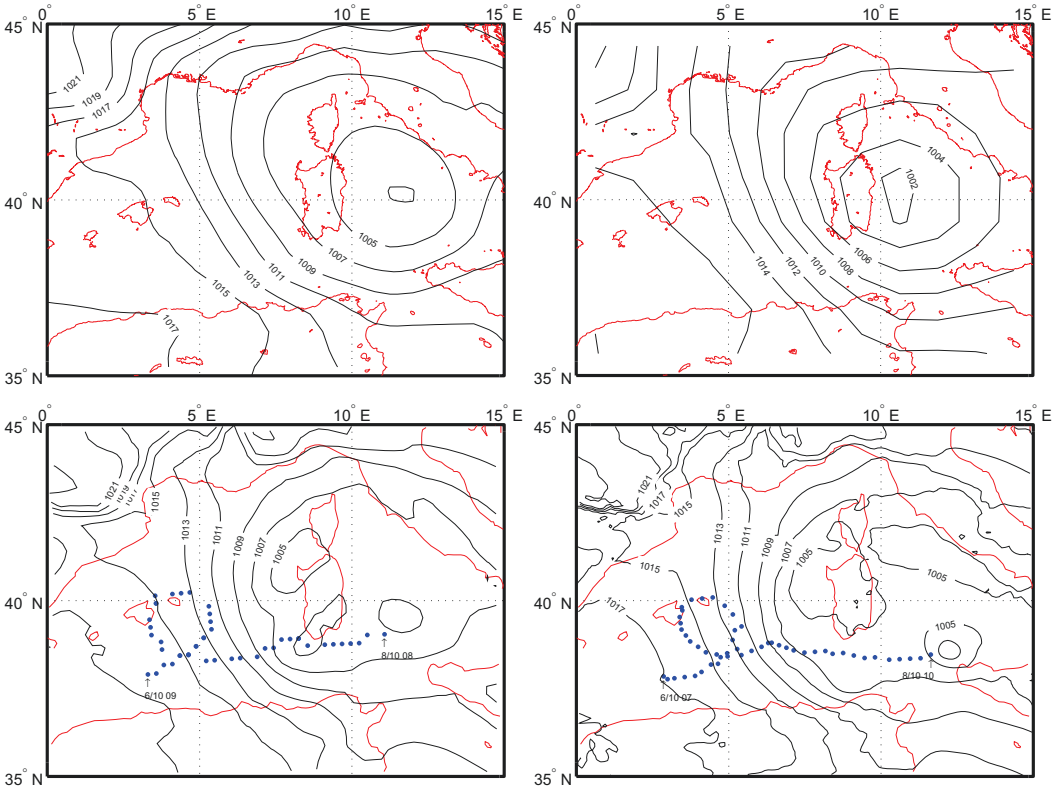

Figure 3.10: The same as Fig. 3.9 on Oct 08 at 12 UTC.

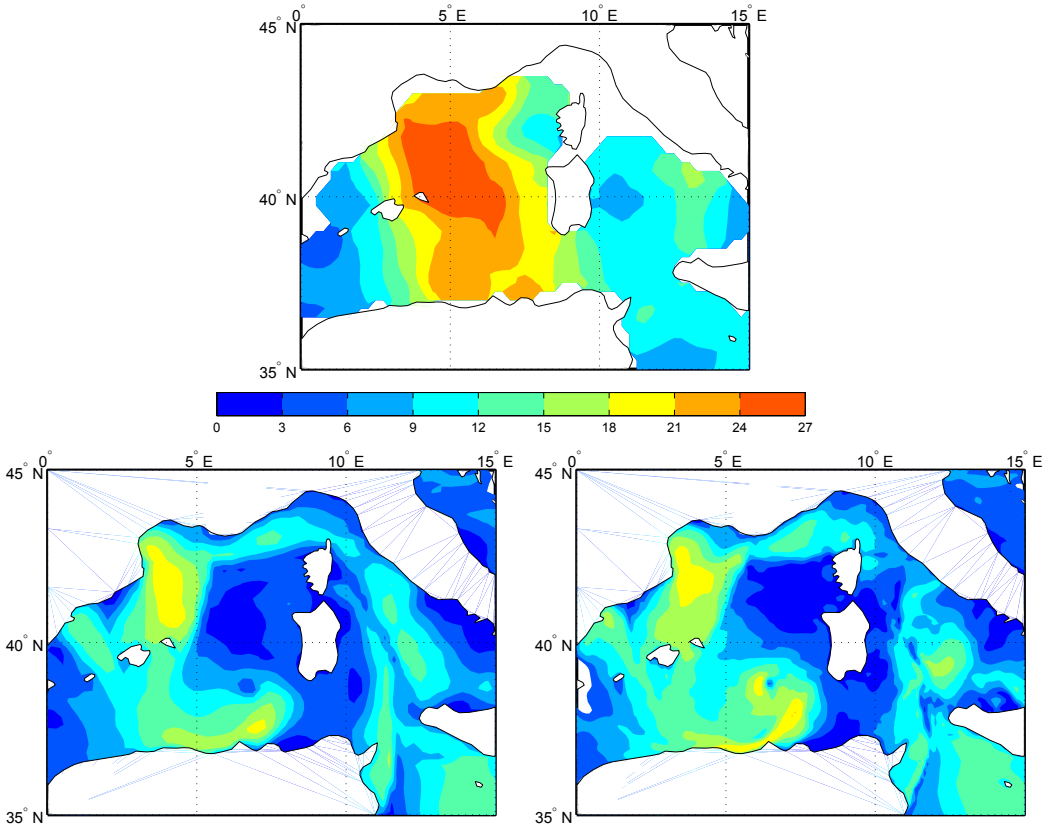

Figure 3.11: Measured wind speed field on Oct 07 at 18 UTC as reconstructed in the NOAA "Blended Sea Winds" (top). 10-meters wind speed in 9610sn2lo (bottom left) and 9610sn2hi (bottom right) simulations. Every contour represents a 3 m/s increment. The label 9610sn2lo/hi refers to the case of October 1996, and the 2nd simulation with a spectrally nudged formulation with low/high grid resolution.

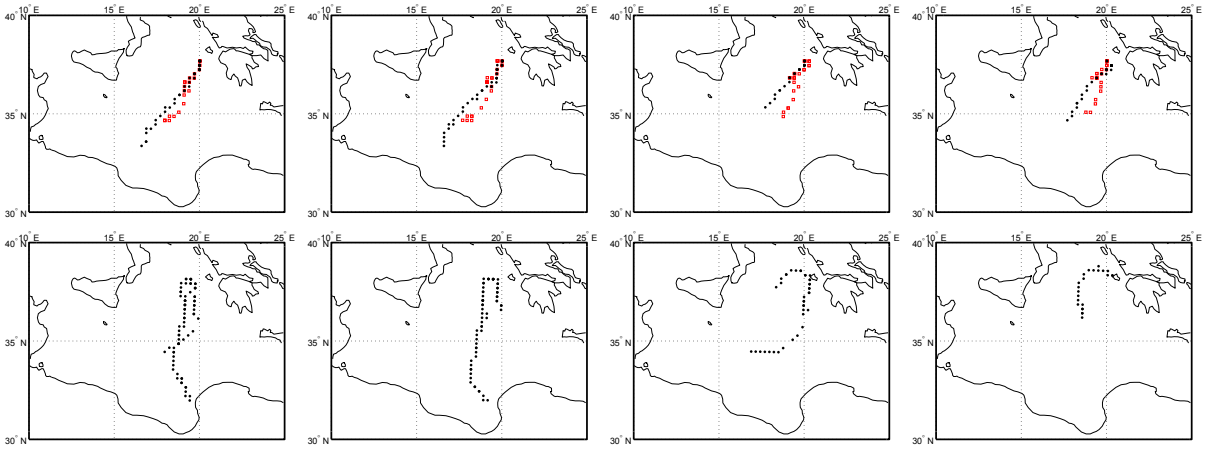

Figure 3.12: January 1995 medicane track in the low resolution spectrally nudged 9501sn1lo-9501sn4lo simulations (top) and low resolution non nudged 9501nn1hi-9501nn4hi simulations (bottom). In the top panels two different markers have been used for a better visualiztion: (red) empty squares correspond to the part of the track moving northwards, (blue) filled circles to the part moving southwards.

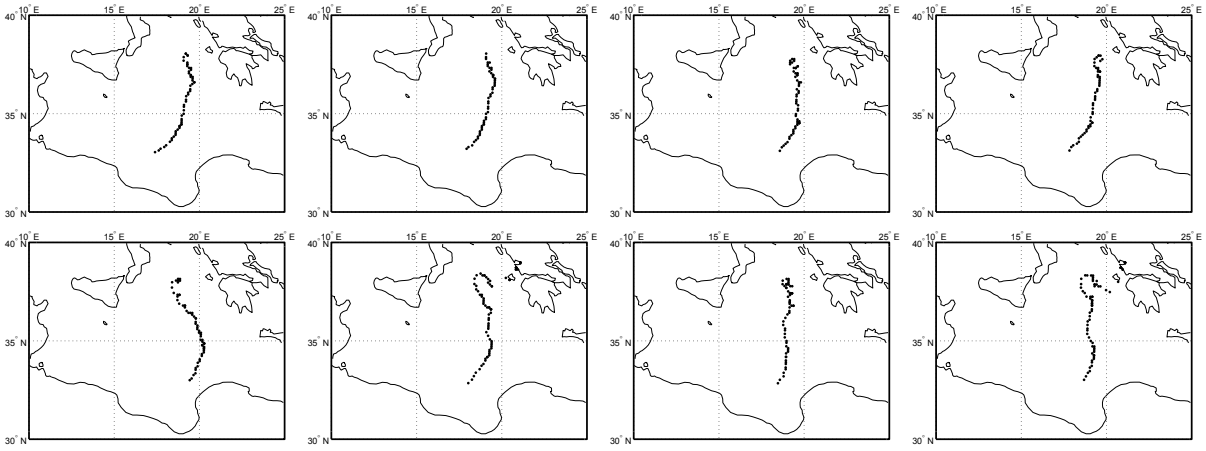

Figure 3.13: January 1995 medicane track in the high resolution spectrally nudged 9501sn1lo-9501sn4lo simulations (top) and high resolution non nudged 9501nn1hi-9501nn4hi simulations (bottom).

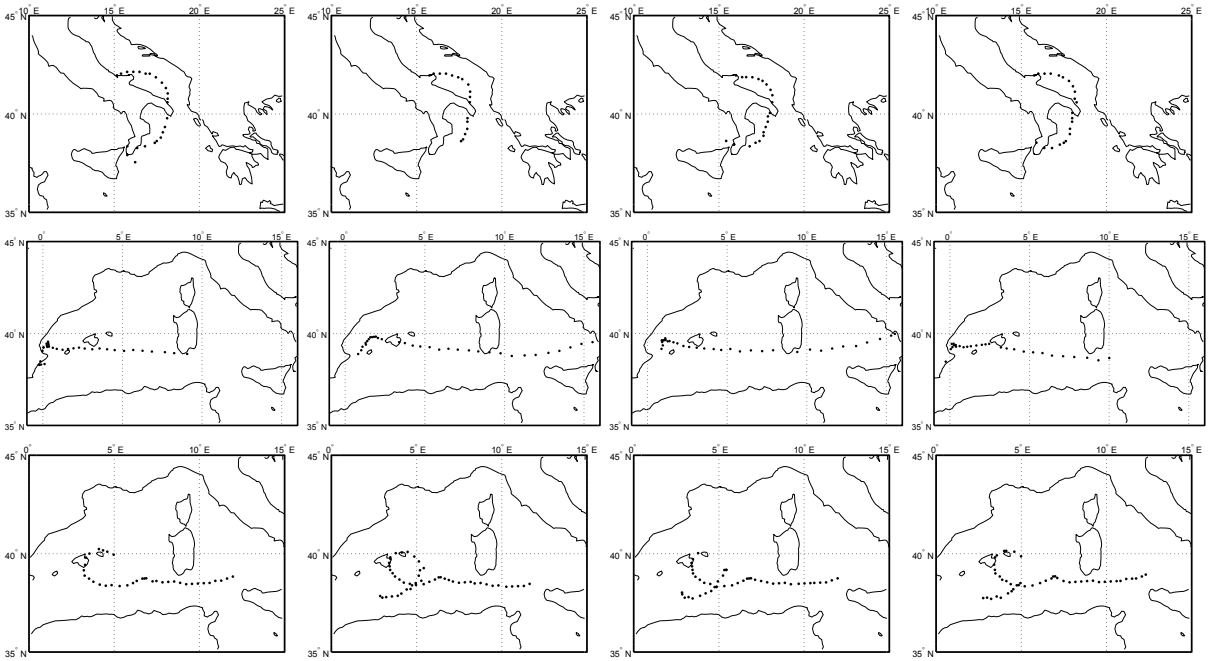

Figure 3.14: Medicane track in high resolution spectrally nudged simulations. 0609sn1hi-0609sn4hi simulations for the September 2006 case (top), 9609sn1hi-9609sn4hi simulations for the September 1996 case (middle) and 9610sn1hi-9610sn4hi simulations for the October 1996 case (bottom).

3.3 Results: Vertical Structure

So far we have devoted our attention to the analysis of the sea level wind and pressure patterns associated with medicanes. However, in order to study the features related to the tropical-like nature of medicanes, such as for example their axis-symmetry or warm core, the full vertical structure of the cyclone has to be taken into account.

Besides giving an insight on the dynamical characterization of medicanes, the analysis of their vertical structure has also a practical interest. Several modelling studies on tropical cyclones (Walsh, 1997; Walsh et al., 2007; Hart, 2003) in fact exploited features of the TCs 3D structure to detect and track them in the model output. It is thus interesting to investigate whether a similar characterization can be applied to the medicanes.

We will focus on the variables that are expected to reflect the most typical signatures of a tropical-like cyclone dynamics: geopotential, potential temperature and horizontal velocity.

Figs. 3.15 and 3.16 show distributions of the aforementioned variables for respectively the 9501 and 0609 cases, in the spectrally nudged high resolution simulations. The two remaining cases (not shown) exhibit a similar behavior. The geopotential profiles show an almost perfect axis-symmetric structure, extending up to 300 hPa. In all the cases, positive temperature anomalies are found in the vicinity of the cyclone center, reflecting the medicanes' warm core structure. Velocity profiles[1] show as well a structure very similar -at a smaller scale- to that tropical cyclones, characterized by a region in the center of the storm with very low tangential velocity, corresponding to the cyclone's eye; outside of this region, tangential velocity has a maximum a few grid points away from the storm center, in the lower troposphere, and then decreases upwards and outwards. The region of maximum wind is interpreted as being associated with the eyewall.

Figs 3.17 shows profiles corresponding to Fig. 3.16 in a coarse resolution run for the 0609 medicane. While the typical structure of the geopotential and velocity profiles is still visible, it is more difficult to keep track of the warm core structure. In the velocity profile, the region of maximum winds is displaced farther from the cyclone center, reflecting a poorer representation of the eye structure. Similar differences between low and high resolution vertical profiles emerge from the analysis of the remaining cases.

[1] In the plot is represented the meridional component of wind. Since both cyclones are propagating in the longitudinal direction at the time corresponding to the snapshot, this is a good approximation for the tangential velocity.

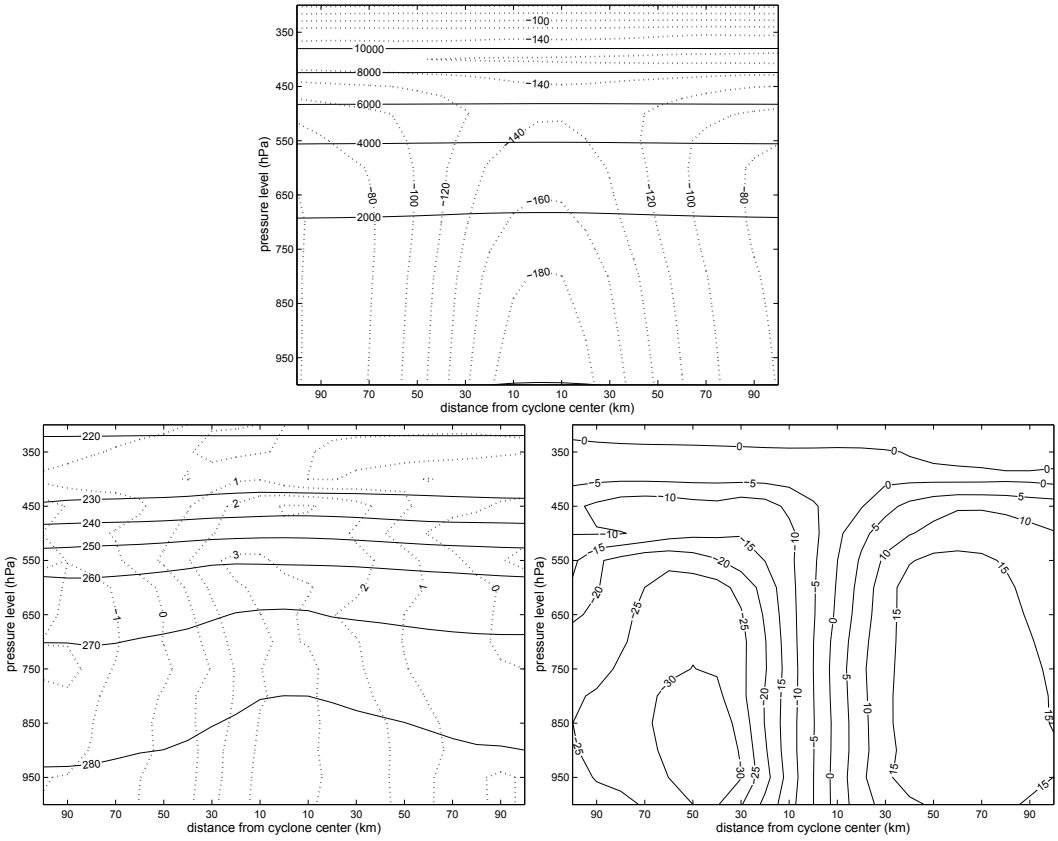

Figure 3.15: Vertical profiles of Jan 95 medicane on 01/16 at 00 UTC in spectrally nudged high-resolution 9501sn2hi simulation. Top: x-z cross section at a fixed latitude corresponding to the center of the storm of geopotential (full lines) and geopotential zonal anomaly (dashed lines). Bottom left: x-z cross section of temperature (full lines) and temperature anomaly (dashed lines). Anomalies are calculated with respect to the zonal mean field. Bottom right: x-z cross section of y component of velocity.

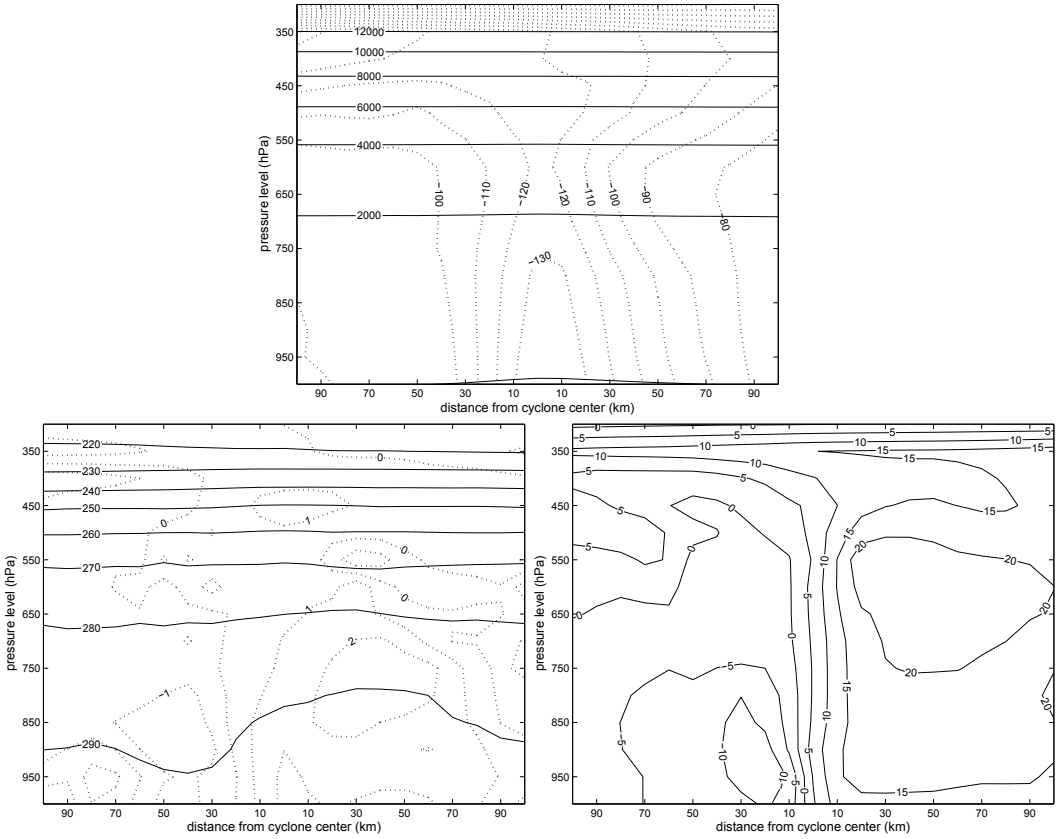

Figure 3.16: The same as Fig. 3.15 for Sept 06 medicane, on 09/26 at 12 UTC in 0609sn2hi simulation.

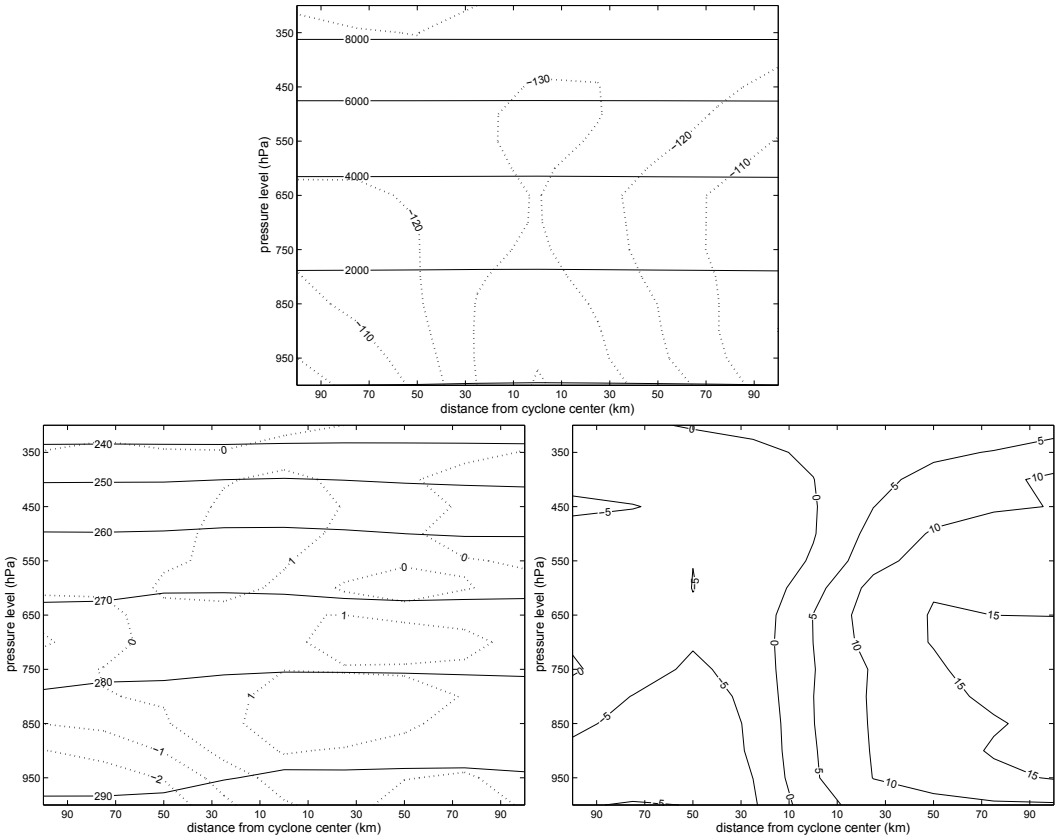

Figure 3.17: The same as Fig. 3.16 in 0609sn2lo low-resolution simulation.

Chapter 4

The multi-decadal statistics of medicanes

Papers on which the Chapter is based:
L. Cavicchia, S. Gualdi and H. von Storch, "The multidecadal statistics of medicanes" in preparation.

4.1 Medicanes climatology

In order to study the climatology of medicanes and to analyze their statistical properties, we performed the downscaling of the full NCEP/NCAR reanalyses data for the period 1948-2011, running the regional model in the same configuration used for the study of historical medicanes, at 10 kilometers resolution and with spectral nudging switched on (the model setup is described in detail in Sec. 2.1). The simulation is referred to as NCEP60 in the following.

After running the model, we identify medicane events by applying the detection algorithm described in Sec. 2.2. The selection efficiency of the different criteria employed in the detection procedure is reported in Table 4.1

We find a total number of 99 medicanes over 63 medicanes seasons (a medicane season is defined to last from August of each year through July of the following year). The frequency of medicanes is thus extremely low, 1.57 ± 1.30 events per year, consistently with the empirical understanding of

Table 4.1: Efficiency of the selection cuts (number of tracks per year).

ΔP	V_{av}	B & V_T	Geometry	V_{shape}	V_{max}
1606	24.6	9.7	7.1	3.75	1

medicanes as rare events.

In the rest of this Chapter, the statistical properties of medicanes are analyzed in detail, and their linkage with the synoptic circulation patterns in the Mediterranean region is discussed.

4.1.1 Geographical distribution, annual cycle and inter-annual variability

The locations of formation of all the medicanes detected over the six decades under study are shown in Fig. 4.1. A great part of the medicanes are formed in two specific areas of the Mediteranean. The region where medicane formation occurs more often is in the western Mediterranean, roughly delimited by the Balearic islands and the Spanish coast on the west, southern France on the north, and the western coast of Corsica and Sardinia on the east. The second preferred formation region extends between the Ionian Sea and the coast of Libya. Two more formation areas, characterized by a lower number of events, are the Aegean Sea and the Adriatic Sea. Almost no activity is found in the Levantine basin in the eastern Mediterranean.

The geographical pattern of medicanes formation is quite different from that of "ordinary" Mediterranean cyclogenesis, whose properties were described in Sec. 1.1.

Figure 4.2 shows the seasonal distribution of the detected medicanes. The distribution is characterized by:

- no events in Summer;
- an high activity during all Autumn (September through December);
- a peak in January;
- a flattish tail extending from February through May.

The number of medicanes per season for the period 1948-2010 is reported in Fig. 4.3. The year-to-year variability is strong. The overall trend is negligible (+ 0.015 events/year).

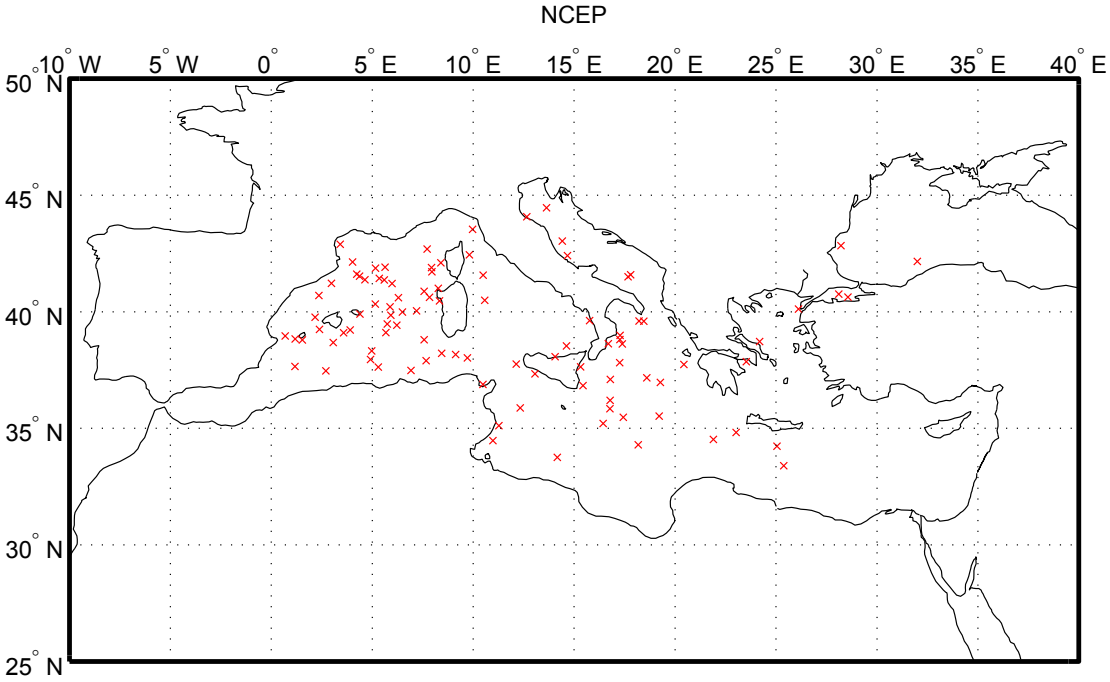

Figure 4.1: Formation locations of all the medicanes detected in the NCEP60 simulation.

It is worth to point out that both the geographical pattern and seasonal cycle of medicanes formation do not exhibit a maximum in the regions/months where the sea surface temperature is highest (that would be respectively the south-eastern part of the basin and the Summer months, see for example Brasseur et al. 1996 and references therein). This result supports the hypothesis discussed in Sec. 1.2, that the formation of medicanes requires cold air intrusions enhancing instability. Further investigation on the factors associated with medicanes genesis is presented in Sec 4.2 below.

4.1.2 Sub-regional features

Due to its complex geography and orography, the Mediterranean region exhibits a great variety of subregional weather features. It is thus interesting to study in further detail the statistical properties of medicanes in different areas within the Mediterranean. We focus on the two areas where the larger number of medicanes is formed, western Mediterranean and "Ionian" (see the map in Fig. 4.4 for the exact definition of those areas).

The seasonal cycle for, respectively, the western Mediterranean and Ionian

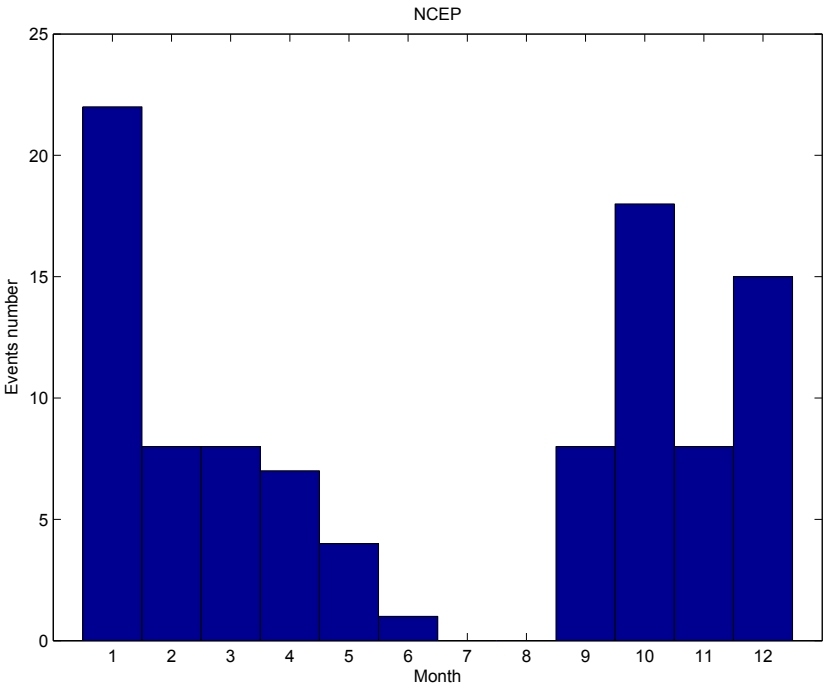

Figure 4.2: Number of medicanes per month (total number in the period 1948-2011) in the NCEP60 simulation.

regions is reported in Fig. 4.5, in analogy with Fig. 4.2. There is a marked difference in the annual cycles in the two areas: the frequency of medicanes formation in the western Mediterranean steadily increases during Fall and starts to decrease in January with a long tail extending in the Spring. On the other hand, the events in the Ionian Sea exhibit a sharp peak in January, with much less activity during Fall and Spring.

The inter-annual variability of the frequency of medicanes in the two considered regions is reported in Fig. 4.6. The average number of events is 0.75 ± 0.95 per year in the western Mediterranean, and 0.32 ± 0.50 in the Ionian Sea. The variability looks mostly uncorrelated between the two regions (the Pearson's correlation coefficient between the two time series is $\rho = -0.03$).

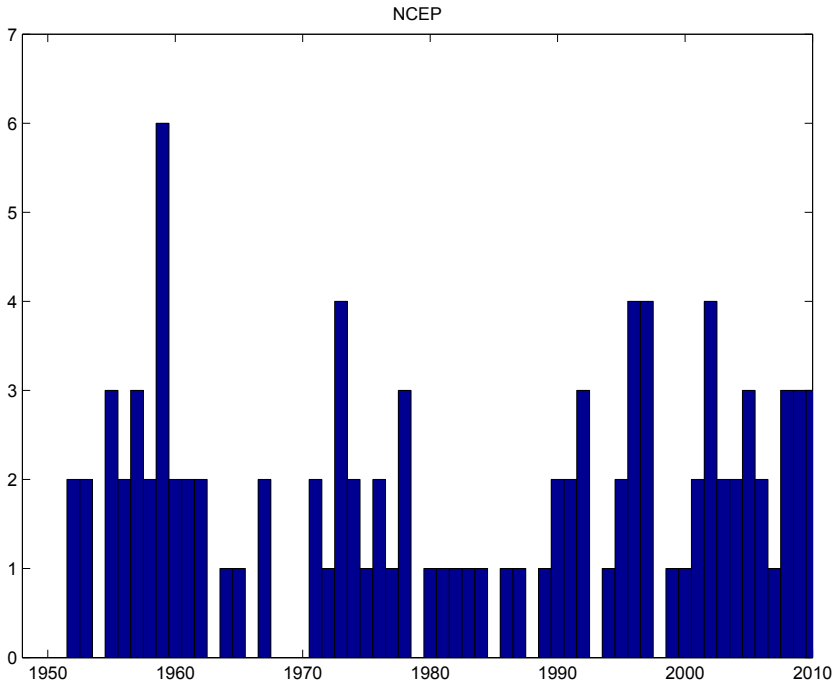

Figure 4.3: Number of medicanes per season in the NCEP60 simulation.

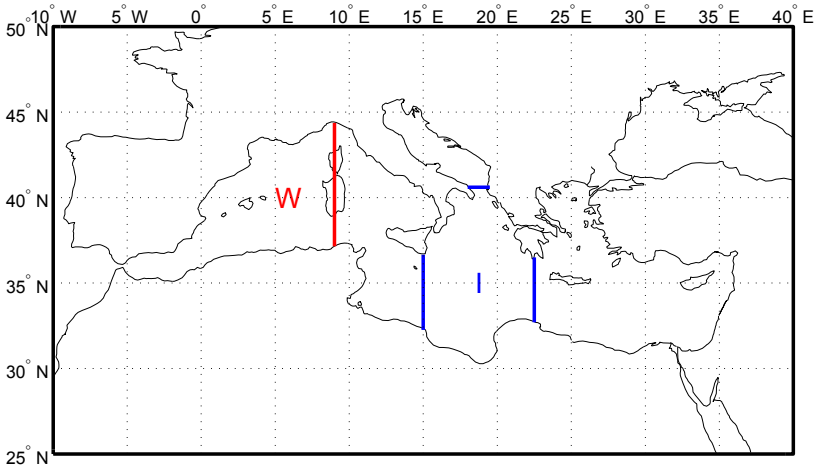

Figure 4.4: Areas used for the analysis of medicanes in western Mediterranean (red line, label W) and Ionian (blue lines, label I) regions.

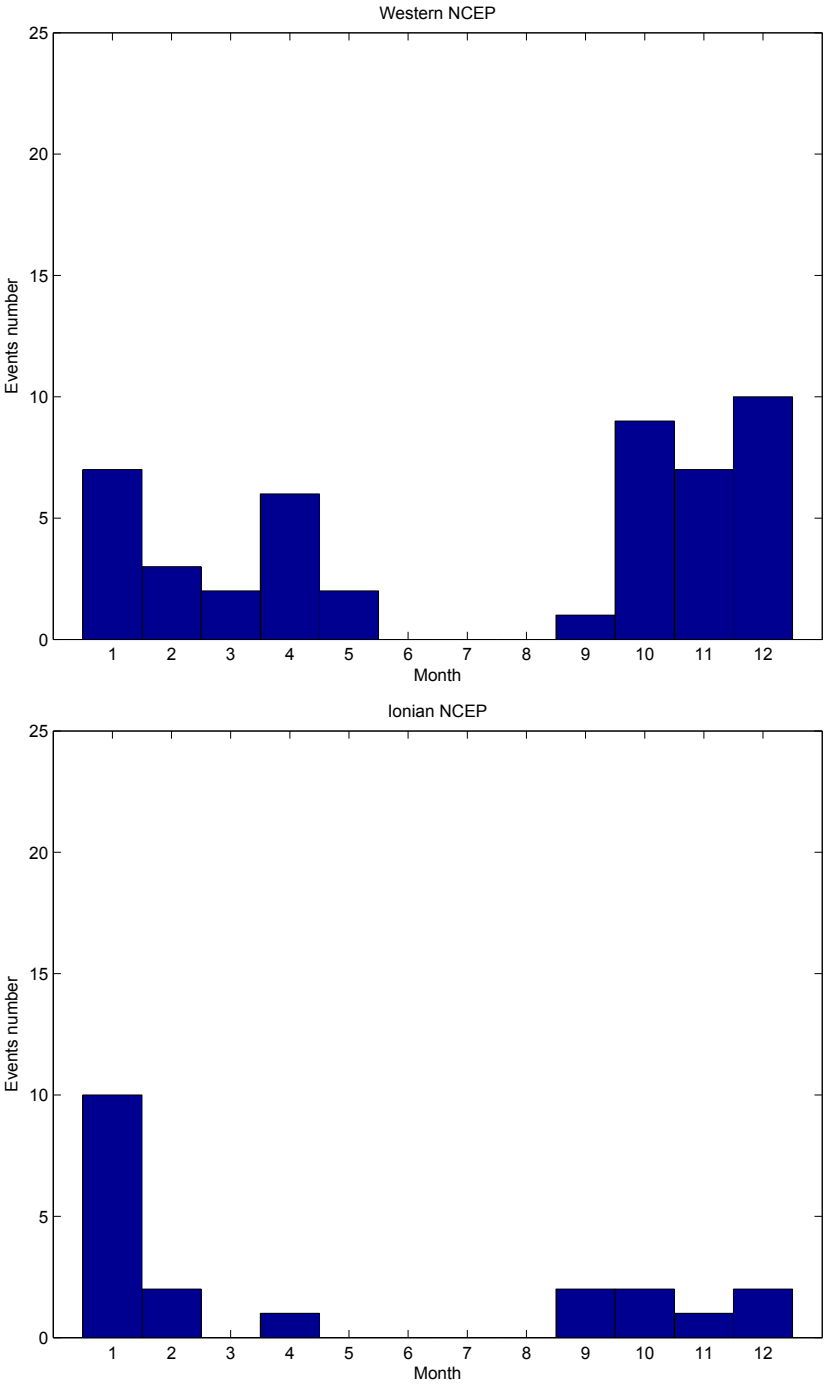

Figure 4.5: Number of medicanes per month (total number in the period 1948-2011) formed in the western Mediterranean (top) and in the Ionian area (bottom), in the NCEP60 simulation.

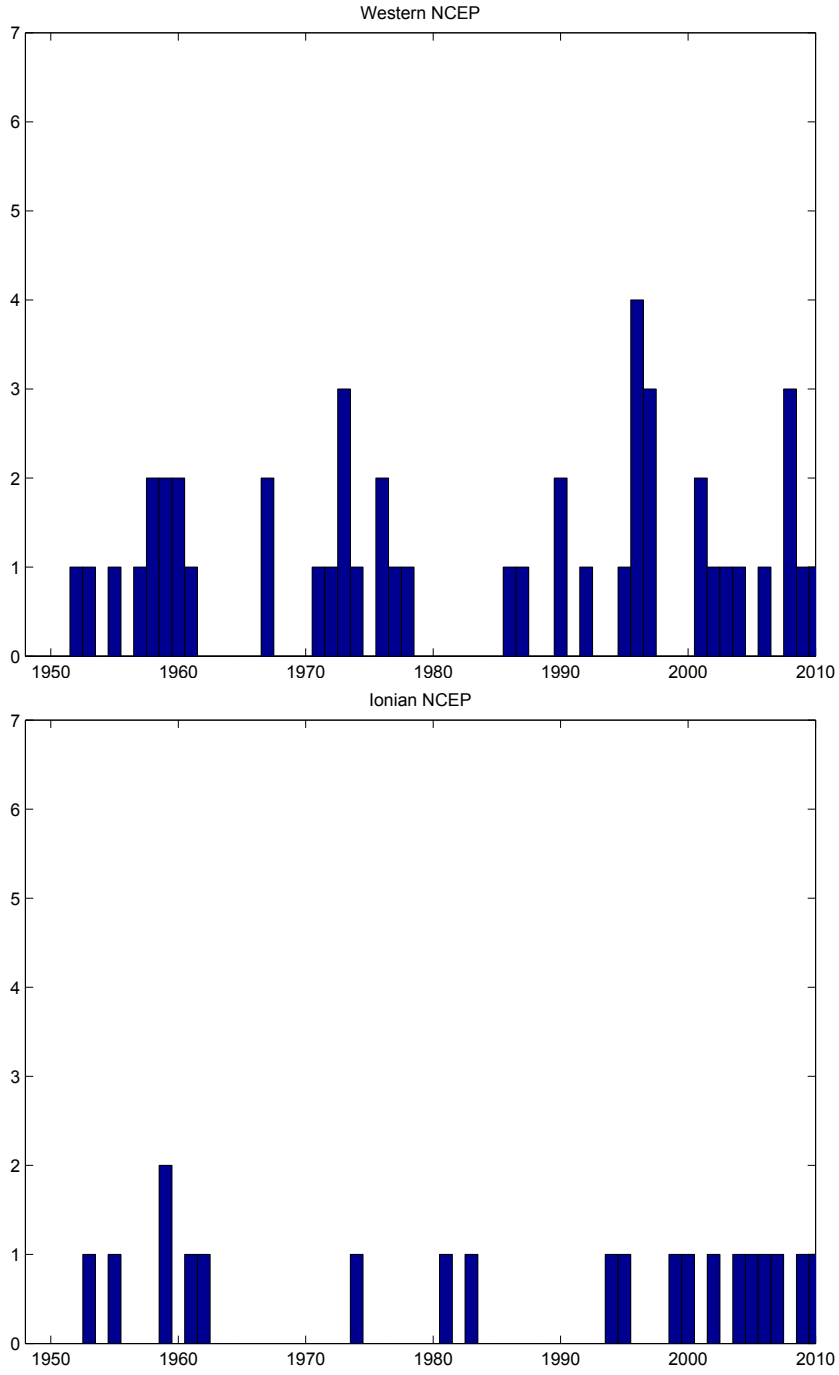

Figure 4.6: Number of medicanes per season formed in the western Mediterranean (top) and in the Ionian area (bottom), in the NCEP60 simulation.

4.2 Linkage between medicanes statistics and large-scale patterns

Several hypotheses about the environmental factors that might influence the development of medicanes have been advanced in the literature (as discussed in Chapter 1), based on the evidence found in event-based case studies, and on the analogy with tropical cyclones. Those factors, mostly related to large-scale circulation patterns, include:

- the presence of a cold cut-off low in the middle and high troposphere;
- a low vertical wind shear;
- a large moisture content of the atmosphere;
- pre-existent low level vorticity;
- a high value of sea surface temperature.

We analyzed the events detected in the six decades simulation, in order to assess whether those factors can be associated to the formation of medicanes on general grounds.

In Figs. 4.7 and 4.8 are reported the composite plots of the anomalies with respect to the climatological (over the simulation period) monthly mean of the aforementioned variables, for all the medicanes formed in respectively the western Mediterranean and Ionian Sea (similar results hold for the other formation regions). The composites are calculated from the daily mean values of the fields, on the day when the pressure minimum is tracked by the detection algorithm for the first time. The patterns of environmental conditions shown in the composite plots can thus be considered to be representative of the precursors of medicanes formation.

A clear signal is visible in the difference ΔT between the 350 hPa temperature and the sea surface temperature (Fig. 4.7, top), showing a negative anomaly between 3° C and 5° C. The deviation from the mean state of the 350 hPa temperature alone (Fig. 4.9, top) shows a pattern very similar in both its shape and magnitude to that of ΔT. On the other hand, the sea surface temperature field (Fig. 4.9, bottom) does not show significant anomalies associated to medicanes formation. It can be inferred that the anomalies of the temperature difference ΔT, leading to the instability responsible for the development of medicanes, are controlled by cold air intrusions in the upper atmospheric levels rather than to a warming of the sea surface.

The wind shear field (850 hPa - 250 hPa) shows (Fig. 4.8, top) as well relevant anomalies - the absolute value of wind shear at the time of medicanes

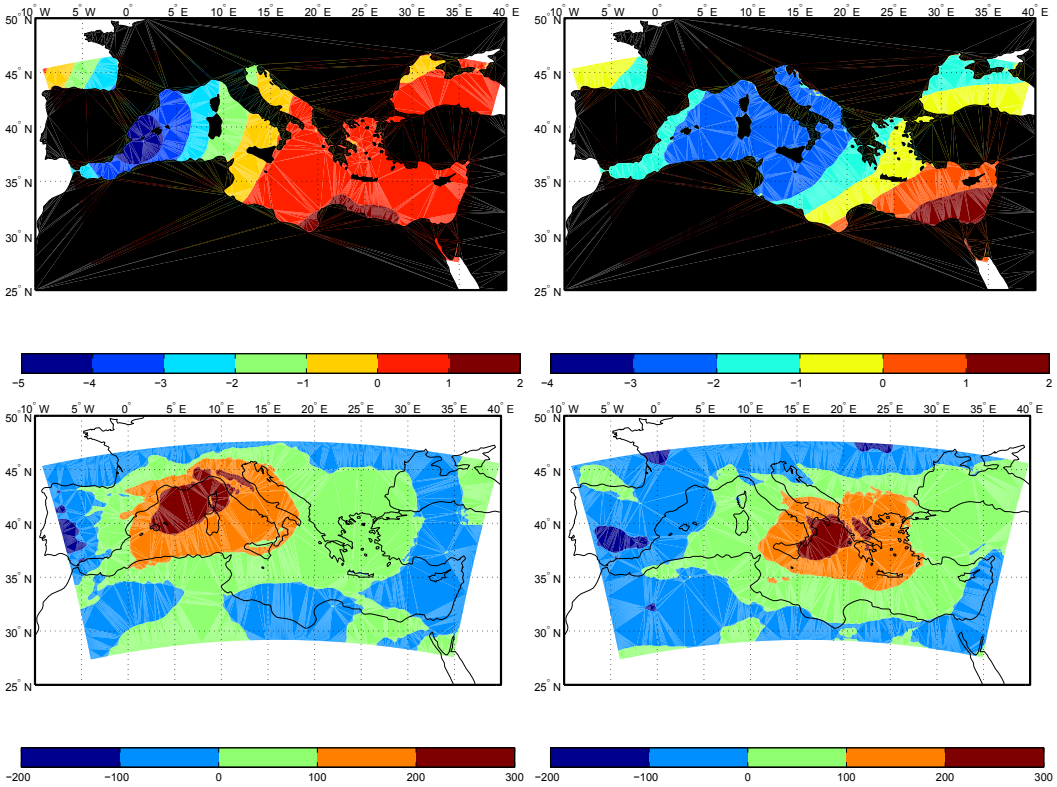

Figure 4.7: Composite plots of the daily means, on the day corresponding to the first point in the track, for medicanes in the western Mediterranean (left panels) and Ionian Sea (right panels) of the anomalies with respect to the climatological monthly means. Top: difference between 350 hPa temperature and SST (1° C contours). Bottom: relative humidity integrated along the atmosphere column (adimensional units, contours at steps of 100).

formation is around 10 - 15 m/s lower than the mean value in the area. The humidity field (integrated over the atmosphere column, Fig. 4.7, bottom) and the relative vorticity field at 850 hPa (Fig. 4.8, bottom) show both positive anomalies at the time of formation of medicanes. It can thus be concluded that those environmental factors - low wind shear, high moisture and vorticity - favor the formation of medicanes, in a similar way as they do for tropical cyclones.

Having singled out a number of variables that exhibit significant deviations from their mean state in correspondence with the formation of medicanes, we further investigate whether the aforementioned deviations are able

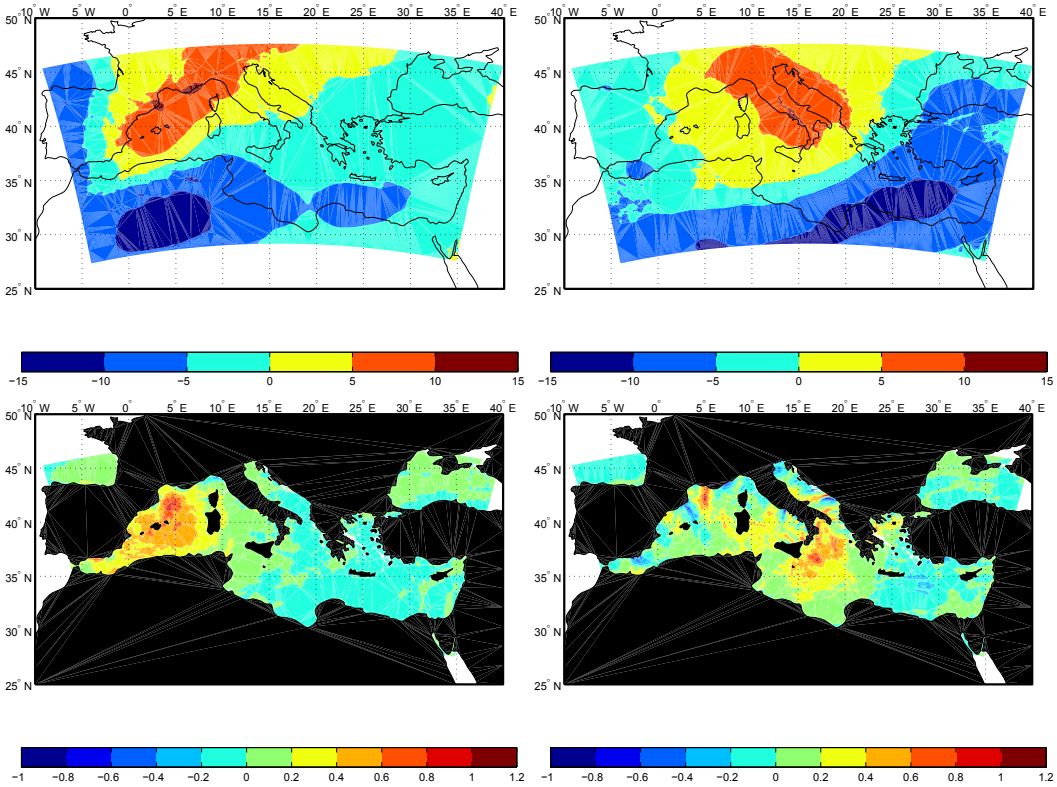

Figure 4.8: Composite plots of the daily means, on the day corresponding to the first point in the track, for medicanes in the western Mediterranean (left panels) and Ionian Sea (right panels) of the anomalies with respect to the climatological monthly means. Top: 850-250 hPa wind shear (5 m/s contours). Bottom: 850 hPa relative vorticity (0.5 s^{-1} contours).

to account for the main features of the statistics of medicanes. Rather than using one of the indexes defined for tropical cyclones, we aim to quantify the effect of each of the considered factors without making any prior assumption on their relative weight.

In order to assess to what extent the geographical distribution of medicanes formation can be explained by the realization of patterns of environmental factors similar to those described above, we computed for each of the four factors analyzed (ΔT, wind shear, relative humidity and vorticity) the probability that it exceeds a threshold corresponding to the value observed in association to the formation of medicanes[1]. Those threshold values are

[1]The probabilities are computed from the daily mean values over all the simulation period as the percentage of days in which the condition is realized.

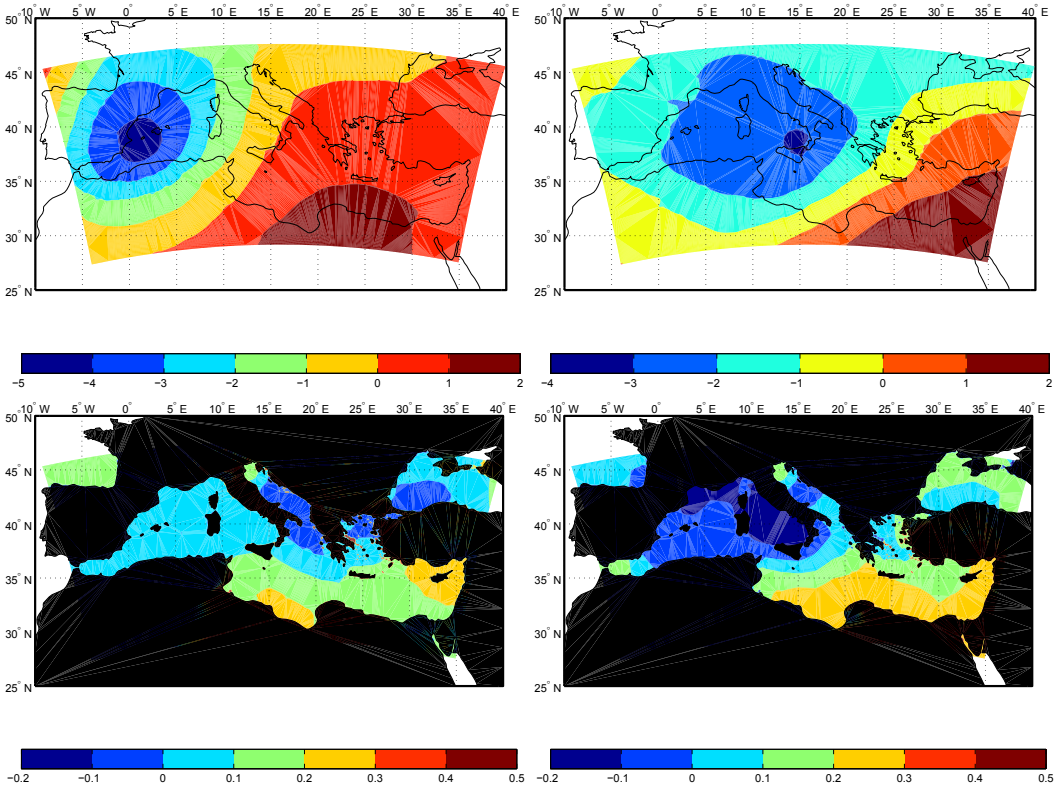

Figure 4.9: Composite plots of the daily means, on the day corresponding to the first point in the track, for medicanes in the western Mediterranean (left panels) and Ionian Sea (right panels) of the anomalies with respect to the climatological monthly means. 350 hPa temperature (top, 1° C contours), sea surface temperature (bottom, 0.1° C contours).

fixed as follows:

- $\Delta T < -58°$ C;
- a wind shear (WS) lower than 4 ms^{-1} (in absolute value);
- a value of the integrated relative humidity (RH) larger than 1100;
- 850 hPa vorticity (VORT) larger than 0.5 s^{-1}.

The maps of the probability distributions for the four variables are reported in Fig. 4.10. All the thresholds are significative - selecting between 5% and 15% of the distribution of the respective variable in the areas of medicanes formation. On the other hand none of the factors, if considered

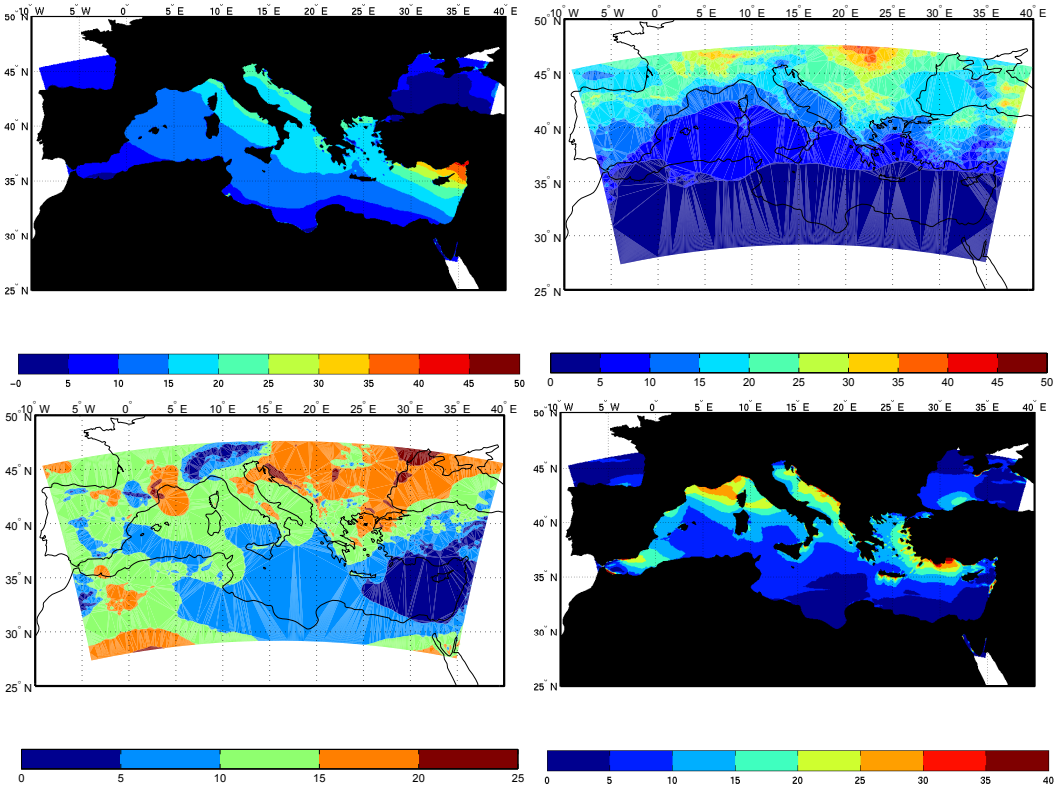

Figure 4.10: Probability for each of the following factors to exceed the threshold value corresponding to medicanes formation: ΔT (top left, 5% contours), RH (top right, 5% contours), WS (top left, 5% contours), VORT (bottom right, 5% contours).

alone, seems to be able to explain the geographical distribution of medicanes events.

Assuming that all the environmental conditions considered have to be realized simultaneously in order to trigger the formation of a medicane, we have calculated the probability that the four factors exceed the respective threshold at the same time (Fig. 4.11). Under this assumption, we find that the probability of having conditions favorable for medicanes development is higher in the north-western part of the Mediterranean basin. Those conditions are realized most frequently over the Adriatic and Aegean seas. We argue, however, that the semi-closed geography of those sub-basins is a limiting factor for the full development of medicanes, as most of the low-pressure systems crossing them stay over sea for a short time. The environmental conditions favorable for medicane formation occur over the Ionan Sea

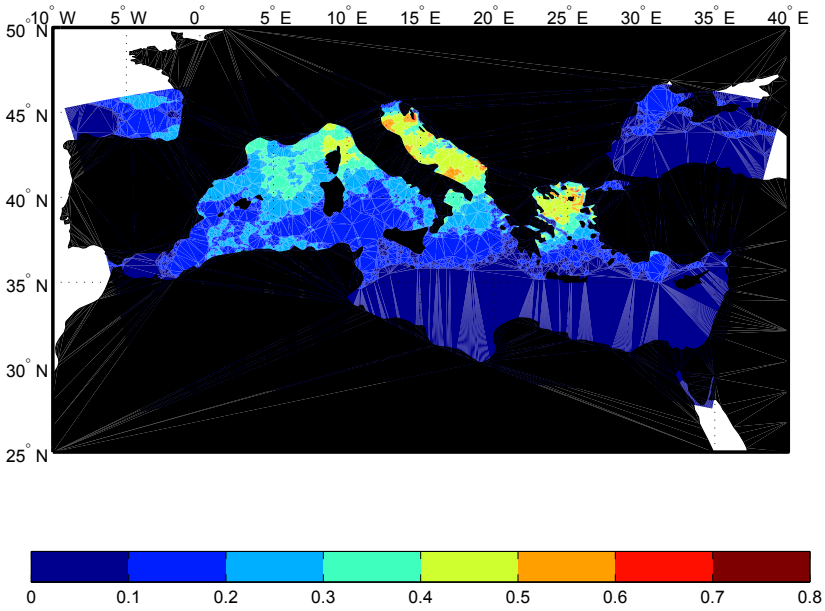

Figure 4.11: Probability of realization of the environmental conditions favorable for medicanes formation (0.1% contours).

approximately half of the times as they do in the western Mediterranean, compatibly with the frequency of detected medicanes.

In order to assess whether the frequency of the environmental conditions considered can explain the seasonal cycle of medicanes, we define an index $\mathcal{M}$ in such a way that it takes the value 1 if all the four factors exceed the respective thresholds over an area larger than 2000 grid-points, and 0 otherwise. The index has been computed in the two boxes shown in Fig. 4.12, that correspond to the areas where the large scale conditions associated to the formation of the detected medicanes respectively in the western Mediterranean and Ionian Sea are observed. In Fig. 4.13 is reported, for each month, the value of the index $\mathcal{M}$ summed for the whole simulation period. Comparing Fig.4.13 with Fig. 4.5, we find that the seasonal variation of the index $\mathcal{M}$ is comparable with that of medicanes formation in both the western Mediterranean and the Ionian Sea.

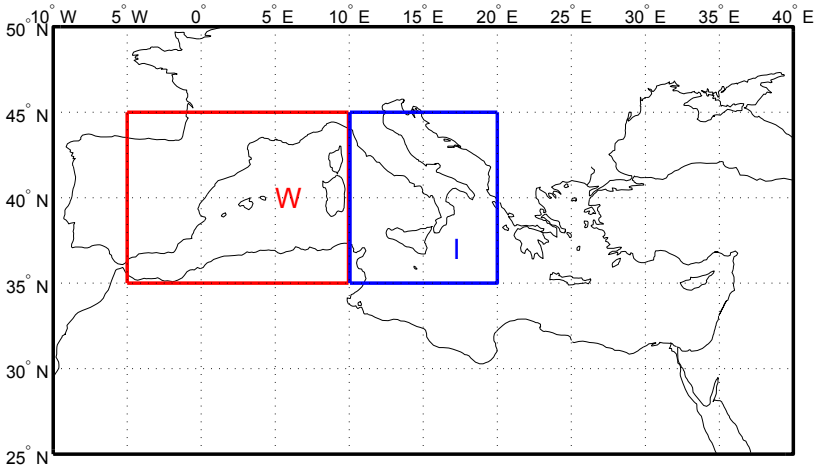

Figure 4.12: Boxes used for the calculation of the index $\mathcal{M}$ for medicanes in western Mediterranean (red box, label W) and Ionian (blue box, label I) regions.

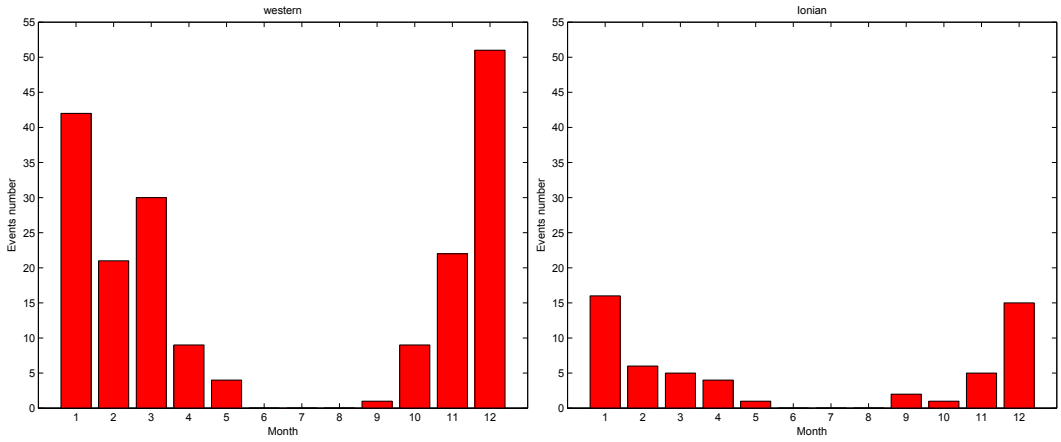

Figure 4.13: Total number of days in the 1948-2011 period where the index $\mathcal{M}$ is equal to 1 in the western Mediterranean (left) and Ionian region (right)

.

Chapter 5

Medicanes and climate change

The development of cyclonic systems relies on the interplay of several environmental and dynamical factors. The assessment of the impact of climate change on their frequency and properties is thus extremely complex. Such complexity has been reflected in a long debate in the literature. The current understanding of the issue can be summarized quoting the IPCC report on extreme events (Intergovernmental Panel on Climate Change, 2012).

"Average tropical cyclone maximum wind speed is likely to increase, although increases may not occur in all ocean basins. It is likely that the global frequency of tropical cyclones will either decrease or remain essentially unchanged. There is medium confidence that there will be a reduction in the number of extratropical cyclones averaged over each hemisphere. While there is low confidence in the detailed geographical projections of extratropical cyclone activity, there is medium confidence in a projected poleward shift of extratropical storm tracks. There is low confidence in projections of small spatial-scale phenomena such as tornadoes and hail because competing physical processes may affect future trends and because current climate models do not simulate such phenomena."

A study on the impact of climate change on polar lows (Zahn and von Storch, 2010), using the same dynamical downscaling approach employed in the current work, found a reduction in the number of polar lows in future climate scenarios, due to an increase in the atmospheric stability, resulting from a faster warming rate of the mid-troposhpere with respect to the North Atlantic sea surface temperature.

No analysis has been published up to date tackling specifically the issue of the changing statistics of medicanes in future climate scenarios . A study on Mediterranean cyclogenesis in 21st century climate projections (Gaertner et al., 2007), however, found an increase in the tendency of the Mediterranean Sea to be prone to the formation of tropical cyclones. This conclusion is

drawn by the analysis of dynamical properties of the most intense cyclones detected in a multi-model ensemble of regional model projections for the A2 IPCC scenario in the period 2071-2100.

In order to assess in a systematic way the impact of climate change on the statistics of medicanes, we use the same downscaling technique applied for the reconstruction of the climatology of medicanes. The initial and boundary conditions are provided by the ECHAM5/MPI-OM model. We apply the downscaling to two 30-years periods: 1960-1989, with present climate greenhouse gas concentration (labeled in the following C20), and 2070-2099, with the IPCC-AR4 A2 future climate scenario greenhouse gas concentration (labeled A2). Apart from the boundary conditions, the system configuration is exactly the same employed to study the climatology of medicanes, described in Chapter 4. The model setup and the detection procedure are described in detail in Chapter 2.

5.1 Present climate control run

We find in the 1960-1989 control run a total number of 31 medicanes over thirty years. The frequency of medicanes, with an average of approximately one medicane per year, is around 35 percent lower than the value found in the reanalyses-driven simulation. In Zahn and von Storch (2010), where the impact of climate change on the statistics of polar lows was studied with the same downscaling approach and the same boundary conditions used in this work, a comparable difference in the number of storms detected in the reanalysis-driven downscaling and in the ECHAM5-driven one was found. That difference has been attibuted to the bias in the mean atmospheric vertical stability found in the ECHAM5 boundary conditions (see Fig. 2 in Zahn and von Storch 2010).

The geographical distribution, seasonal cycle and inter-annual variability of the medicanes detected in the C20 simulation are reported, respectively, in Figs. 5.1, 5.2 and 5.3. A comparison of Fig. 5.1 with Fig. 4.1 shows that the geographical distributions of the medicanes in the C20 simulation and NCEP-driven simulation are similar, with the larger number of medicanes formed in the western Mediterranean and "Ionian" areas. The long-term time-series are also similar, showing both strong year-to-year variability and negligible trend. The peak in the annual cycle is slightly shifted towards the end of Fall. The long-term statistical properties of medicanes detected in the C20 simulation are thus compatible with those found in the NCEP60 simulation, in spite of the fact that the frequency of storms produced over the 30 years period is lower.

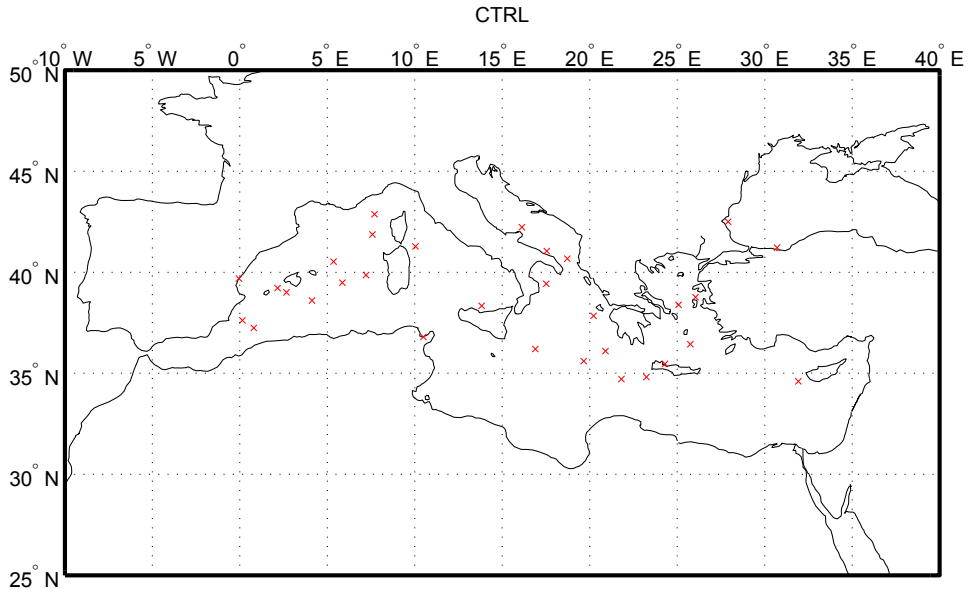

Figure 5.1: Formation locations of all the medicanes detected in the C20 simulation.

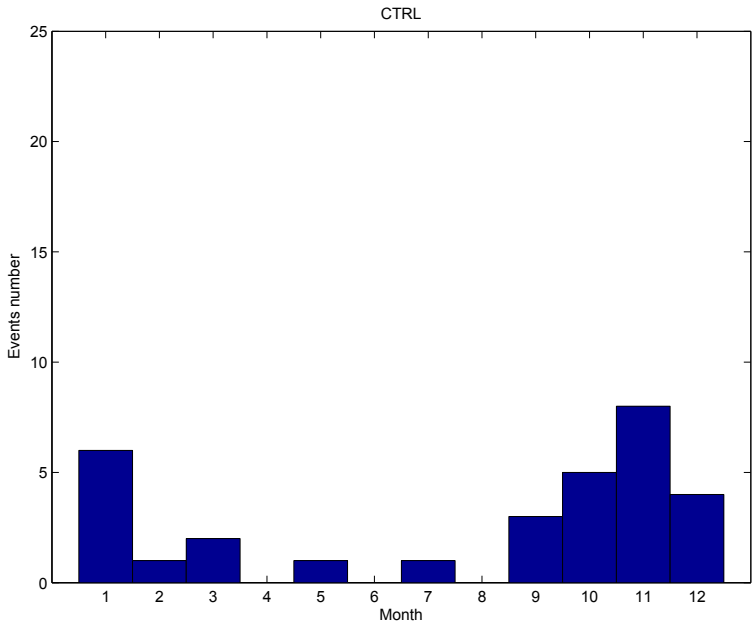

Figure 5.2: Number of medicanes per month (total number in the period 1960-1989) in the C20 simulation.

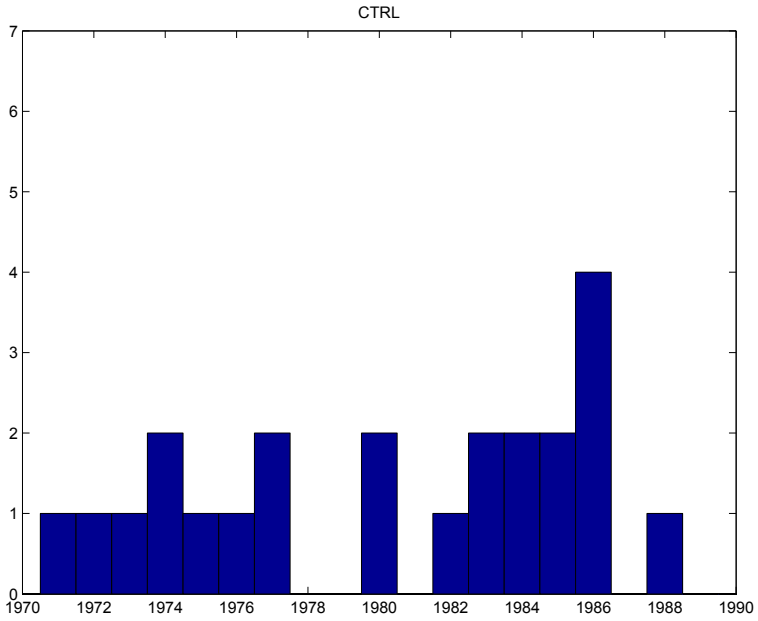

Figure 5.3: Number of medicanes per season in the C20 simulation.

5.2 Projected frequency of medicanes in the A2 IPCC scenario

The number of detected medicanes in the A2 simulation is eighteen over thirty years, a forty percent decrease with respect to the C20 simulation. The geographical distribution, seasonal cycle and inter annual variability are reported, respectively in Figs. 5.4, 5.5 and 5.6.

There is no visible difference in the preferred medicanes formation regions. On the other hand, the maximum of medicane activity is shifted from November to October.

In order to explain the reduction in the number of detected medicanes, we repeat the analysis of the favorable environmental conditions for medicanes development performed in Chapter 4 for past medicanes, analyzing how their frequency changes between the control run and the scenario simulation. In Fig. 5.7 is reported the probability of the simultaneous occurrence of the environmental factors favoring medicanes for the A2 scenario, and the difference with respect with the control experiment. The probability is decreased with respect to the control simulation over most of the basin, the decrease being larger in the northwestern part of the basin where most of the medicanes develop. In order to assess the reasons of the reduction in the probability of medicanes formation, we analyze the four large-scale factors (ΔT, wind shear, humidity and vorticity) separately. The probability to exceed the threshold for medicane formation for each of the factors in the A2 simulation is reported in Fig. 5.8, while Fig. 5.9 shows the difference between the A2 scenario and the control run.

The strongest effect is visible in ΔT, whose probability shows a significant decrease in all the basin. The probability of having values of both the moisture content of the atmosphere and low level vorticity suitable for the development of medicanes also show a decrease, but less strong than that of ΔT.

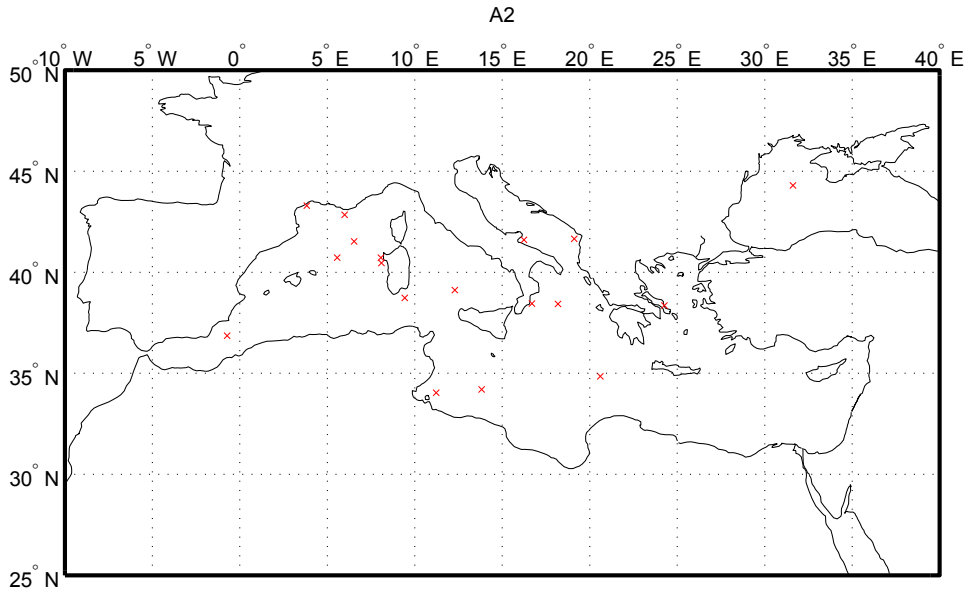

Figure 5.4: Formation locations of all the medicanes detected in the A2 simulation.

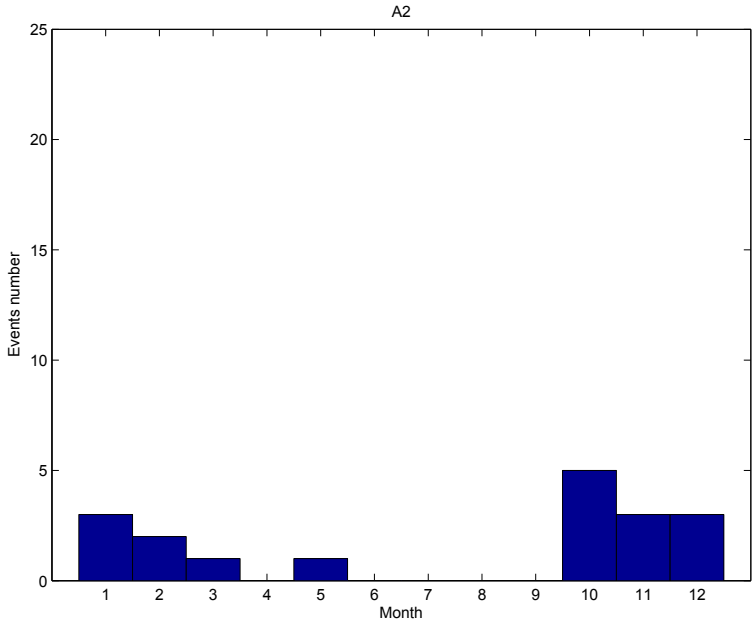

Figure 5.5: Number of medicanes per month (total number in the period 2070-2099) in the A2 simulation.

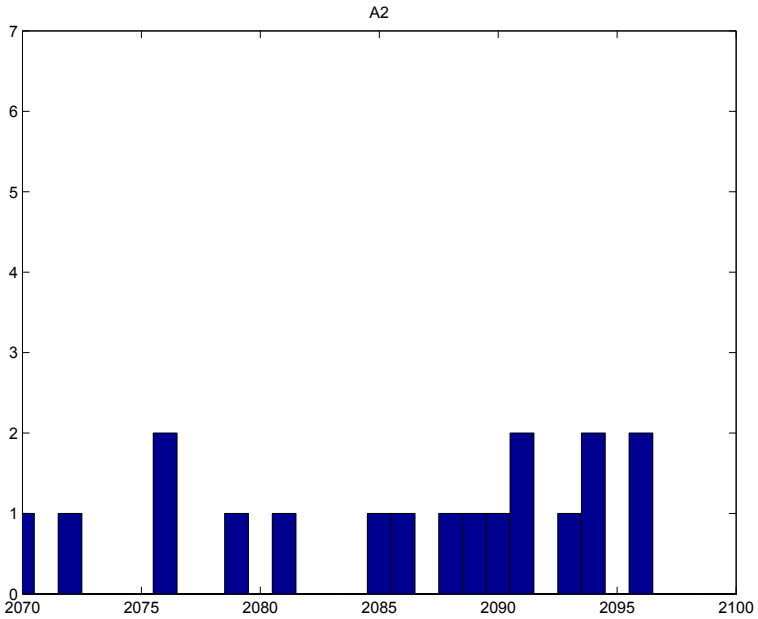

Figure 5.6: Number of medicanes per season in the A2 simulation.

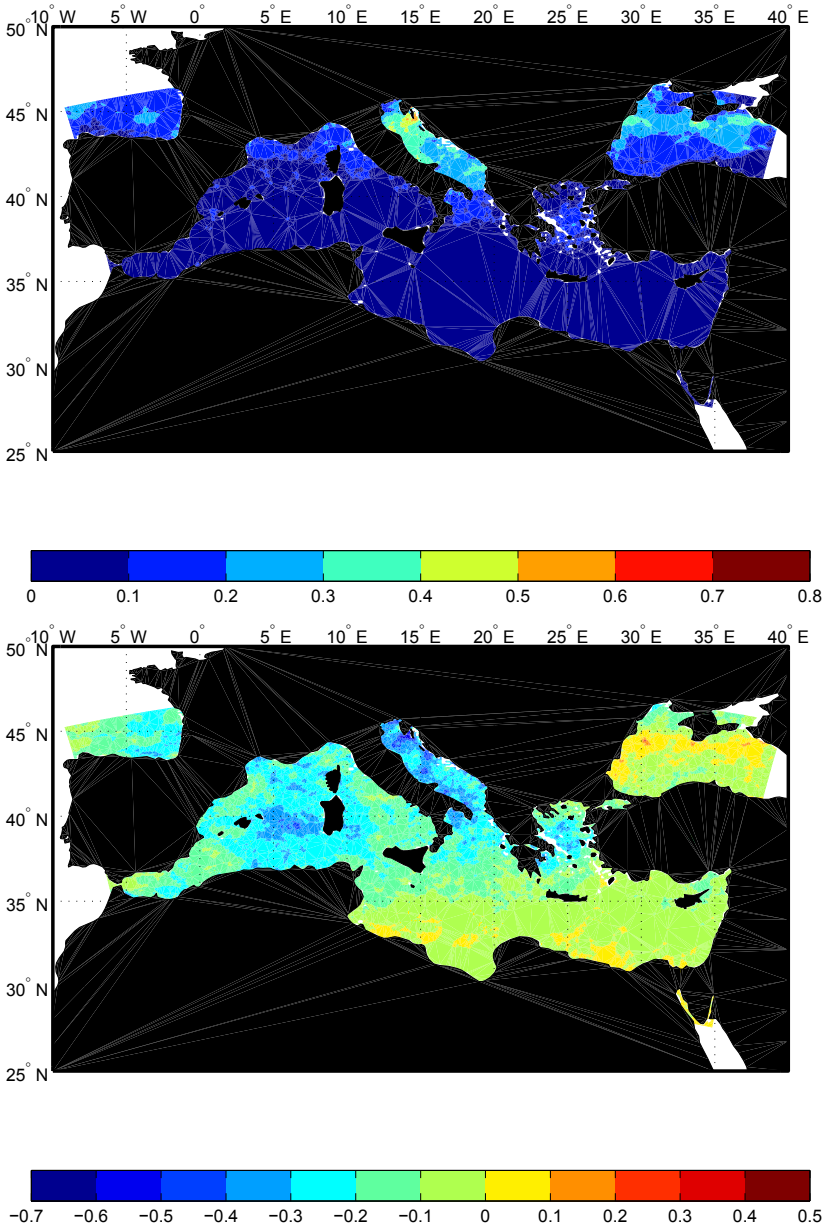

Figure 5.7: Probability of simultaneous realization of the environmental conditions favorable for medicanes formation. Top: A2 scenario (0.1% contours). Bottom: difference between scenario and control run (0.1% contours).

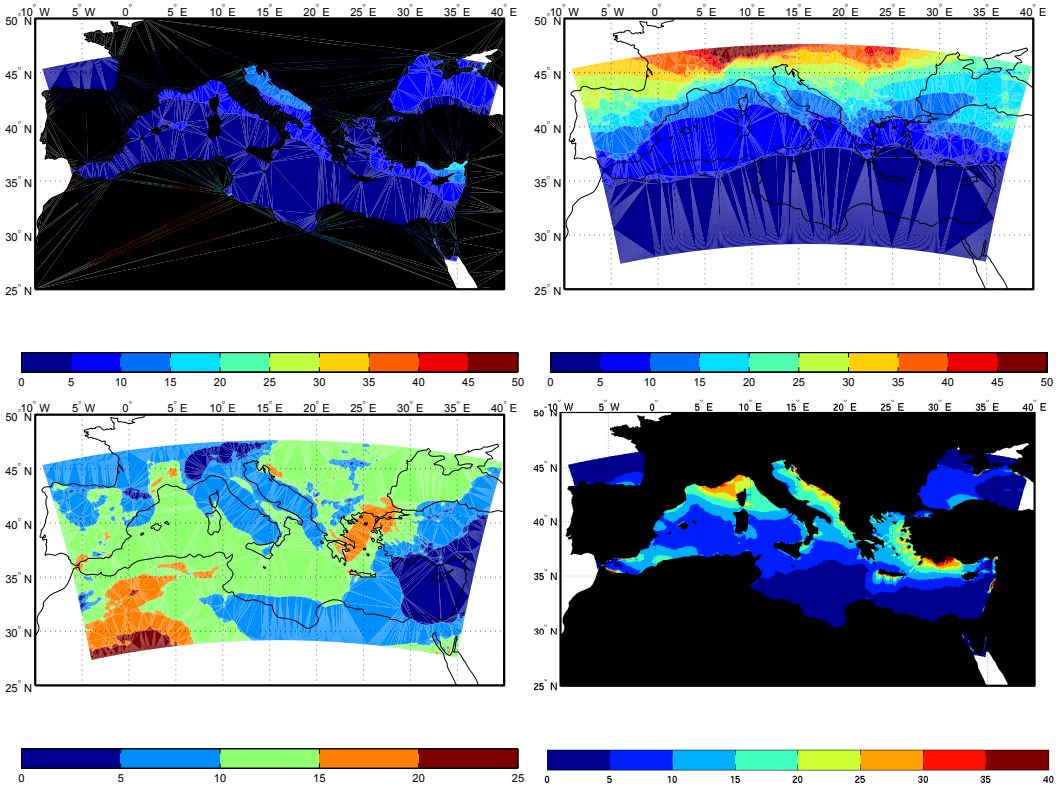

Figure 5.8: Probability for each of the following factors to exceed the threshold value corresponding to the formation of medicanes in the A2 simulation: ΔT (top left, 5% contours), RH (top right, 5% contours), WS (bottom left, 5% contours), VORT (bottom right, 5% contours).

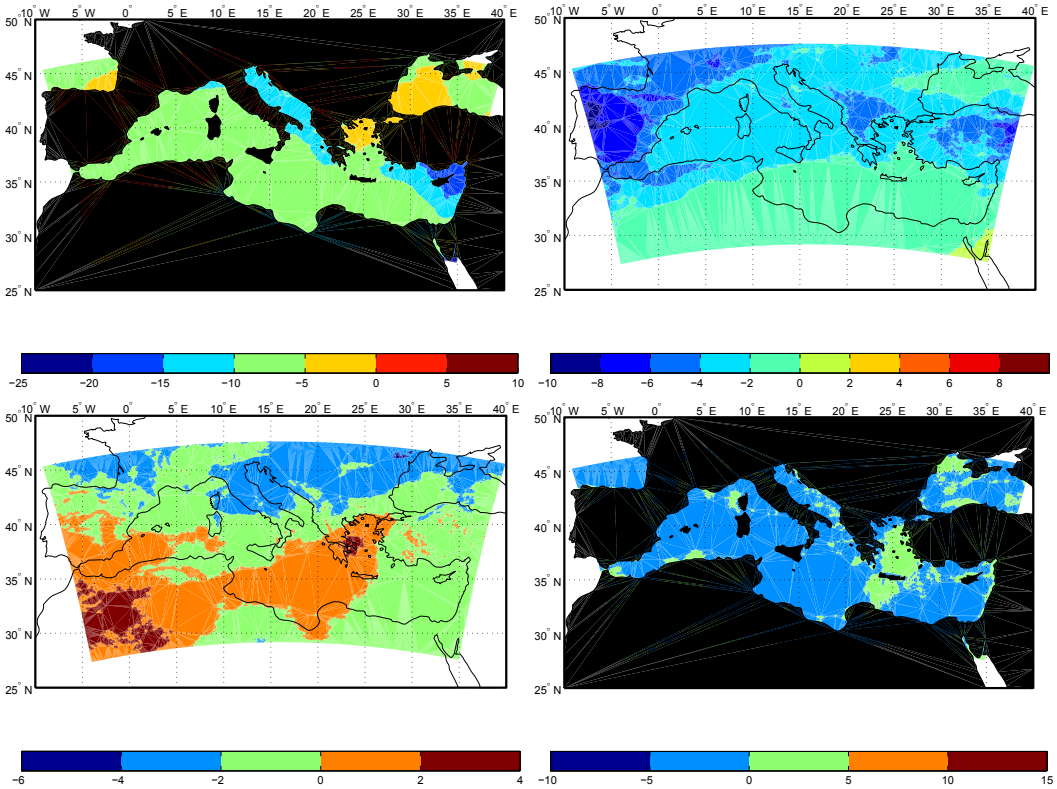

Figure 5.9: Probability for each of the following factors to exceed the threshold value corresponding to the formation of medicanes (A2-C20 difference): ΔT (top left, 5% contours), RH (top right, 5% contours), WS (bottom left, 5% contours), VORT (bottom right, 5% contours).

Conclusions and outlook

In the present work we investigated the long-term statistics of the emergence, tracking and of dynamical properties of medicanes, a rare kind of Mediterranean storms that show features similar to those of tropical hurricanes. The climatology of medicanes over the last six decades was studied using a high resolution regional climate model (CCLM) to perform the dynamical downscaling of reanalysis data, and the impact of climate change on the statistics of medicanes was estimated applying the same method on the future climate scenarios produced by a global circulation model.

We showed that the regional model, driven by boundary conditions derived by NCEP/NCAR reanalysis, is able to reproduce a number of medicanes cases documented in the literature, provided spectral nudging is applied. Not only are the medicanes generated at about the correct time and location, but also their internal dynamical structure, including characteristic features such as vertical symmetry and warm core, is well simulated. For both the surface variables and the vertical structure, the degree of accuracy of the values of the atmospheric fields produced by the model in the vicinity of the storm depends on the resolution; most details are fully resolved only in the high resolution (10 km) simulations. The depths of pressure minima coincide with good accuracy with the ones found in large-scale analyses of comparable resolution in the 25 km resolution simulation, while a deepening due to the better resolved cyclone fine structure generally occurs in the high resolution simulations. The value of wind speed in the coarse resolution simulations, on the other hand, tends to be underestimated by 10-30% with respect to the one inferred from satellite-based measurements.

Applying the downscaling to the full NCEP/NCAR reanalysis data for the 1948-2011 period, and using an objective detection procedure, we studied the statistical properties of the medicanes detected over six decades. We find that medicanes occur with a very low frequency (about 1.6 per year over the whole Mediterranean basin), and that they are formed mostly in the western Mediterranean and in the region extending between the Ionian Sea and the North-African coast. The annual cycle of medicanes formation has a peak at

the beginning of Winter, with a relevant number of events during Fall, and a few over Spring. The year-to-year variability is strong, but no significant trend is found in the last sixty years.

We investigated the environmental factors related with the formation of medicanes. We find that the triggering of medicanes requires a sufficiently large difference between the sea surface temperature and the temperature in the upper atmospheric layers, in order to increase the atmospheric instability. For the detected medicanes, such a difference is generally produced by the presence of a cold temperature anomaly in the high troposphere, rather than by a large deviation of the sea surface temperature from the mean state. A low wind shear, high moisture content, and high low-level vorticity are all factors that favor the development of medicanes. It was shown that the frequency of simultaneous realization of all the favorable conditions described above exhibits a geographical distribution and a seasonal cycle compatible with the frequency of medicanes formation.

Finally, we used the same downscaling approach used for the reconstruction of the climatology of past medicanes to estimate the impact of climate change on medicanes statistics. We find that the number of medicanes produced in the 2070-2099 period within the A2 SRES-IPCC scenario is about forty percent lower than those produced in the 1960-1989 simulation with 20th century radiative forcing. The decrease in medicanes frequency corresponds to a comparable decrease in the occurrence of the environmental conditions associated with their formation. In particular, the main effects are found to be the decreased frequency of synoptic states with large atmospheric instability, and with high atmospheric moisture.

A decrease in the frequency in future climate comparable to that of medicanes, has been found for several kinds of cyclonic systems based on air-sea interaction, such as tropical cyclones in most of the ocean basins, polar lows and so on. On the other hand, the decrease in the frequency of such systems is often associated to an increase in the mean intensity of the events. It would thus be interesting extend the results discussed in this Thesis by performing a systematic analysis of the intensity of medicanes in both present and future climate. Moreover, it would be useful to complement the results obtained in this Thesis for the A2 scenario, by repeating the analysis on different future climate scenarios, in order to gain a better understanding of the impact of climate change on the statistics of medicanes.

Medicanes are often associated to extreme weather events, such as for example severe flooding in southern Italy associated with the storm of October 1996, or, more recently, the flood in Genoa occurred simultaneously to the formation of a medicane in the wester Mediterranean area, in November

2011. A thorough analysis of the linkage between extremes in wind and precipitation related to medicanes would thus be extremely useful in order to quantify the impacts of such storms on coastal areas.

Acknowledgements

The Author's research has been funded by the Institute for Coastal Research of the Helmholtz-Zentrum Geesthacht, Zentrum für Material- und Küstenforschung, and by CMCC, Centro Euro-Mediterraneo sui Cambiamenti Climatici.

The Author acknowledges Burkardt Rockel and Beate Geyer for their precious help with the model, and Antonio Navarra, Matthias Zahn, Giuseppe Zappa and Paolo Davini for many valuable and stimulating discussions. The Author thanks Marcello Miglietta and Kevin Walsh for their careful review and many useful suggestions that helped to ameliorate this manuscript.

Appendix A

The cyclone phase space

A parametrical classification of cyclones according to their dynamical properties has been proposed in Hart (2003), to study the extratropical transition of tropical cyclones. A cyclone phase space is defined, based on the dynamical parameters (cold core/warm core and symmetrical/asymmetrical vertical structure) that optimize the discrimination between tropical and extra-tropical cyclones.
The parameters are defined as follows.

$$B = \left(\overline{Z_{600\ \mathrm{hPa}} - Z_{900\ \mathrm{hPa}}}\big|_R - \overline{Z_{600\ \mathrm{hPa}} - Z_{900\ \mathrm{hPa}}}\big|_L \right) , \tag{A.1}$$

$$-|V_T^L| = \left. \frac{\partial(\Delta Z)}{\partial \ln p} \right|_{900\ \mathrm{hPa}}^{600\ \mathrm{hPa}} , \tag{A.2}$$

and

$$-|V_T^U| = \left. \frac{\partial(\Delta Z)}{\partial \ln p} \right|_{600\ \mathrm{hPa}}^{300\ \mathrm{hPa}} . \tag{A.3}$$

In Eqns. (A.1 - A.3), Z represents the geopotential height, at the indicated level. The bar in Eq. (A.1) indicates an area average over semicircles of 500 km radius respectively to the left and right with respect to the direction of motion of the storm. The parameter B represents the thermal symmetry of the cyclone: a threshold value of B=10 m has been empirically determined by analyzing a large sample of both tropical and extra-tropical cyclones. The thermal wind parameters are defined in such a way that positive and negative values of $-V_T$ indicate respectively a warm-core or cold-core in the relevant layer. Studying the diagrams of the three dimensional phase space it is possible to classify a specific cyclone as tropical or extra-tropical at each stage of its lifetime (see Fig. A.1).

The warm-core and symmetry criteria applied in the objective detection algorithm of medicanes (Sec. 2.2) are based on the phase space analysis described above. Only the radius used for the calculation of the B and V_T parameters has been modified to a value of 100 km, in order to adapt the analysis to the characteristic spatial scale of medicanes. As an example, the evolution of the simulated January 1995 medicane in the phase space diagrams is reported in Fig. A.2.

The radius for the calculation of the parameters has to be chosen in such a way that it includes the thermal symmetry of the cyclone, but does not extend into other systems, smoothing out the warm core structure. In the case of tropical cyclones, the value is fixed as the average radius over which convergent inflow is observed over a large sample of events (Frank, 1977). In the case of medicanes such a large sample of events to estimate the radius is not available. The used value of 100 km used correctly reproduced the warm-core structure of the four test cases discussed in Chapter 3. It was verified however that different values in the range 100- 200 km do not alter the results in a relevant way(see Table 2.1).

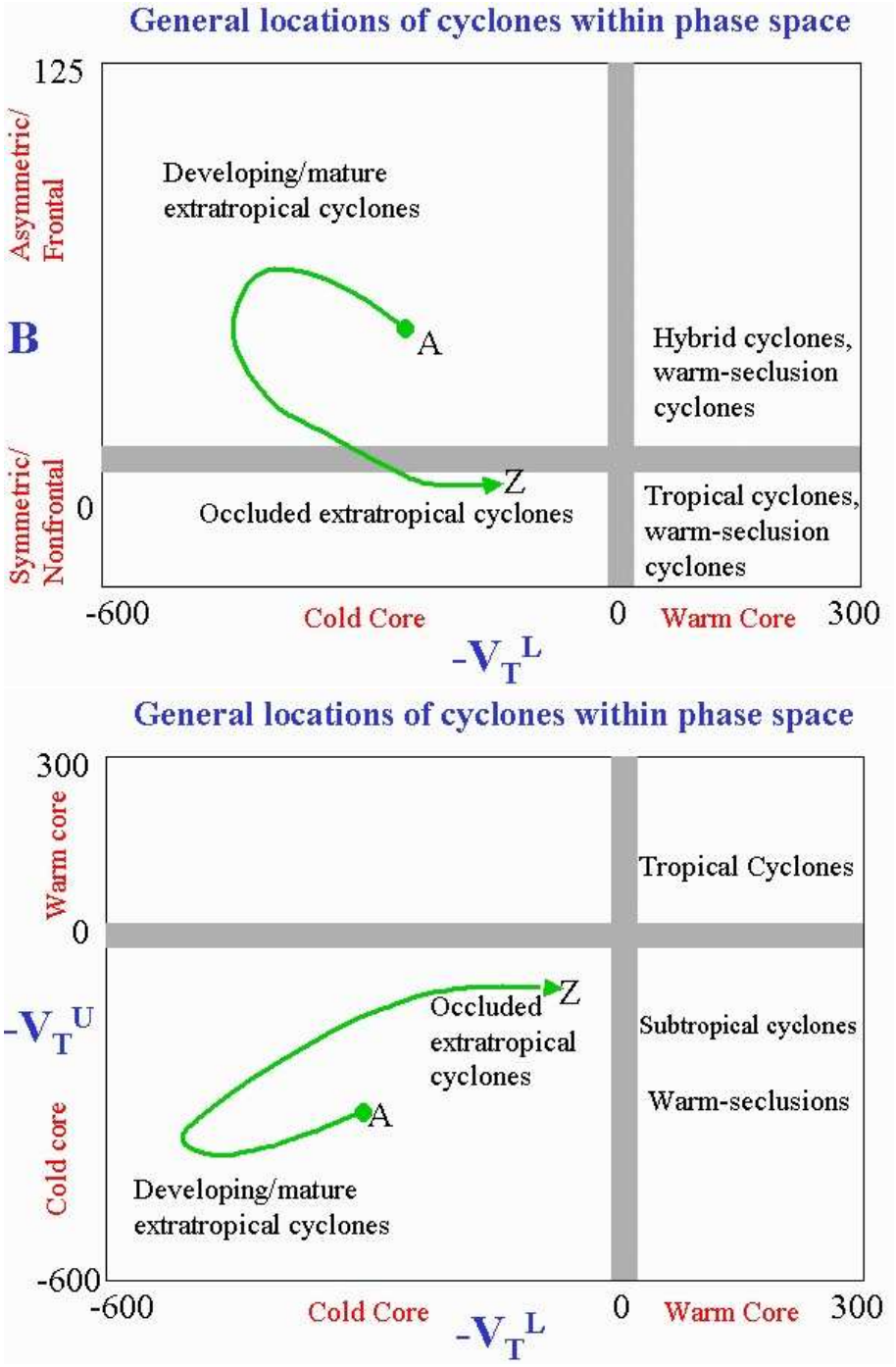

Figure A.1: Classification of cyclones based on phase space diagrams (from the website `http://moe.met.fsu.edu/cyclonephase/`).

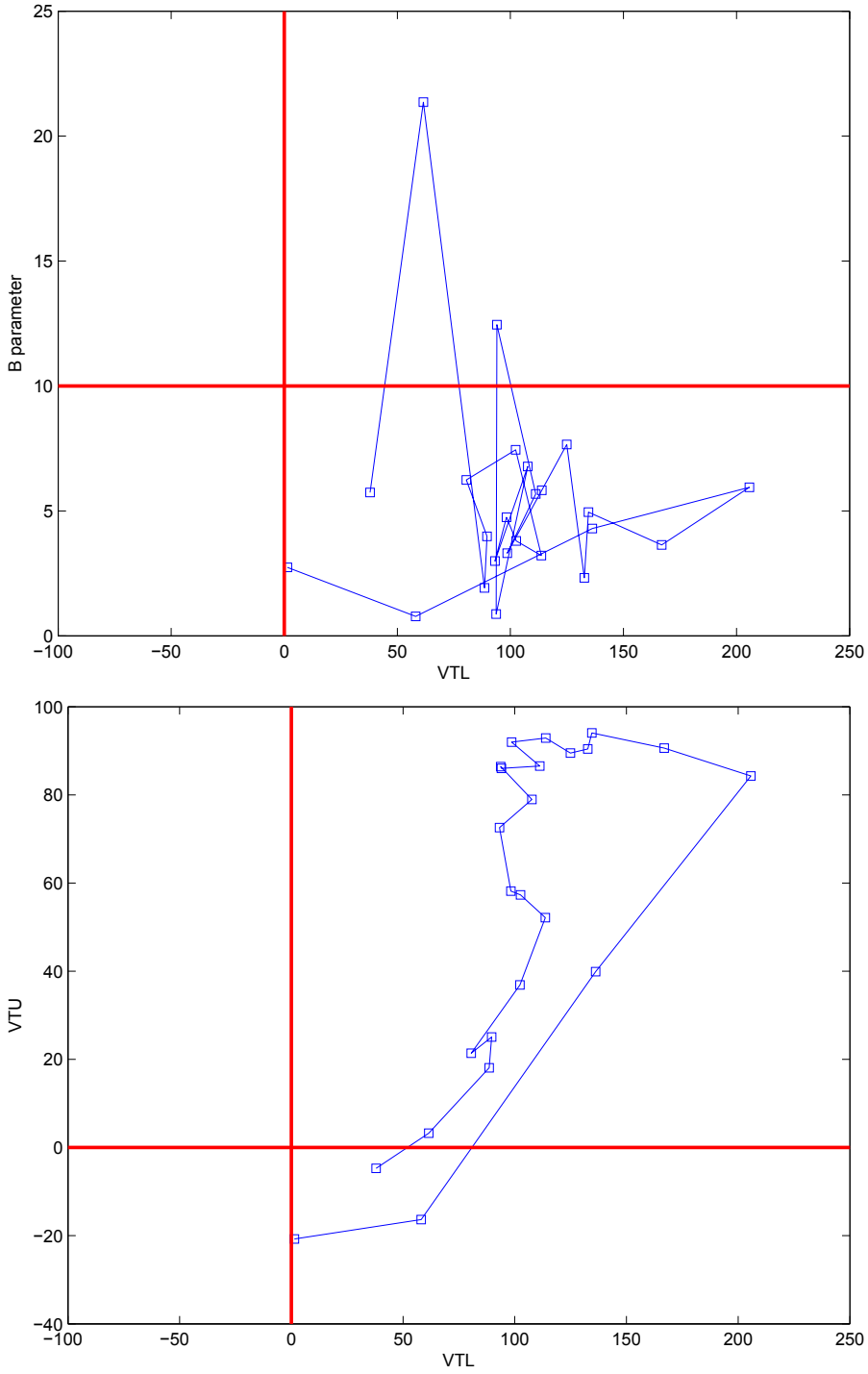

Figure A.2: Evolution of the 9501 medicane in the phase space diagrams (9501sn2hi simulation).

Appendix B

Detection algorithm sensitivity test

In order to assess the robustness of the statistical properties of medicanes against the variation of the threshold values used in the detection algorithm, the analysis was repeated on the full downscaled NCEP data with the following sets of parameters P1 and P2, to be compared with the set of parameters P0 used to obtain the results in Chapter 4 and 5.
P1:

- ΔP=20 Pa;
- R_{wc}= 100 km;
- V_{av}= 15 m/s;
- V_{max} = 25 m/s;
- t_{vmax} =4 h.

P2:

- ΔP=20 Pa;
- R_{wc}= 100 km;
- V_{av}= 18 m/s;
- V_{max} = 30 m/s;
- t_{vmax} =6 h.

The resulting geographical distributions, seasonal cycle and year-to-year variability are reported respectively in Figs. B.1, B.2 and B.3. As it was discussed in Sec. 2.2, the choice between the parametrizations P0 and P2 is to some extent arbitrary, as in one case more importance is given to minimize missed detections and in the other to minimize false positives. The comparison between Figs. B.1, B.2 and B.3 with the corresponding Figs. 4.1, 4.2 and 4.3 shows that the main statistical properties are to a large extent unaffected by the change in the parametrization. On the other hand, by changing the parameters in a more radical way such as in P1, larger differences arise in both the geographical distribution and seasonal cycle. This results support the conclusion that the results presented in Chapters 4 and 5 are statistically robust with respect to the choice of the parametrization P0 against P2.

R_{wc} = 100 km, t_{vmax} = 6h

V_{av} \ V_{max}	25	26	27	28	29	30
14	22	19	15	13	10	6
15	21	19	15	13	10	6
16	21	19	15	13	10	6
17	21	19	15	13	10	6
18	21	19	15	13	10	6

R_{wc} = 100 km, t_{vmax} = 4h

V_{av} \ V_{max}	25	26	27	28	29	30
14	25	22	19	16	15	7
15	24	22	19	16	15	7
16	24	22	19	16	15	7
17	23	21	18	15	14	7
18	22	20	17	15	14	7

R_{wc} = 150 km, t_{vmax} = 6h

V_{av} \ V_{max}	25	26	27	28	29	30
14	20	18	14	12	10	6
15	19	18	14	12	10	6
16	19	18	14	12	10	6
17	19	18	14	12	10	6
18	19	18	14	12	10	6

R_{wc} = 200 km, t_{vmax} = 6h

V_{av} \ V_{max}	25	26	27	28	29	30
14	18	16	12	10	8	4
15	17	16	12	10	8	4
16	17	16	12	10	8	4
17	17	16	12	10	8	4
18	17	16	12	10	8	4

Table B.1: Number of medicanes detected in the 2000-2005 period, varying the algorithm parameters as indicated.

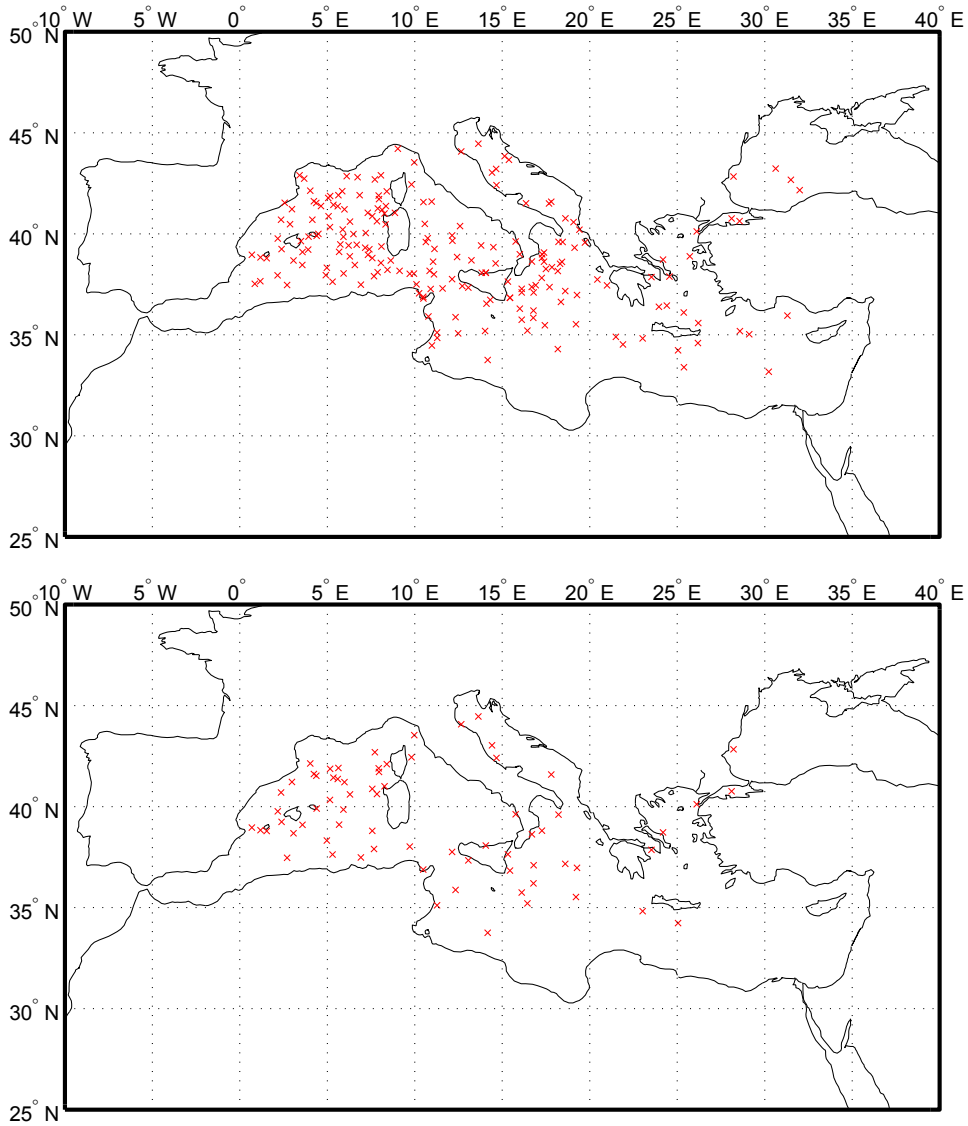

Figure B.1: Formation locations of the medicanes detected in the NCEP60 simulation, using the set of detection parameters P1 (top) and P2 (bottom).

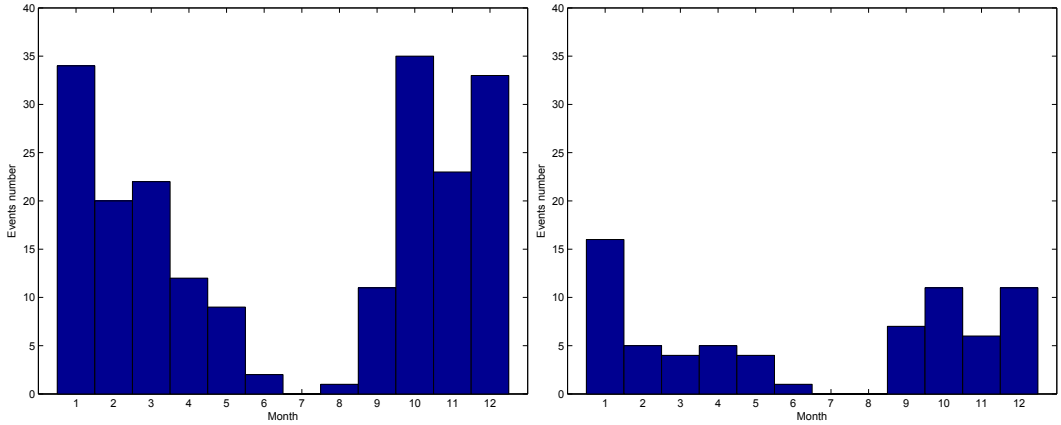

Figure B.2: Number of medicanes per month (total number in the period 1948-2011) in the in the NCEP60 simulation, using the set of detection parameters P1 (left) and P2 (right).

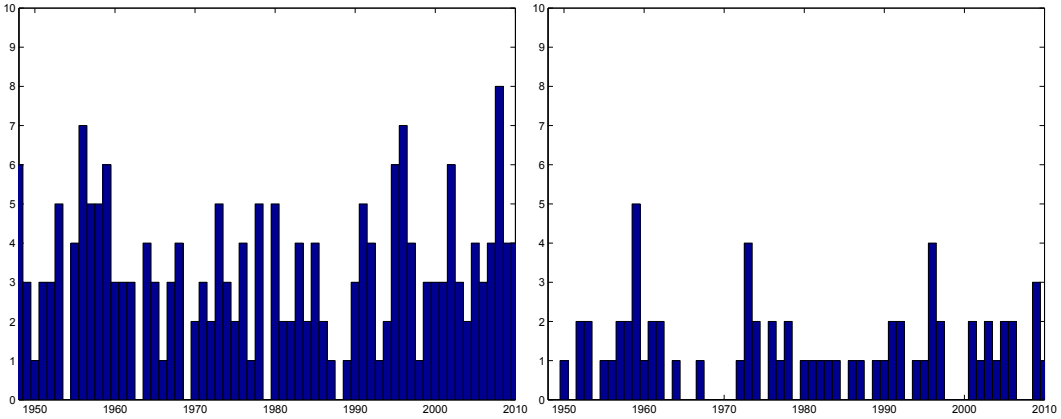

Figure B.3: Number of medicanes per season in the in the NCEP60 simulation, using the set of detection parameters P1 (left) and P2 (right).

Bibliography

M. Bister and K.A. Emanuel. Low frequency variability of tropical cyclone potential intensity 1. Interannual to interdecadal variability. *Journal of Geophysical Research*, 107:4801, 2002.

P. Brasseur, J.M. Beckers, JM Brankart, and R. Schoenauen. Seasonal temperature and salinity fields in the Mediterranean Sea: Climatological analyses of a historical data set. *Deep Sea Research Part I: Oceanographic Research Papers*, 43:159–192, 1996.

A. Buzzi and S. Tibaldi. Cyclogenesis in the lee of the Alps: A case study. *Quarterly Journal of the Royal Meteorological Society*, 104:271–287, 1978.

S.J. Camargo, K.A. Emanuel, and A.H. Sobel. Use of a genesis potential index to diagnose ENSO effects on tropical cyclone genesis. *Journal of Climate*, 20:4819–4834, 2007a.

S.J. Camargo, A.H. Sobel, A.G. Barnston, and K.A. Emanuel. Tropical cyclone genesis potential index in climate models. *Tellus A*, 59:428–443, 2007b.

J. Campins, A. Jansà, and A. Genovés. Three-dimensional structure of western Mediterranean cyclones. *International journal of climatology*, 26:323–343, 2006.

J. Campins, A. Genovés, MA Picornell, and A. Jansà. Climatology of Mediterranean cyclones using the ERA-40 dataset. *International Journal of Climatology*, 31:1596–1614, 2011.

D. Conte, M. M. Miglietta, and V. Levizzani. Analysis of instability indices during the development of a Mediterranean tropical-like cyclone using MSG-SEVIRI products and the LAPS model. *Atmospheric Research*, 101:264–279, 2011.

S. Davolio, M. M. Miglietta, A. Moscatello, F Pacifico, A. Buzzi, and R. Rotunno. Numerical forecast and analysis of a tropical-like cyclone in the Ionian Sea. *Natural Hazards and Earth System Sciences*, 9:551–562, 2009.

N. Ebuchi, H. C. Graber, and M. J. Caruso. Evaluation of wind vectors observed by QuikSCAT/SeaWinds using ocean buoy data. *Journal of Atmospheric and Oceanic Technology*, 19:2049–2062, 2002.

K. Emanuel. Genesis and maintenance of "Mediterranean hurricanes". *Advances in Geosciences*, 2:217–220, 2005.

K.A. Emanuel. An air-sea interaction theory for tropical cyclones. Part I: Steady-state maintenance. *Journal of the Atmospheric Sciences*, 43:585–605, 1986.

K.A. Emanuel. Thermodynamic control of hurricane intensity. *Nature*, 401: 665–669, 1999.

K.A. Emanuel and D. Nolan. Tropical cyclone activity and the global climate system. In *Preprints, 26th Conf. on Hurricanes and Tropical Meteorology, Miami, FL, Amer. Meteor. Soc. A*, volume 10, 2004.

J. A. Ernst and M. Matson. A Mediterranean Tropical Storm? *Weather*, 38: 332–337, 1983.

F. Feser and H. von Storch. A dynamical downscaling case study for typhoons in SE Asia using a regional climate model. *Monthly Weather Review*, 136: 1806–1815, 2008.

F. Feser, B. Rockel, H. von Storch, J. Winterfeldt, and M. Zahn. Regional Climate Models Add Value to Global Model Data: A Review and Selected Examples. *Bulletin of the American Meteorological Society*, 92:1181–1192, 2011.

L. Fita, R. Romero, A. Luque, K. Emanuel, and C. Ramis. Analysis of the environments of seven Mediterranean tropical-like storms using an axisymmetric, nonhydrostatic, cloud resolving model. *Natural Hazards and Earth System Sciences*, 7:41–56, 2007.

W.M. Frank. The structure and energetics of the tropical cyclone I. Storm structure. *Monthly Weather Review*, 105:1119–1135, 1977.

MA Gaertner, D. Jacob, V. Gil, M. Domínguez, E. Padorno, E. Sánchez, and M. Castro. Tropical cyclones over the Mediterranean Sea in climate change simulations. *Geophysical Research Letters*, 34:L14711, 2007.

V. Gil, A. Genovés, MA Picornell, and A. Jansà. Automated database of cyclones from the ECMWF model: Preliminary comparison between West and East Mediterranean basins. In *Proc. Fourth Plinius Conf. on Mediterranean Storms*, 2003.

W.M. Gray. Hurricanes: Their formation, structure and likely role in the tropical circulation. *Meteorology over the tropical oceans*, 19:155–218, 1979.

W.M. Gray et al. *Tropical cyclone genesis*. Department of Atmospheric Science, Colorado State University, 1975.

R. E. Hart. A cyclone phase space derived from thermal wind and thermal asymmetry. *Monthly Weather Review*, 131:585–616, 2003.

V. Homar, R. Romero, D. J. Stensrud, C. Ramis, and S. Alonso. Numerical diagnosis of a small, quasi-tropical cyclone over the western Mediterranean: dynamical vs. boundary factors. *Quarterly Journal of the Royal Meteorological Society*, 129:1469–1490, 2003.

Intergovernmental Panel on Climate Change. *Managing the risks of extreme events and disasters to advance climate change adaption*. Cambridge University Press, 2012.

E. Kalnay et al. The NCEP/NCAR 40-year reanalysis project. *Bulletin of the American Meteorological Society*, 77:437–470, 1996.

K. Lagouvardos, V. Kotroni, S. Nickovic, D. Jovic, G. Kallos, and C. J. Tremback. Observations and model simulations of a winter sub-synoptic vortex over the central Mediterranean. *Meteorological Applications*, 6:371–383, 1999.

A. Luque, L. Fita, R. Romero, and S. Alonso. Tropical-like Mediterranean storms: an analysis from satellite. In *EUMETSAT 07 proceedings*, 2007.

C.E. Menkes, M. Lengaigne, P. Marchesiello, N.C. Jourdain, E.M. Vincent, J. Lefèvre, F. Chauvin, and J.F. Royer. Comparison of tropical cyclogenesis indices on seasonal to interannual timescales. *Climate dynamics*, 38:301–321, 2012.

M. M. Miglietta, A. Moscatello, D. Conte, G. Mannarini, G. Lacorata, and R. Rotunno. Numerical analysis of a Mediterranean "hurricane" over south-eastern Italy: Sensitivity experiments to sea surface temperature. *Atmospheric Research*, 101:412–426, 2011a.

M. M. Miglietta, A. Moscatello, D. Conte, G. Mannarini, G. Lacorata, and R. Rotunno. Numerical analysis of a Mediterranean "hurricane" over south-eastern Italy: Sensitivity experiments to sea surface temperature. *Atmospheric Research*, 101:412–426, 2011b.

A. Moscatello, M. M. Miglietta, and R. Rotunno. Observational analysis of a Mediterranean "hurricane" over south-eastern Italy. *Wheather*, 63: 306–311, 2008a.

A. Moscatello, M. M. Miglietta, and R. Rotunno. Numerical analysis of a Mediterranean "hurricane" over south-eastern Italy. *Monthly Weather Review*, 136:4373–4396, 2008b.

E. Palmen. On the formation and structure of tropical hurricanes. *Geophysica*, 3:26–38, 1948.

I. Pytharoulis, G. Craig, and S. Ballard. The hurricane-like Mediterranean cyclone of January 1995. *Meteorological Applications*, 7:261–279, 2000.

E. Rasmussen and J. Turner. *Polar Lows: Mesoscale Weather Systems in the Polar Regions*. Cambridge University Press, Cambridge, 2003.

E. Rasmussen and C. Zick. A subsynoptic vortex over the Mediterranean with some resemblance to polar lows. *Tellus A*, 39:408–425, 1987.

O. Reale and R. Atlas. Tropical cyclone-like vortices in the extratropics: observational evidence and synoptic analysis. *Weather Forecast*, 16:7–34, 2001.

L. Ricciardulli and F. Wentz. Reprocessed QuikSCAT (V04) wind vectors with Ku-2011 geophysical model function. Technical Report 043011, Remote Sensing Systems, 2011.

M. M. Rienecker et al. MERRA: NASA's modern-era retrospective analysis for research and applications. *Journal of Climate.*, 24:3624–3648, 2011.

B. Rockel, A. Will, and A. Hense. The regional climate model COSMO-CLM (CCLM). *Meteorologische Zeitschrift*, 17:347–348, 2008.

M.J. Rodwell and B.J. Hoskins. Monsoons and the dynamics of deserts. *Quarterly Journal of the Royal Meteorological Society*, 122:1385–1404, 1996.

L.R. Schade. *The ocean's effect on hurricane intensity*. PhD thesis, Massachusetts Institute of Technology, 1994.

A. J. Simmons. Observations, assimilation and the improvement of global weather prediction – some results from operational forecasting and ERA-40. In T.N. Palmer and R. Hagedorn, editors, *Predictability of Weather and Climate*, pages 459–488. Cambridge University Press, 2006.

M. Tous and R. Romero. Meteorological environments associated with medicane development. *International Journal of Climatology*, 33:1–14, 2013.

M. Tous, R. Romero, and C Ramis. Surface heat fluxes influence on medicane trajectories and intensication. *Atmospheric Research*, 2012. doi: 10.1016/j.atmosres.2012.05.022.

I. F. Trigo, T. D. Davies, and G. R. Bigg. Objective climatology of cyclones in the Mediterranean region. *Journal of Climate*, 12:1685–1696, 1999a.

I.F. Trigo, T.D. Davies, and G.R. Bigg. Objective climatology of cyclones in the Mediterranean region. *Journal of Climate*, 12:1685–1696, 1999b.

UIB. Website. URL `http://www.uib.es/depart/dfs/meteorologia/METEOROLOGIA/MEDICANES`.

H. von Storch, H. Langenberg, and F. Feser. A spectral nudging technique for dynamical downscaling purposes. *Monthly Weather Review*, 128:3664–3673, 2000.

K. Walsh. Objective detection of tropical cyclones in high-resolution analyses. *Monthly Weather Review*, 125:1767–1779, 1997.

K. Walsh and I. G. Watterson. Tropical cyclone-like vortices in a limited area model: comparison with observed climatology. *Journal of Climate*, 10:2240–2259, 1997.

K. J. E. Walsh, M. Fiorino, C. W. Landsea, and K. L. McInnes. Objectively determined resolution-dependent threshold criteria for the detection of tropical cyclones in climate models and reanalyses. *Journal of Climate*, 20:2307–2314, 2007.

M. Zahn and H. von Storch. Tracking polar lows in CLM. *Meteorologische Zeitschrift*, 17:445–453, 2008.

M. Zahn and H. von Storch. Decreased frequency of North Atlantic polar lows associated with future climate warming. *Nature*, 467:309–312, 2010.

M. Zahn, H. von Storch, and S. Bakan. Climate mode simulation of North Atlantic Polar Lows in a limited area model. *Tellus A*, 60:620–631, 2008.

H.-M. Zhang, J. J. Bates, and R. W. Reynolds. Assessment of composite global sampling: Sea surface wind speed. *Geophysical Research Letters*, 33:L17714, 2006.